– *An international journal for New Concepts in Global Tectonics* –

NCGT JOURNAL

Editor-in-Chief: Bruce LEYBOURNE (leybourneb@iascc.org)

NCGT Journal
New Concepts in Global Tectonics

Volume 13, Number 10
December 2025

ISSN 2202-0039

WWW.ncgtjournal.com

Ionizations in the atmosphere, vapor clouds and earthquakes

by Valentino Straser

See Fig. 3

Cloud sighted November 1, 2024

~Aligned with the course of the Taro River

~In the middle valley between Solignano and Borgotaro

~Province of Parma

4th Quarterly Issue

NCGT Journal
New Concepts in Global Tectonics

New Concepts in Global Tectonics Journal
Volume 13, Number 10, December 2025

ISSN number; ISSN 2202-0039

– An international journal for New Concepts in Global Tectonics –

NCGT JOURNAL

Volume 13, Number 10, December 2025. ISSN 2202-0039.

CONTENTS

For donations, please feel free to contact the Research Director of the Geoplasma Research Institute, Mr. Bruce Leybourne, at leybourneb@iascc.org. For contact, correspondence, or inclusion of material in the NCGT Journal please use the following methods: *NEW CONCEPTS IN GLOBAL TECTONICS.* 1. E-mail: leybourneb@iascc.org (files in MS Word or ODT format, and figures in gif, bmp or tif format) as separate files; 3. Telephone, +61 402 509 420. *DISCLAIMER*: The opinions, observations and ideas published in this journal are the responsibility of the contributors and do not necessarily reflect those of the Editor and the Editorial Board. *NCGT Journal* is a refereed quarterly international online journal and appears in March, June, September and December. *ISSN number*; ISSN 2202-0039.

NCGT Journal
New Concepts in Global Tectonics

New Concepts in Global Tectonics Journal
Volume 13, Number 10, December 2025

ISSN number; ISSN 2202-0039

EDITOR's CORNER: - Comments by Editor in Chief - Bruce Leybourne

Announcements on Upcoming Conferences - "CALL FOR PAPERS"

Next year - 21-24 September 2026 – NCGT in Italy is being organized by Valentino Straser (valentino .straser @gmail. com). Please contact Valentino if you wish to become involved in any aspect of the conference . Again , we are looking for Session Topics , Abstracts , Papers , Session Chairs , Organizers , Workers , Financial Contributions etc. Let me and Valentino know how you' d like to be involved, and we may accommodate.

September 2026 in Italy we currently have several sessions being locally organized by Valentino Straser

1.) Straser - EQ forecasting (Abstracts requested)

2.) Leybourne - Stellar Transformer - Global Space Weather interactions (6 Abstracts in Editor's Corner within New Concepts in Global Tectonics Journal - Volume 12, Number 4, December 2024)

3.) Anokhin - Lake Ladoga - Siberia (2 Abstracts in Editor's Corner within New Concepts in Global Tectonics Journal - Volume 13, Number 1, March 2025 pp. 5-8, more abstracts requested)

4.) Longhinos - Indian Tectonics (Abstracts requested)

Cover Image : Ionizations in the atmosphere , vapor clouds and earthquakes - Valentino Straser: See Fig. 3. Cloud sighted on November 1, 2024, aligned with the course of the Taro River, in the middle valley between Solignano and Borgotaro, in the province of Parma.

NCGT Journal
New Concepts in Global Tectonics

New Concepts in Global Tectonics Journal
Volume 13, Number 10, December 2025

ISSN number; ISSN 2202-0039

New Book

G. P. Gregori (born 1938), Degree in Physics (1961, Univ. of Milan),

B. G. Gregori (born 1967), Degree in Medicine and Surgery (1992) and Specialization in Neurology (1999)

Science is suffering an identity crisis. Our "widespread scientific knowledge" is "static".

Our mind dislikes uncertainty. Not relying on the mainstream is uncomfortable, but we gain better awareness of the world and of ourselves. This book is challenging. It stimulates the reader also on a psychological level, and tries to explain concepts that to most people consider abstruse. It is a journey where mind can dance between quantum physics, cosmology, theology, Greek philosophy and the mystery of life and death. Science is logic, and a scientist can never give up. Many present unsolved paradoxes can find a solution.

At present, we are biased by: 3 "original sins" in Newton's principles, by an Einstein's mistake, and by a misconception of "absolute" time and of the perception of time passing. A new formulation is presented, which is a substantial advancement compared to Galileo, Newton, Maxwell and Einstein.

https://www.europebookstore.com/products/the-universe-out-of-the-box-worlds-and-anti-worlds-g-p-gregori-and-b-g-gregori/

.

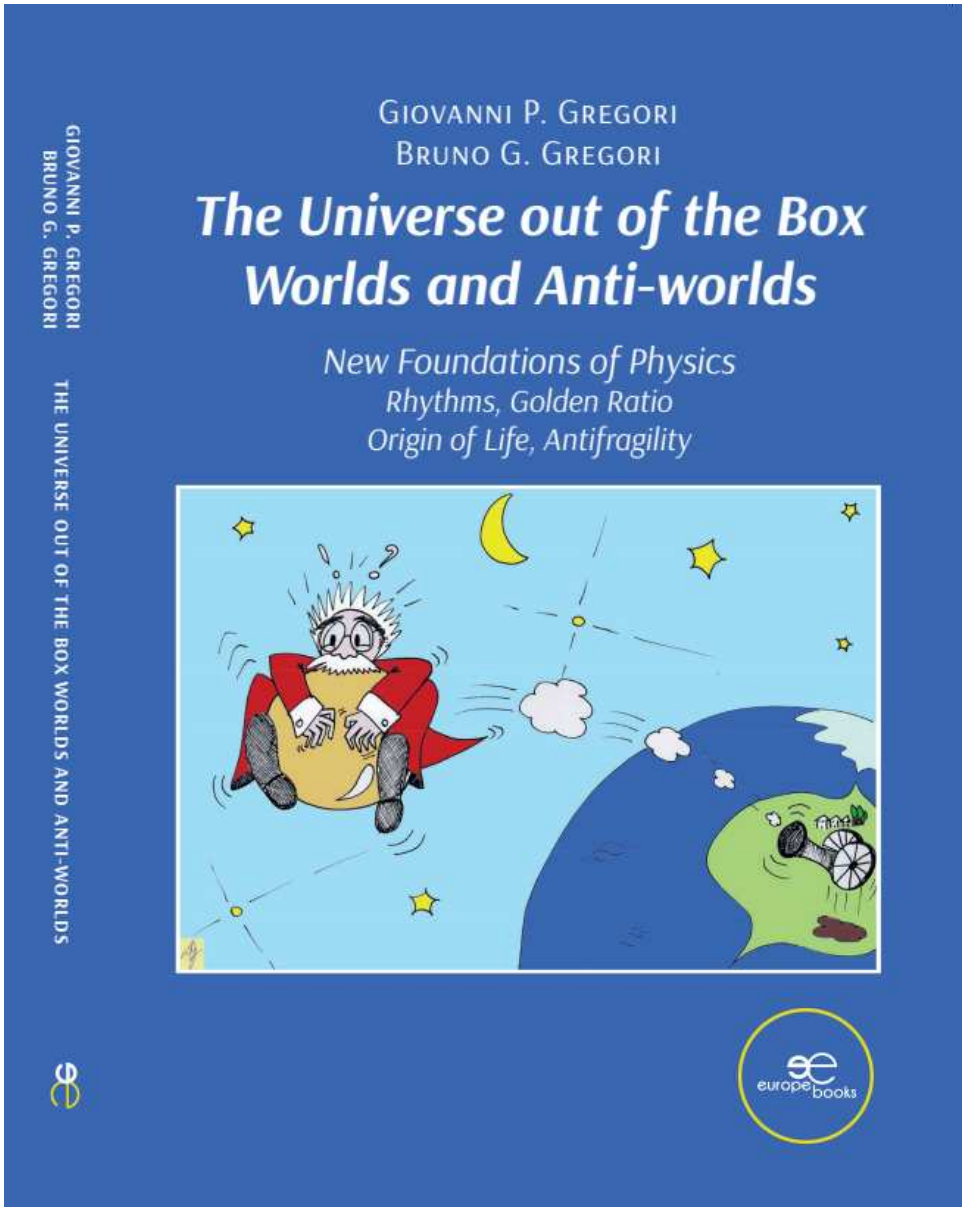

ISSN number; ISSN 2202-0039

Company Profiles:

Tesla 3D, Inc. is an independent research and development company with a strong applied science foundation, enabling rapid and practical innovation in the energy and exploration sectors. While not a large enterprise, Tesla 3D, Inc. stays well informed about breakthroughs in electrical generation, storage, and mining technologies. When called upon, the company can comprehend complex challenges and develop strategic, real-world plans that effectively navigate regulations, funding mechanisms, and policies. Tesla 3D, Inc. actively contributes to national and industry advancement through volunteer leadership, including participation in the Homeland Security Taskforce focused on energy resilience and EMP (electromagnetic pulse) threats. The company also set a precedent by independently qualifying for federal Innovation (R&D) Tax Credits; demonstrating that small, agile innovators can leverage these incentives to streamline regulatory solutions and tackle critical infrastructure challenges. This involvement underscores Tesla 3D, Inc.'s commitment to advancing energy security and shaping the transformative role of technology in resource development. Founded: 2011 Colorado by R. Miller.

Geo-Transect LLP (www.tgeo.co.in) Geo-Transect LLP is a knowledge-driven geoscience consultancy, specializing in subsurface exploration and environmental intelligence across India. With core expertise in subsurface mapping, groundwater zonation, aquifer recharge quantification, coastal and shoreline analysis, landscape and topological planning, and island conservation, the firm delivers data-driven insights that empower sustainable planning and development. Representing the forefront of India's earth-science services sector, Geo-Transect blends scientific precision with advanced technologies to support governmental, industrial, and research-based initiatives across southern India and beyond. Integrating indigenous knowledge with global best practices, the firm is committed to environmental stewardship and responsible resource management. Guided by the ethos "With Wisdom in Nature," Geo-Transect envisions a future where scientific understanding harmonizes development with the natural world.

Stellar Transformer Technologies (https://stellartransformertechnologies.com/) is a private geophysical modeling company specializing in modeling the dynamic electro-magnetic Stellar Transformer interactions between Earth-Sun and planets within our solar system. Original research started in 1995 by the current owner and founder during investigations of the seafloor as a geophysicist with the Naval Oceanographic Office at Stennis Space Center. Leading to an understanding and application of new tectonic theories. Later research confirmed dynamic links to space weather affecting a myriad of environmental factors: such as everyday weather; hurricanes; tornadoes; sever weather outbreaks; earthquakes; global climate-change; and certain types of wildfire outbreaks from passing coronal mass ejections induced by internal core generated Electro-Magnetic Pulses (EMP). Current and planned services include mapping of Stellar Transformer circuits; innovative modeling of deep earth magnetics, forecasting Earth's natural hazards listed above; database development and more. Combining big data and AI to find inter-relationships. Developing algorithm inputs for forecasting, data visualization and simulations. All leading to new forecasting technologies. We are actively assisting the EMP Task Force power grid protection efforts with direct input and evaluation of EMP threats. Our company comprehends the complex challenges of geophysical modeling and development of real-world forecasting applications. Electro-magnetic or magnetic induction is the production of an electromotive force, or voltage, across an electrical conductor in a changing magnetic field. The Stellar Transformer Concept contends that simple step-down energy induction occurs between Sun and Earth, much like the transformer process that steps down your household energy from higher voltage transmission lines sourced from the power company. The Sun represents a large coil from the power company, while the Earth represents the smaller coil to your home. The larger coil element generally excites current into the smaller coil element by induction of "step down energy", although lesser feedback mechanisms occur due to the action/reaction principles. Layers within the Earth hold and release charge acting as condensers, or capacitance layers. Thus, the Earth operates somewhat like a battery where energy is either stored or released through time-change of state-of-matter. We combine new Geophysical Intelligence with AI for a winning combination of innovations that will bring new mitigation strategies for space weather to the forefront. Bringing a paradigm shift to the business community for global environmental forecasting based on solar and planetary effects. This will save lives and mitigate property damage using new science and innovative technologies. Many of these ideas were first presented at EU2015 - Electric Universe (https://www.youtube.com/watch?v=IoqgZhbxhhU). Followed up at EU2016 with discussions on geometrical modeling applications, adhering to golden ratio principles (https://www.youtube.com/watch?v=Q355Haapq-0). Founded: 2023 in Colorado by Bruce Leybourne – Owner/Operator.

NCGT Journal
New Concepts in Global Tectonics

New Concepts in Global Tectonics Journal
Volume 13, Number 10 December 2025

ISSN number; ISSN 2202-0039

India Lightning Studies Reveal Relationship to Monsoons, Stellar Transformer Circuits, and Solar Activity: Plausible India Subcontinent Research Scenarios

Bruce A. Leybourne[1], Biju Longhinos[2], Girish T. Easwaraiyer[3], Jishma R. Jayan[4]

[1]*StellarTransformerTechnologies.com,* Aurora, CO, USA
[2]*College of Engineering* Trivandrum, India
[3] *University College* Trivandrum, India (Retired)
[4]*GeoTransect LLP,* Trivandrum, India

*Corresponding Author:
B. A. Leybourne, *Stellar Transformer Technologies, Aurora, Colorado, USA*
Email:*leybourneb@iascc.org*

Abstract: Rising lightning incidence with related climate change, has motivated extensive research of lightning phenomena on the India subcontinent. The focus was on understanding lightning patterns and identifying vulnerable regions that currently may be attributed to factors such as global warming and environmental changes. Our focus is to develop forecasting models to mitigate associated risks based on *Stellar Transformer* innovation concepts that are more directly related to *Stellar Transformer* circuit magnetic moment alignments, variations of solar activity and the ongoing solar minimum.

Keywords: lightning hotspots, climate change, Indian subcontinent, forecasting models, *Stellar Transformer*, solar activity, diurnal solar induction, Central Indian Ridge (CIR), Mid-Pacific, magnetotail moment alignment

Introduction

Lightning studies by Climate Resilient Observing Systems Promotion Council (CROPC) and the India Meteorological Department (IMD) reported a 57% rise in lightning incidents from April 2019 to March 2024. Research suggests that higher air temperatures create more water vapor, which, upon cooling at altitude, generates electric charges that spark lightning. CropC+1ndma.gov.in+1ndma.gov.inphys.org

Regional Vulnerabilities

Some regions in India are more susceptible to lightning hazards. Coastal Regions in Central West India have highest concentrations of "Cloud to Ground" lightning activity (Fig. 1, Taori, et.al, 2023). Additionally, significant heating during the pre-monsoon period with increased moisture enhances lightning occurrences in many areas (Fig. 2). "*Diurnal characteristics often show two peak times of occurrences with one peak in early morning hours while the other in afternoon-evening hours.*" (Taori, et.al, 2023). Lightning hotspots identified with satellite observations especially in Central India before active monsoons suggest lightning data could help forecast monsoon activity. PreventionWebNCERT

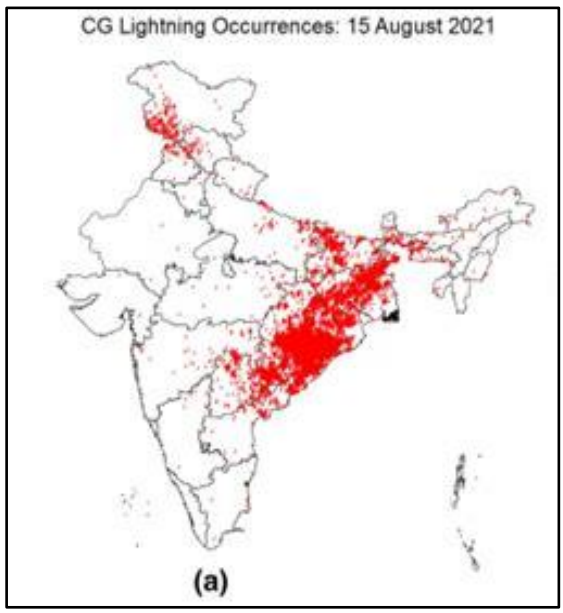

Fig. 1. India Subcontinent Cloud to Ground Lightning Distributions (From: Taori, et.al, 2023).

ISSN number; ISSN 2202-0039

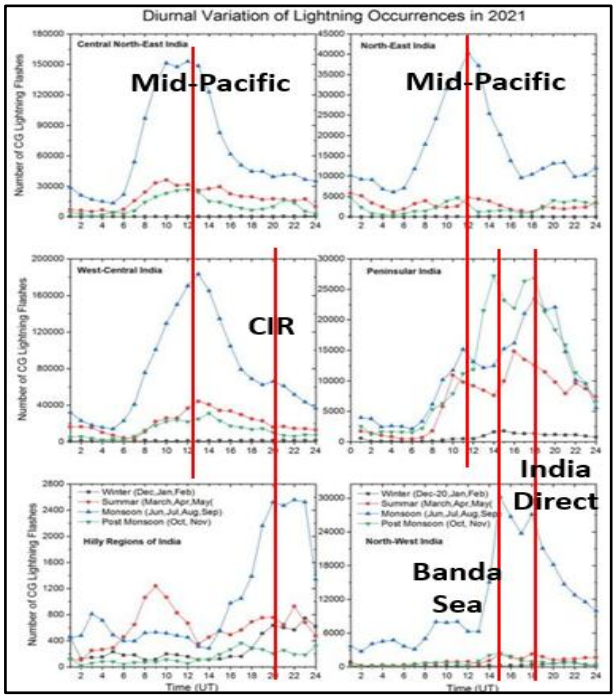

Fig. 2. Regional and Seasonal Diurnal Lightning Data on India Subcontinent "*Diurnal characteristics often show two peak times of occurrences with one peak in early morning hours while the other in afternoon-evening hours.*" (From: Taori, et.al, 2023). Vertical red lines reveal timing relationships with peak diurnal lightning to Earth's magnetotail, driven by solar wind magnetic moment alignment to tectonic elements of the Global Electric Circuit (GEC) proposed by the *Stellar Transformer* concept. Lunar and other planetary influences are likely but not confirmed by these data sets. (From: Taori, et.al, 2023)

Forecasting and Technological Advances

Recent research has employed artificial neural networks (ANNs) and other deep learning methods to define predictors of lightning occurrence and intensity, utilizing variables such as the K-index—a long-established geomagnetic activity measure related to solar disturbances (Märcz, 2018). Predictive relationships involving Aerosol Optical Depth (AOD) and Convective Available Potential Energy (CAPE) have also been widely demonstrated (Zhu et al., 2019; Qie et al., 2021). These parameters influence atmospheric convection and electrical field buildup leading to lightning initiation.

Hybrid models that combine deep learning frameworks with physics-based dynamic systems have recently been developed for lightning *nowcasting*, significantly improving the accuracy of short-term lightning forecasts (Liu et al., 2023; Jayawardena et al., 2024). Such integrative approaches link solar-geomagnetic variability and atmospheric thermodynamics, advancing our ability to predict lightning behavior over the Indian subcontinent.

Stellar Transformer Concepts

While predictive modeling advancements have improved lightning forecasting in India, *Stellar Transformer* concepts connect tectonics and space weather (Leybourne and Gregori, 2020; Leybourne and Orr, 2018; Leybourne et.al., 2017) brings a unique innovation in understanding the timing of peak lightning events. Evolving from Earth Endogenous Energy theory (Gregori, 2002) concerning *"An precedented challenge for humankind survival: Energy exploitation from the atmospheric electrical circuit"* (Gregori and Leybourne, 2021). This relationship is indicated in Fig. 2, by vertical red lines labeled with the associated tectonic elements that align with Earth's magnetotail. The *Stellar Transformer* concept determines equatorial induction in the tropics driven by sweeping electrical plasma currents within local space weather manifests as lightning. While solar magnetism magnitude variation drives axial induction within Earth's dipole field. The energy within the Global Electric Circuit (GEC) equalizes charge within the water layer. Thus, the interplay between lightning and earthquake energy charge equalization occurs mostly within the larger global water layer interface, i.e. supercritical water. This charge equalizing factor within the GEC is the innovation realized by the *Stellar Transformer* concept. This type of simple step-down leaky transformer energy induction occurs between the larger Solar magnetic coil and a smaller Earth magnetic coil. Much like the man-made transformer processes manage this charge within transformers that step down household energy from the power company.

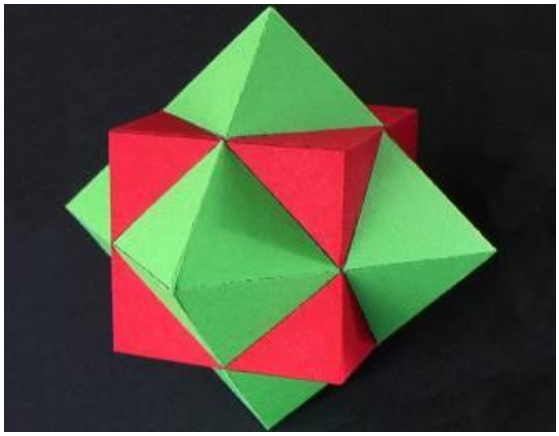

Fig. 3 Cubic/Octahedral Duality Platonic Solid configuration pattern reflects Earth's lightning distribution at tips of the octahedron along the equator and north-south *MOR* distribution patterns along the edges of the cube in the second order e.m. harmonic duality of the plasma double layer i.e. Birkeland Current. The vibrational component is strongly linked to the daily *TD* dynamo and Earth's other tidal cycles implying Golden Ratio applications. (Creative Commons 4.0 International license)

NCGT Journal
New Concepts in Global Tectonics
New Concepts in Global Tectonics Journal
Volume 13, Number 10 December 2025
ISSN number; ISSN 2202-0039

Stellar Transformer magnetotail magnetic moment aligns with Earth's cubic/octahedral duality e.m. vibrational harmonic in Fig. 3. Mid-Ocean Ridges (MOR) align with the cube corners while lightning hotspots occur at the equatorial tips of the octahedron (Fig. 4 and 5).

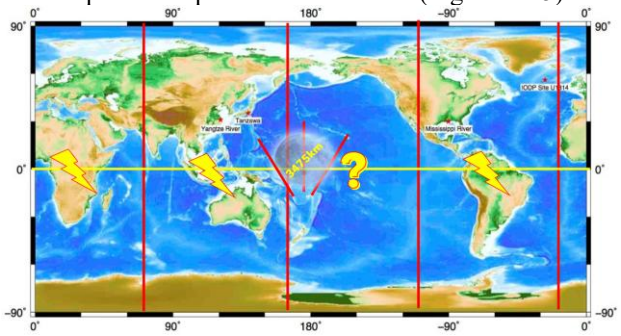

Fig. 4. Earth Cubic/Octahedral e.m Duality Harmonic modeled in Fig. 3, Platonic solids, reflected in 90° separation of the East Pacific Rise (EPR), the Mid-Atlantic Ridge (MAR) and the Central Indian Ridge (CIR). Interestingly the CIR and EPR are separated by 180° with no midocean ridge structure between and is hypothesized as to where the 3475 km diameter of the moon originated from a blown Mid-Pacific Circuit. Lightning bolts represent tropical lightning hotspots in Fig. 5, except where (**?**) mark is inserted in the Mid-Pacific. (Supplemental addition to Creative Commons 4.0 International license). (Leybourne et. al. 2025)

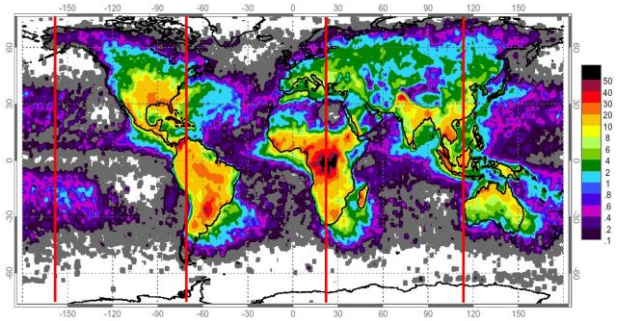

Fig. 5. Distribution of Global Lightning Hotspots (NASA) exhibiting an e.m. harmonic 90° octahedral configuration of the strongest lightning hotspots along the equatorial region in Catatumbo in Lake Maracaibo Venezuela, Congo, and Indonesian-North Australian. Also represented by adding tropical lightning bolts for hotspots noted in Fig. 4, except where (**?**) mark is inserted in the Mid-Pacific. Hypothesized as to where the 3475 km diameter of the moon originated from a blown Mid-Pacific Circuit. (Supplemental addition to *NASA* non-commercial use)

Lightning Peaks Stellar Transformer Analysis

The largest monsoon lightning peaks (Fig. 5) in North-East, Central North-East, and West Central India occur during magnetotail alignment with the Mid-Pacific blown circuit (Fig. 4 – From Leybourne et.al., 2025). Analogous to magnetic hoops bursting when Coronal Mass Ejections leave the Sun. The logic reasons that Hawaii and Fiji are left as dangling open circuits much more attuned to space weather and lunar influence, thus a strong influence on regional monsoons throughout Indian and Pacific Ocean in the tropics. Although the open circuit in Fiji (large vortex structure), seems to reconnect through the Central Pacific Megatrend rerouting to the north via the Western Pacific Rim.

North-West India has two lightning peaks during the monsoon season when magnetotail alignment passes over the Banda Sea Mantle Vortex (Leybourne and Adams, 2020, 1999), also a tropical lightning hotspot. And when the magnetotail aligns with the India subcontinent itself. While the Peninsular India has lightning peaks during the monsoon and post monsoon seasons with magnetotail alignments to all the aforementioned tectonic elements. The Hilly Region of the mining districts monsoon season peaks during magnetotail alignment with the Central Indian Ridge (CIR). While a minor lightning peak is noted in West Central India.

We leave the summer and winter lightning peaks for later interpretations with higher resolution data which may discern more correlations within the India subcontinent. Thus, vertical red lines in Fig 2 compared with Figs. 4 and 5, reveal timing relationships to *Stellar Transformer* tectonic elements of the GEC aligned with magnetotail magnetic moments. Magnetotail variations driven by the solar wind, are likely to be seen in higher resolution lightning studies (Albrecht et.al., 2016), and correlating relationships to solar activity should increase weather forecasting ability. Lunar and other planetary influences are also likely but not confirmed by these data sets.

We analyze the Lightning Detection Sensor Network data on cloud-to-ground (CG) lightning occurrences in Fig. 2, during September 2019–December 2021 over India. The data are grouped into six homogeneous zones as specified by the India Meteorological Department to investigate the seasonal variation of the CG lightning occurrences (Fig. 2). The CG lightning occurrences are found to be the most during August–September months over all the six zones while they are at minimum during December–January months with a small peak in occurrences during March–April. The diurnal characteristics of CG lightning flash occurrences are studied by clubbing data into winter, summer, monsoon and post-monsoon seasons. Diurnal characteristics often show two peak times of occurrence with one peak in early morning hours while the other in afternoon-evening hours. It is also noted that all the zones show increase in the lightning occurrences from the year 2019 to 2021. It is noted that CG lightning occurrences over the north-east central north-and peninsular India were nearly doubled.

ISSN number; ISSN 2202-0039

Thus, solar induction from magnetotail alignments associated with the Banda Sea, Central Indian Ridge (CIR) and the blown circuit in the Mid-Pacific (Fig. 4 – From Leybourne et.al., 2025) may drive peak energy in lightning hotspots related to the India subcontinent. Adding to the Stellar Transformer story (Leybourne and Gregori, 2020).

Sunspot–Lightning Inverse Relationship

Analysis of lightning data near Trivandrum, India, by Girish and Eapen (2008) using thunderstorm observations from the Indian Meteorological Department (IMD) and sunspot and geomagnetic indices (aa, Ak)—found statistically significant inverse correlations between sunspot activity and lightning frequency. More thunderstorms occur during sunspot minima and fewer during sunspot maxima, a pattern that remains consistent across both modern (1986–1999) and historical data sets. This inverse correlation near the dip equator implies that variations in solar magnetic output influence regional convective electrical activity.

Monsoon Relationships

Peak thunderstorm activity is observed in April, during the pre-monsoon season (March–May), consistent with the climatological buildup to the Indian monsoon. Lightning patterns during this period may act as early indicators of monsoon-related atmospheric processes modulated by solar and ionospheric interactions (Girish & Eapen, 2008). Pre-monsoon convection, enhances ionospheric conductivity and modifies potential gradients, influencing large-scale moisture transport and circulation (Singh et al., 2020).

Pre-Monsoon Lightning Activity and Monsoon Onset

The pre-monsoon season over India is characterized by intense convective activity and frequent thunderstorms, particularly along the Western Ghats and northeastern India. These result from strong surface heating, orography, and sea-breeze penetration (Rao & Basha, 2018). As the monsoon advances, convective precipitation transitions from isolated deep convection to widespread stratiform rain (Houze et al., 2015).

Relationship Between Pre-Monsoon Rainfall and Monsoon Onset

Studies over the Indochina Peninsula show that total pre-monsoon rainfall does not directly control monsoon onset timing, suggesting complex coupling between convection and large-scale dynamics (Huang et al., 2019).

Impact on Monsoon Rainfall Patterns

A strong positive correlation exists between lightning and rainfall during the pre-monsoon period in central India, which weakens once the monsoon sets in due to altered thermodynamics (Pawar et al., 2020).

Influence on Monsoon Dynamics

The Rodwell–Hoskins mechanism describes how monsoon-induced ascent can generate subsidence in adjacent regions, influencing circulation and rainfall distribution (Rodwell & Hoskins, 2001). Interactions between this mechanism and pre-monsoon convection may modulate large-scale monsoon variability.

Seasonal Characteristics of Storms

Pre-monsoon storms are typically more intense but shorter-lived, exhibiting higher echo tops and faster propagation speeds. In contrast, monsoon storms have broader coverage and longer lifespans, sustaining prolonged rainfall (Kumar et al., 2021).

In summary, pre-monsoon lightning and thunderstorm activity play a vital role in atmospheric thermodynamics preceding monsoon onset. While they significantly affect regional rainfall and local climate, their influence on the monsoon's onset and evolution is nonlinear and spatially variable underscoring the need for continued high-resolution lightning and geomagnetic observations across the Indian subcontinent.

Global Electric Circuit

Geomagnetic Effects of Thunderstorms

Geomagnetic data from the Indian Institute of Geomagnetism (IIG) shows increases in the diurnal range of magnetic declination (Rd) correlate with thunderstorm activity on geomagnetically quiet days. Suggesting that lightning-induced processes modulate E-region dynamo currents (which affect Earth's magnetic field near the equator).

Modulation of the Global Electric Circuit

Girsh and Eapen (2008) propose that thunderstorms help regulate the electric potential gradient (Vi) between the ionosphere and Earth, especially near the magnetic equator. During sunspot maxima (Fig. 6), increased solar ionization raises Vi. Thunderstorms reduce this excess to maintain balance. Thus, lightning acts as a "moderator" in

ISSN number; ISSN 2202-0039

the global electric circuit, particularly near the dip equator.

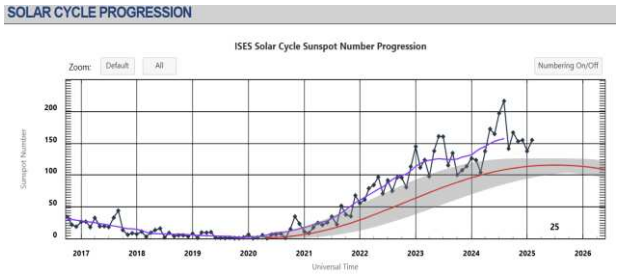

Fig. 6. Solar Cycle Sunspot Number Progression (ISES).

Magnetotail Coupling Dip-Equator Aligned Currents

For solar–terrestrial coupling diagnostics we reference the Geocentric Solar Magnetospheric (GSM) coordinate system, in which the X_GSM axis points toward the Sun and Z_GSM lies in the plane containing Earth's dipole axis and X_GSM (perpendicular to X_GSM and completing a right-handed system). Evaluating the Z_GSM component of the geomagnetic field at (or projected to) an earthquake epicenter (Fig. 7, Khachikyan et.al., 2012). is useful when considering currents aligned with the magnetotail and plasma sheet, which map to low-latitude ionospheric footprints near the dip equator (Hapgood, 1992; Kivelson & Russell, 1995).

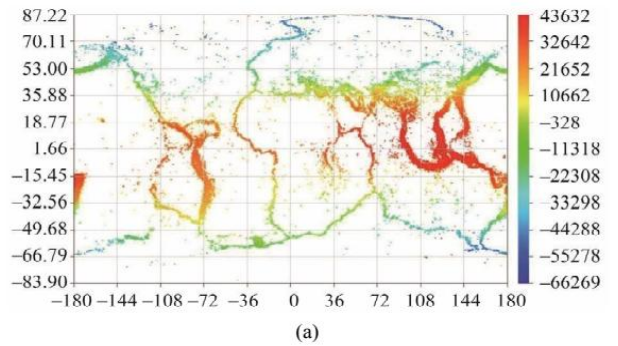

Fig. 7 Map of Dip Equator Value of geomagnetic ZGSM-component in the point of epicenter (Khachikyan et.al., 2012). Geocentric Solar Magnetospheric (GSM) system map of epicenters of earthquakes with magnitude M ≥ 4.5 occurred on the globe in 1973-2010 years (173477 events) from the global seismological catalogue NEIC, where the color corresponds to value of geomagnetic Z_{GSM}-component in the point of epicenter in the moment of earthquake occurrence, as calculated by Geopack- 2008.

Magnetotail energy input and lightning variability

Energy extracted from the solar wind and stored in the magnetotail plasma sheet is intermittently released during substorm activity, altering ionospheric conductivity and the global atmospheric electric circuit (GEC) (Rycroft, Israelsson, & Price, 2000; Harrison, 2014). These changes modulate the fair-weather current and can influence deep convection and lightning occurrence—particularly in the tropics where the ionosphere–troposphere coupling is strongest (Rycroft & Harrison, 2012; Singh, Bhattacharya, & Srivastava, 2020). Consistent with this view, Girish and Eapen (2008) reported a robust inverse relationship between sunspot activity and thunder/lightning near Trivandrum: lightning tends to be enhanced during solar minima and suppressed during solar maxima.

Seismo-electromagnetic Charge Balance Hypothesis

Crustal deformation and rock fracturing can generate charge carriers and electric fields via defect activation and related processes, potentially producing seismo-electromagnetic (SEM) effects that couple to the atmosphere and ionosphere (Freund, 2011; Hayakawa & Hobara, 2010; Pulinets & Ouzounov, 2011). Within this conceptual framework, we hypothesize a balancing tendency: when magnetotail-driven external charging of the GEC is relatively weak (e.g., during solar minima), enhanced atmospheric convection and lightning may act as an efficient discharge pathway. Conversely, when external solar/geomagnetic forcing is strong (e.g., solar maxima), part of the planetary electrical imbalance may be expressed through increased SEM activity associated with the lithosphere, including rare luminous phenomena sometimes reported near earthquakes (so-called earthquake lights; Thériault et al., 2014). This balancing view is a working hypothesis that aligns with observed sunspot–lightning anticorrelation (Girish & Eapen, 2008) and with broader GEC–space-weather couplings (Rycroft et al., 2000; Harrison, 2014), but it requires further targeted observations and co-located datasets (lightning, geomagnetic/ionospheric, and seismic) to test causality.

India's crustal fabric and coastal lightning

Reports of basaltic paleomagnetic remnant patterns and hypothesized "spike-like" structural lineaments along India's west and east coasts (Fig. 8) could, in principle, guide studies of localized conductivity pathways that focus lightning attachment or SEM emissions. However, without systematic paleomagnetic mapping and conductivity profiling, such site-specific claims remain preliminary. A rigorous evaluation would require integrating lightning location networks with magneto-telluric and aeromagnetic surveys and high-temporal-resolution space-weather indices (e.g., AE, Kp, and local Z_GSM projections). A plausible India Subcontinent integration research project is justified**.**

ISSN number; ISSN 2202-0039

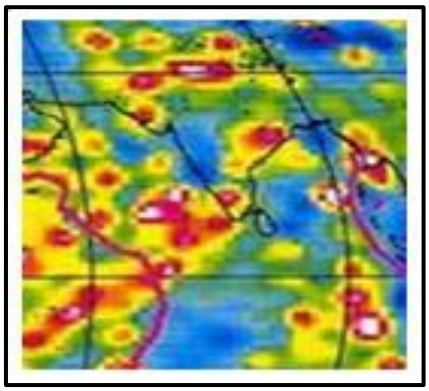

Fig. 8 Basalt Flow Remnant Signatures - Quinn associated with Giovanni's Sea Urchin Spikes. See areas with increased lightning near Trivandrum and the western coastal area in India and lightning hotspots along coastal areas of India's East coast (Quinn, 2012).

Conclusions

This study reveals a complex and dynamic interaction between solar activity, geomagnetic modulation, magnetotail dynamics, atmospheric convection, and lightning behavior over the Indian subcontinent. Evidence from lightning detection networks, geomagnetic indices, and published solar–terrestrial studies shows that India's lightning environment is strongly influenced not only by conventional meteorological drivers but also by deeper electromagnetic couplings extending from the Sun to the Earth's ionosphere, atmosphere, and lithosphere.

A consistent pattern emerges in which solar minima correspond to enhanced lightning activity, particularly near the dip equator, while solar maxima correlate with reduced lightning but increased seismo-electromagnetic signals. This inverse lightning–sunspot relationship, strongly expressed in Trivandrum-region data, supports the hypothesis that the global atmospheric electric circuit (GEC) responds dynamically to solar cycle–driven changes in ionospheric potential, conductivity, and magnetotail energy input.

The Stellar Transformer framework provides a unifying conceptual model linking magnetotail magnetic-moment alignments to peak lightning incidence over India. Timing correlations between magnetotail position, mid-ocean ridge structures, and tropical lightning hotspots suggest that large-scale electromagnetic geometry may modulate regional convective energy release. These relationships, combined with the doubled lightning incidence documented from 2019–2021, underscore the urgency of integrating space-weather diagnostics into India's lightning and monsoon forecasting systems.

Pre-monsoon lightning patterns show additional predictive value. Convective buildup in March–May precedes monsoon onset and corresponds to enhanced ionospheric conductivity and potential gradients. This phase of atmospheric electrical intensification may provide 2–4 weeks of lead time for monsoon forecasting when combined with deep learning and hybrid physics-ML approaches. ANN-based models using K-index, AOD, and CAPE—supplemented with magnetotail alignment—offer a promising pathway toward operational prediction.

The study also explores a speculative but physically grounded charge-balancing hypothesis in which internal lithospheric electrical processes (e.g., piezoelectric and SEM effects during tectonic stress) may complement magnetospheric charging under different solar conditions. Lightning from energy derived from the plasma sheet in the magnetotail balances charge from internal electric charge from earthquake piezoelectric effects of oscillating magnetic planetary dipole effects. Although unproven, this dual-source energy perspective provides testable predictions for future multi-sensor campaigns.

In aggregate, the findings demonstrate that lightning behavior in India cannot be explained solely by atmospheric thermodynamics. Instead, it arises from a multi-domain electromagnetic system driven by solar wind, magnetotail configuration, crustal conductivity architecture, and atmospheric convection. A proposed digital twin testbed—integrating real-time lightning, geomagnetic, solar wind, TEC, conductivity, and MHD simulations—offers a practical roadmap for converting these insights into operational lightning hazard and monsoon forecasting systems.

By integrating Stellar Transformer physics, deep learning, and India's growing observational infrastructure, this research provides a foundation for next-generation forecasting tools capable of reducing lightning-related fatalities and advancing our understanding of Earth–Sun electromagnetic coupling.

Taken together, contemporary space-weather theory and observations suggest:

- Solar cycle modulation of the magnetosphere–ionosphere system alters the GEC
- This modulation is consistent with enhanced lightning during solar minima in low-latitude India (Girish & Eapen, 2008)
- Seismo-electromagnetic processes provide a plausible (but still unproven) complementary pathway through which the Earth system redistributes charge during periods of stronger external forcing. Establishing the phase

ISSN number; ISSN 2202-0039

relationships among lightning, Z_GSM at epicentral longitudes, and regional seismicity remains an important target for future multi-sensor campaigns

This study uncovers a dynamic interplay between solar cycles, geomagnetic variation, lightning activity, and the ionosphere, particularly in equatorial regions like Trivandrum. In summary, lightning studies in India encompass a broad spectrum, from analyzing climatic influences and regional susceptibilities to developing sophisticated predictive models. The *Stellar Transformer* adds to these efforts, which are crucial for mitigating the adverse effects of lightning and safeguarding communities across the nation.

Acknowledgements

Pioneering work by Indian scientists has laid the foundation for current lightning research. Notably, S.V. Chandrashekhar Aiya (1956), a prominent figure in the mid-20th century, mathematically demonstrated the effects of thunderstorms and lightning on radio and television broadcasting signals. His contributions have been instrumental in understanding atmospheric noise and its impact on communication systems. Ref. en.wikipedia.org. We want to acknowledge all co-workers that, in different ways and at different times, contributed to the exploitation of the analyses mentioned in the present study. We like also to thank the many outstanding scientists for their warm encouragement.

Funding Information

No funding was sought or implemented in this original work by Geoplasma Research Institute for publishing in the NCGT Journal.

Author's Contributions

This study derived from a long-lasting cooperation by all authors. The backbone draft was prepared by the first author, although many ideas resulted from the emergence of long-lasting discussions between all authors.

Ethics

This article is original and contains unpublished material. Authors declare that there are no ethical issues and no conflict of interest that may arise after the publication of this manuscript.

Acronyms

ANNs - Artificial Neural Networks
AOD - Aerosol Optical Depth
CAPE - Convective Available Potential Energy
CIR – Central Indian Ridge
CME – Coronal Mass 'ejection
CROPC - Climate Resilient Observing Systems Promotion Council
EMP – Electro-Magnetic Pulse
GRACE Gravity Recovery and Climate Experiment
IMD India Meteorological Department
MOR - mid-ocean ridge
NCGT - New Concepts of Global Tectonics
NASA - National Aeronautics and Space Administration
NOAA - National Oceanic and Atmospheric Administration
SEIR – Southeast Indian Ridge
SOHO - Solar and Heliospheric Observatory
USGS. U.S. Geological Survey

References

Albrecht, R. I., Goodman, S. J., Buechler, D. E., Blakeslee, R. J., & Christian, H. J. (2016). *Where are the lightning hotspots on Earth?* Bulletin of the American Meteorological Society, 97(11), 2051–2068. https://doi.org/10.1175/BAMS-D-14-00193.1

Chandrashekhar Aiya, S. Noise Radiation from Tropical Thunderstorms in the Standard Broadcast Band. *Nature* 178, 1249 (1956). https://doi.org/10.1038/1781249a0

CROPC. (2024). *Annual Lightning Report 2023–24.* Data from IITM, NRSC, WWLLN, Vaishala.

Freund, F. T. (2011). Pre-earthquake signals: Underlying physical processes. *Journal of Asian Earth Sciences*, 41, 383–400. https://doi.org/10.1016/j.jseaes.2010.03.009

Girish, T. E., & Eapen, P. E. (2008). Geomagnetic and sunspot activity associations and ionospheric effects of lightning phenomena at Trivandrum near dip equator. *Journal of Atmospheric and Solar–Terrestrial Physics*, 70, 2222–2232. https://doi.org/10.1016/j.jastp.2008.07.003

Gregori, G. P. (2002). *Galaxy–Sun–Earth Relations: The origin of the magnetic field and of the endogenous energy of the Earth*. Beiträge zur Geschichte der Geophysik und Kosmischen Physik, 3(3), 471 pp.

Gregori, G. P., & Leybourne, B. A. (2021). An unprecedented challenge for humankind survival: Energy exploitation from the atmospheric electrical circuit. *American Journal of Engineering and Applied Science*, 14(2), 258–291. https://doi.org/10.3844/ajeassp.2021.258.291

Hapgood, M. A. (1992). Space physics coordinate transformations—A user guide. *Planetary and Space Science*, 40(5), 711–717.

Harrison, R. G. (2014). The global atmospheric electric circuit and climate. *Surveys in Geophysics*, 35, 221–259.

Hayakawa, M., & Hobara, Y. (2010). Current status of seismo-electromagnetics for short-term earthquake prediction. *Terrestrial, Atmospheric and Oceanic Sciences*, 21(3), 407–413.

Houze, R. A., Jr., et al. (2015). Monsoon convection and its implications for weather and climate prediction. *Bulletin of the American Meteorological Society*, 96(12), 2397–2412.

Huang, W., Zhang, C., & Chen, W. (2019). Pre-monsoon rainfall and its relationship with the monsoon onset over the Indochina Peninsula. *Frontiers in Earth Science*, 7, 259.

IMD Lightning Detection Sensor Network (2019–2021).

Jayawardena, T., Cooray, V., & Liyanage, D. (2024). *Physics-informed deep learning for lightning nowcasting using satellite and reanalysis data. Atmospheric Research*, 301, 107238. https://doi.org/10.1016/j.atmosres.2023.107238

Khachikyan, G., A. Inchin and A. Lozbin, 2012, "Spatial Distribution of Seismicity: Relationships with Geomagnetic Z-Component in Geocentric Solar Magnetospheric Coordinate System," *International Journal of Geosciences*, Vol. 3 No. 5, pp. 1084-1088. doi: 10.4236/ijg.2012.35109.

Kivelson, M. G., & Russell, C. T. (1995). *Introduction to Space Physics*. Cambridge University Press.

Kumar, A., Jain, S., & Das, S. K. (2021). Seasonal characteristics of thunderstorms over India. *Scientific Reports*, 11, 7845.

Leybourne, B. A., & Adams, M. B. (2020). Mantle dynamics in the Banda Sea Triple Junction and link to ENSO. *Journal of Systemics, Cybernetics and Informatics*, 18(4), 97–106.

Leybourne, B.A., D.W. Johnson, G.P. Gregori, 2025. Arc Blast as Static Electricity or Interplanetary Lightning Short Circuits in Stellar Transformers: A Plausible North American Scenario, *New Concepts in Global Tectonics Journal*, 13, (2): 229-251

Leybourne, B. A., & Gregori, G. P. (2020). Introduction to Plasma Tectonics & Electric Geology. *Journal of Systemics, Cybernetics and Informatics*, 18(2), 7–13.

Leybourne, B. A., & Orr, D. (2018). Stellar Transformer Concepts. *Journal of Systemics, Cybernetics and Informatics*, 16(4), 26–37.

Leybourne, B. A., Davis, J. M., Gregori, G. P., Quinn, J. M., & Smoot, N. C. (2017). Evolution of Earth as a Stellar Transformer. *New Concepts in Global Tectonics Journal*, 5(1), 144–155.

Liu, X., Zhang, Y., & Chen, D. (2023). *Hybrid deep learning–physical model for lightning prediction based on environmental variables. arXiv preprint* arXiv:2302.05491. https://arxiv.org/abs/2302.05491

Märcz, F. (2018). *Geomagnetic activity indices and their relevance to space weather and atmospheric electricity. Annales Geophysicae*, 36, 345–355. https://doi.org/10.5194/angeo-36-345-2018

Pawar, S. D., et al. (2020). Lightning activity and rainfall. *Quarterly Journal of the Royal Meteorological Society*, 146, 2076–2091.

Phys.org. (2024). "'Alarming' rise in deadly lightning strikes in India," Aug. 27, 2024.

Potdar, S. and D. Siingh, 2024, The Atmospheric Global Electric Circuit: A Review, J. Ind. Geophys. Union, 28(4), 247-267

Pulinets, S., & Ouzounov, D. (2011). LAIC model for earthquake precursors. *Journal of Asian Earth Sciences*, 41, 371–382.

Qie, X., Yuan, T., & Wu, X. (2021). *Relationships between aerosol optical depth, convective available potential energy, and lightning activity in tropical regions. Journal of Geophysical Research: Atmospheres*, 126(9),e2020JD034972. https://doi.org/10.1029/2020JD034972

Quinn, J.M., 2012. Mapping the global lithosphere: of mega-diameter meteorite impact sites within the global lithosphere, 154 pp. Solar-Terrestrial Environmental Research Institute (STERI), Lakewood, CO.

Rao, T. N., & Basha, G. (2018). Thunderstorm characteristics from VHF radar. *Journal of the Atmospheric Sciences*, 75(6), 1823–1838.

Rodwell, M. J., & Hoskins, B. J. (2001). Subtropical anticyclones and monsoons. *Journal of Climate*, 14, 3192–3211.

Rycroft, M. J., Israelsson, S., & Price, C. (2000). GEC and solar–terrestrial relations. *Journal of Atmospheric and Solar–Terrestrial Physics*, 62, 1563–1576.

Rycroft, M. J., & Harrison, R. G. (2012). Electromagnetic atmosphere–Earth coupling. *Atmospheric Research*, 135–136, 1–7.

Sandwell, D. T. et al. (2014). Global seafloor topography from satellite altimetry and ship-depth soundings. *Science*, 346(6205), 65–67.

Singh, R., Bhattacharya, A., & Srivastava, S. K. (2020). Solar–terrestrial influences on lightning and monsoon variability. *JGR Space Physics*, 125, e2019JA027778.

Thériault, R., et al. (2014). Earthquake lights in rift environments. *Seismological Research Letters*, 85(1), 159–173.

Taori, A., Suryavanshi, A., & Bothale, R. V. (2023). Cloud-to-ground lightning over India. *Natural Hazards*, 116, 4037–4049.

Zhu, Y., Li, Z., & Li, C. (2019). *Machine-learning-based lightning prediction using satellite aerosol and thermodynamic parameters. Remote Sensing of Environment*, 233, 111389. https://doi.org/10.1016/j.rse.2019.111389

NCGT Journal
New Concepts in Global Tectonics

New Concepts in Global Tectonics Journal
Volume 13, Number 10, December 2025

ISSN number; ISSN 2202-0039

Ionizations in the atmosphere, vapor clouds and earthquakes

Valentino Straser[1]

[1]*Faculty of Agriculture University of Makeni, Makeni, Sierra Leone*

Corresponding Author:
Valentino Straser;
Email:
valentino.straser@gmail.com

Abstract: Anomalous atmospheric phenomena, "vapor clouds" or "seismic clouds," represent a controversial theory that hypothesizes that ionization phenomena in tectonically active zones can give rise to unusual clouds that appear before an earthquake near the future epicenter. This study, conducted in the Northwestern Apennines, along the Taro System seismic line, presents several cases of "coincidences" between the appearance of specific "feather"-shaped clouds and subsequent seismic events, whether single earthquakes or brief seismic swarms, or those lasting several months, with a magnitude less than 4.5.

Keywords: earthquakes, seismic swarms, anomalous atmospheric phenomena, earthquake clouds, Taro System, tectonic stress

Introduction

Earthquake forecasting represents one of the greatest challenges of modern science, with enormous implications for human safety, urban planning, and the resilience of societies. International research has gradually advanced over the past thirty years thanks to the establishment of working groups and technological development. The overall objectives are multiple and encompass multiple fields, starting with the scientific field, which has been engaged for years primarily in crustal diagnosis based on a profound understanding of the mechanisms that govern the behavior of the Earth's crust. This includes the study of faults, ground deformations, microseisms, and the geophysical and geochemical signals that can precede an earthquake [Brady, B.T. and Rowell, 1986; Freund, 2003]. From a social perspective, however, the topic of seismic forecasting stimulates ethical and political reflection: how can scientific uncertainty be communicated without creating alarmism, but at the same time without underestimating the risks? Given the complexity and the attribution of responsibility, the debate remains open. Experiments currently underway in Italy, involving the interception of electromagnetic signals, detectable according to a precise azimuth several days before the seismic event, are being conducted by the Radio Emission Project in Rome with the Radio Direction Finding project [Straser et al, 2019; Straser et al., 2020(b)]. These experiments also include the observation of anomalous light phenomena in the atmosphere and presumed vapors released from the ground before the seismic event in seismically active areas, such as the study area [Fig. 1] in the province of Parma (Italy) [Straser 2020(a); Straser 2022], pioneered in the 1980s and 1990s, and the Po Valley area by 45°GRU [Straser, 2010].

Fig. 1. Index map

The hypothesized air ionization phenomena sometimes give rise to unusual cloud formations [Shi et al., 2019]. These effects have already been hypothesized by other authors in other parts of the world over the past 25 years [Guo, 2022; Shou, 1999]. "Vapor clouds" or "seismic

ISSN number; ISSN 2202-0039

clouds," currently not fully accepted by the international scientific community, are included in a theory that suggests that unusual cloud formations that appear before or after an earthquake are a precursor to seismic activity within certain intervals, which can precede an earthquake from a month to a few days before the event [Thomas et al., 2015; Guo et al., 2008]. The formations of these particular ionizations would be concentrated in the epicentral area of the future earthquake, approximately ten kilometers in radius.

The proposed mechanisms consist of an increase in gas emissions, typically radon, from tectonically active faults, which ionizes the air [Cataldi et al., 2020]. This interaction results in an electric field that attracts water molecules, causing condensation and the formation of unusual clouds, such as "feather clouds," in the area under investigation. The agglomeration and condensation of ions in the atmosphere, near the future seismic epicenter, attract water molecules, forming larger clusters that act as condensation centers, leading to the formation of unique clouds, different from those usually described by atmospheric physics. These processes are hypothesized to occur in crustal stress zones determined by active faults. These faults, during deformation during the pre-seismic phase, produce gas emissions into the atmosphere. These gases are agglomerated by an unusual electric field produced around tectonic structures, contributing to the upward migration of ions and, consequently, the formation of "earthquake clouds." Although some studies suggest a correlation between these cloud anomalies and earthquakes, the scientific community does not consider this method reliable for earthquake prediction. Instead, they could be associated with other precursor signals. The concordance of different signals, such as electromagnetic signals detected by satellites or ground deformations, and of course those currently being tested, could provide a more reliable framework for seismic forecasting [Pulinets et al., 2014]. Each advance in understanding these phenomena not only brings us closer to the possibility of predicting an earthquake, but also contributes to improving the geological and seismological models that describe the dynamics of planet Earth.

Tectonic context

In the geodynamic context, the Taro Valley connects, also geographically, the Lunigiana extensional zone to the compressional zone of the Apennine front, which continues beneath the Po Valley. The fault displacements in the two zones connected by the "Taro System" are very different: in the Apennine foothills, they are metric in magnitude, while in the Lunigiana system, if combined, they are kilometric in magnitude [Molli et al., 2018]. Earthquake foci are also deeper in the Lunigiana-Garfagnana area, as well as in the Apennines. Many faults are considered seismic sources due to the reciprocal slippage of their two sides. Bernini and Papani [1987], based on seismological data, indicate a seismogenic source in Lunigiana, dipping slightly to the northeast, located at a depth of about 10 kilometers, interpreted as a consequence of the main detachment between the basement and the overlying cover.

Other authors have surveyed and classified the "blind seismogenic faults" in the Po Valley, detected thanks to the numerous geophysical surveys made possible by oil exploration since the Second World War. The faulting process, caused by the shortening of the Northern Apennines, is closely related to the construction of the Apennine chain, still active at a rate of 1-3 meters per millennium. The Po Valley faults, however, do not cut the surface but stop at depth. Conversely, surface geological features found in the Northern Apennines indicate a deformation process still underway, with ground displacements dating back to the Late Pleistocene-Holocene (starting from the Last Glacial Maximum, approximately 18,000-23,000 years ago). Further analyses have allowed us to inventory active faults and associated earthquakes, particularly those with a magnitude of 5.5 or greater. The presence of active tectonics primarily concerns the boundary structures of the entire intra-Apennine basin system of Lunigiana and Garfagnana, and some fault segments extend as far as ten kilometers, as in the case of the Cisa Pass. Analysis of the active faults of the Cisa Pass, Arzengio-Gigliana-Corlaga, Buto, and Codolo-Tresana also allows us to trace a "transversal" system of the Taro River to the northeast. The sectors of the "Taro System": The "Taro System" can be divided into the following sectors: Bedonia-Borgotaro, Berceto-Solignano (upper valley), Fornovo-Medesano (middle valley), and the foothills. The three sectors were distinguished based on the distribution of subsurface and surface tectonic structures. THE UPPER VALLEY. The Bedonia area, known in the literature as a seismic zone characterized by shallow epicenters, marks the boundary between zones of more superficial seismic activity. Direct or "normal" faults, extensional faults in which the two blocks of rock move apart, are recognized between Bedonia and Borgotaro. These faults involve Monte Zuccone and the Gotra Valley. The faults mapped between Bedonia and Borgotaro may be the northwestern terminal portion of extensional systems in the Lunigiana; in other cases, such as the important north-south normal fault of Montegroppo, they can be interpreted as transtensions that developed along the "Taro System" [Vescovi, 1998]. The recurrent seismicity in this sector is an expression of the geological and geodynamic context of the Upper Taro Valley and, more generally, of the Tuscan-Emilian Apennines. The earthquakes originating in the Borgotaro area have hypocenters that are concentrated in the interval between 11 and 15 kilometers of depth, and

ISSN number; ISSN 2202-0039

to a lesser extent between 5 and 10 kilometers. The seismic events, likely associated with the fracture lines of the "transversal" Taro system, are concentrated in the Borgotaro area, where a fault system crosses the valley floor. The stretch of the Upper Taro Valley between Bedonia and Borgotaro corresponds to an uplift of the crystalline basement that generates a southwest/northeast transverse fault system that accompanies the main orographic divide between Monte Molinatico and Monte Gottero and is closely related to the seismically active zone of the Taro River seismic line. The fracture system is masked on the surface by poorly lithified fluvio-lacustrine deposits that amplify seismic waves and the ground shaking produced by the earthquake. The combination of active tectonics, coupled with the amplification effects caused by fluvio-lacustrine deposits, may explain both the frequency of earthquakes and the ground shaking effects in this area. In the Middle Taro Valley, tectonic lineaments coexist and can be grouped into three preferred trends: northwest/southeast-trending normal faults; southwest/northeast transverse faults; and north-south-trending extensional fractures. Some studies show that the faults along the "Taro System" belt are congruent, in direction and kinematics, with a left-handed strike-slip system that developed along a southwest/northeast direction. This does not mean that the "Taro System" can be synthetically traced back to a single strike-slip fault (which, however, is not recognized at the surface), but that at depth, tectonic stress acts on the crust with a left-handed transpressive kinematics in a southwest/northeast direction, capable of generating innumerable faults along the Taro belt, distributed along the zones of greatest weakness.

Methods

The method used in this study compares the appearance of particular clouds in the sky, especially plume-shaped clouds or the rise of presumed vapors released from the ground along the fault or the tectonic overlap of the Taro System, with data published in real time by the National Institute of Geophysics and Volcanology in Rome, Italy.

Instruments use

The tools used are the website of the National Institute of Geophysics and Volcanology in Rome, Italy, and the 200MP Xiaomi Redmi Note camera.

Data

Discussion and Conclusions

There is insufficient field data to establish a correlation between anomalous atmospheric phenomena and a correlation index. At present, therefore, we can only hypothesize a potential link between the two phenomena, attributing an "element of coincidence." More generally, although some research has demonstrated a statistical correlation between specific cloud anomalies and earthquakes, this does not prove that clouds are a direct cause or a reliable warning signal of earthquakes.

However, for about forty years, an experiment has been underway in the same area, namely along the Taro System Seismic Line, investigating the potential link between the production of plasmas in the atmosphere, likely induced by electrical and electromagnetic phenomena, and earthquakes [Straser, 2007]. Therefore, it cannot be ruled out that the production of ionizations caused by tectonic stress could give rise to particular cloud formations, which have nothing to do with those of classical meteorology. The clouds in question, those examined for this study, are plume-shaped, known in the literature as "cirrus fibratus." The mechanism that could explain the cloud's morphology is not yet clear, but the limited data collected over the last two years suggests a potential link, at least for the tectonic context of the "Taro System," with time lags of about ten days [Figs. 2,3,4] between the appearance of the cloud and the subsequent epicenter of the earthquake [Tables 1, 2].

Fig. 2. Cloud sighted on July 14, 2024, near Mount Prinzera, in the province of Parma, remaining visible in the sky and in the same position for about an hour. The sighting was made during a Science Camp organized by the "G. Marconi" High School in Parma, with the support of the Civil Protection Agency.

NCGT Journal
New Concepts in Global Tectonics

New Concepts in Global Tectonics Journal
Volume 13, Number 10, December 2025

ISSN number; ISSN 2202-0039

Fig. 3. Cloud sighted on November 1, 2024, aligned with the course of the Taro River, in the middle valley between Solignano and Borgotaro, in the province of Parma.

Fig. 4. Cloud sighted on July 7, 2025, in the Taro River Valley area, remaining in the same position for about ten minutes.

Table 1. Comparison between the appearance of the feather-shaped cloud and the subsequent earthquake, in relation to the distance from the epicenter or epicentral zone of the seismic swarms.

N	Cloud (Day)	Earthquake (Day)	Interval time (Day)	Apparent distance (Km)	Cloud typology
1	14 July 2024	21 July 2024	7 days	1 Km	feather
2	1 November 2024	8 November 2024	7 days	16 Km	feather
3	7 July 2025	18 July 2025	11 days	16 Km	feather
4 / 5	6 October 2025	25 October 2025	19 days	1 Km	Steam

Table 2. List of earthquakes considered in this study, taken from the website www.ingv.it

N	Day, [hh]:[mm]:[ss]	Latitude	Longitude	Deep	Magnitude (Ml)	Event type
1	21.07.2024 23:06:20	44.6402	10.0508	19 Km	2.5	Single
2	08.11.2024 01:29:01	44.5172	9.7892	9 Km	2.4	Single
3	18.07.2025 18:45:39 (UTC)	44.5073	10.2263	23 Km	2	Single
	25.10.2025 15:38:34	44.62	10.02	21 Km	2.5	Single
	26:10.2025 17:25:37	44.47	9.75	72	2.5	Single
4	29.10.2025 23:19:27	44.65	10.19	21	2.2	Short seismic swarm
	29.10.2025 23:34:06	44.65	10.17	20	2.3	
	30.10.2025 00:25:43	44.65	10.16	21	2.3	
	30.10.2025 00:28:50	44.65	10.18	21	2.3	
5	02.11.2025 00:00:48	44.50	10.08	23	2.5	Short seismic swarm
	02.11.2025 00:01:15	44.46	10.08	9	3.2	
	02.11.2025 00:06:39	44.48	10.09	10	2.5	

Earthquakes studied over the last four decades, potentially related to air ionization phenomena, generally have magnitudes less than ML3, consistent with the seismic recurrence of the Apennine area of the province of Parma. As has been observed for anomalous atmospheric light phenomena (UAP), it can also be said for particular cloud formations that not all earthquakes are preceded by anomalous light phenomena or characteristic clouds. Instead, the reverse is true: ionization phenomena precede the seismic event, or seismic swarm, in a tectonically active area [Doda, L., Pulinets, 2006; Piscini et al., 2017; Heidari et al., 2024]. One example concerns the photograph of at least sixteen "ball lightning," perfectly aligned along the tectonic fracture of the Taro River in the mid-valley area [Fig. 5]. These anticipated the start of the seismic swarm by approximately 40 days, beginning in early February 2024, with over 120 earthquakes with magnitudes greater than ML2 in just two days along the fracture zone of the Taro System.

ISSN number; ISSN 2202-0039

Fig. 5. Photo taken on December 23, 2023, from Cassio, looking towards Varano Melegari. There are at least sixteen white globes suspended in the sky, aligned along the fracture of the Taro System, in the middle valley of the river, near Monte Sant'Antonio.

This finding is further supported by the interception of electromagnetic precursors detected using the experimental method of the Radio Direction Finding network in Rome. Among the daytime observations made in the central zone of the Taro System, a presumed vaporization phenomenon with a vertical development was observed in the central zone of the Taro System fault. This phenomenon anticipated three clusters of earthquakes that occurred along the Taro's active tectonic line [Fig. 6].

Fig. 6. Alleged release of steam caused by tectonic stress along the Taro seismic line, near Collecchio, in the province of Parma.

At the current stage of research, this study cannot be considered a true conclusion, as it is only partial. Rather, it is hoped that it will point to a new direction for research, allowing for a better understanding of tectonic phenomena and a more reliable crustal diagnosis. This data can be modeled and compared with other research fields to establish a broader, interdisciplinary framework for Earth Sciences mechanisms.

Acknowledgement

I would like to express my sincere thanks to Jerry Ercolini for his constant support in providing information on anomalous light phenomena in the atmosphere and to Gabriele and Daniele Cataldi for having made available the data collected with the Radio Direction Finding system, relating to electromagnetic emissions intercepted in the study area, and to Prof. Giovanni Gregori for his constant encouragement to continue my research.

Funding Information

This study was conducted without funding, independently.

Ethics

This article is original and contains unpublished material. Authors declare that there are not ethical issues and no conflict of interest that may arise after the publication of this manuscript.

References

Bernini M., Papani G. (1987) - Alcune considerazioni sulla struttura del margine appenninico emiliano fra il T. Stirone ed il T. Enza. Ateneo Parmense, Acta Nat., 23, 4, 219-240. Atti del Meeting «Brittle deformation analysis in Neotectonics» Firenze, 17 Aprile 1986.

Brady, B.T. and Rowell, G.A., 1986. Laboratory investigation of the electrodynamics of the rock fracture. Nature, 321, 29 May 1986, 488-492.

Cataldi D., Giuliani G. G., Straser V., Cataldi G., 2020. Radio signals and changes of flow of radon gas (Rn222) which led the seismic sequence and the earthquake of magnitude mw 4.4 rock fracture. that has been recorded in central Italy (Balsorano, L'Aquila) on November 7, 2019 –- New Concepts in GeoplasmaTectonics Journal, 8(1), 32-42.

Doda, L., Pulinets, 2006. Earthquake clouds and physical mechanism of their formation. American Geophysical Union, Fall Meeting 2006, abstract id. T31A-0426.

Freund, F., 2003. Rocks that Crackle and Glow-Strange Pre-Earthquake Phenomena. Journal of Scientific Exploration, 17, 37-71.

Guo, G., 2022. On the relation between anomalous clouds and earthquakes in Italian land. Frontiers in Earth Science, 10, 1–7. https://doi.org/10.3389/feart.2022.812540.

Guo, G., and Wang, B., 2008. Cloud Anomaly before Iran Earthquake. Int. J. Remote Sensing 29, 1921–1928. doi:10.1080/01431160701373762.

Heidari, M., Mazidi, A., & Rousta, I., 2024. Investigating the Earthquake Cloud Precursor in the 2017 Azgeleh Earthquake in Kermanshah, Iran. Journal of Geography and Environmental Hazards, 13(1), 151-172. DOI: 10.22067/geoeh.2022.75548.1186

Molli, G., Carlini, M., Vescovi, P., Artoni, A., Balsamo, F., Camurri, F. et al., 2018. Neogene 3-D Structural Architecture of The North-West Apennines: The Role of the Low-Angle Normal Faults and Basement Thrusts. Tectonics, 37 (7), 2165–2196. doi: https://doi.org/10.1029/2018tc005057

Piscini, A., De Santis, A., Marchetti, D., and Cianchini, G., 2017. A Multi-Parametric Climatological Approach to Study the 2016 Amatrice-Norcia (Central Italy) Earthquake Preparatory Phase. Pure Appl. Geophys. 174 (10), 3673–3688. doi:10.1007/s00024-017-1597-8.

Pulinets, S. A., Morozova, L. I., and Yudin, I. A., 2014. Synchronization of Atmospheric Indicators at the Last Stage of Earthquake Preparation Cycle. Res. Geophys. 4 (1), 45–50.doi:10.4081/rg.2014.4898.

Shi G., Yang F., Zhang L., Zhao T., Hu J., 2019. Impact of Atmospheric Circulation and Meteorological Parameters on Wintertime Atmospheric Extinction in Chengdu and Chongqing of Southwest China during 2001-2016. Aerosol and Air Quality Research, 19: 1538–1554, ISSN: 1680-8584 print / 2071-1409 online doi: 10.4209/aaqr.2018.09.0336.

Shou, Z. H., 1999. Earthquake Clouds, a Reliable Precursor. Sci. Utopya 64, 53–57.

Straser V., Cataldi D., Cataldi G., 2019. Electromagnetic monitoring of the New Madrid Fault us area with the RDF system – Radio Direction Finding of the radio emissions Project. New Concepts in Global Tectonics Journal, 7(1), 43-62.

Straser, V., 2007. Precursory luminous phenomena used for earthquake prediction the taro valley, Northwestern Apennines, Italy. New Concepts in Global Tectonics Newsletter, 44(3), 18-32.

Straser, V., 2010. Variations in gravitational field, tidal force, electromagnetic waves and earthquakes. New Concepts in Global Tectonics Newsletter 57(4), 98-108.

Straser, V., 2020(a). Atmospheric Plasmas that Precede Earthquakes in Seismically Active Areas. Plasma Tectonics and Electric Geology, 62–67.

Straser, V., 2022. Atmospheric plasmas research linked to electromagnetic signals and earthquakes. In: Technology audit and production reserves 6 (1/68), S. 6 - 9. http://journals.uran.ua/tarp/article/download/270465/266575/624972. doi:10.15587/2706-5448.2022.270465.

Straser, V., Cataldi, G., Cataldi, D., 2020(b). Radio direction finding for short-term crustal diagnosis and pre-seismic signals. The case of the Colonna Earthquake, Rome (Italy). European Journal of Advances in Engineering and Technology, 7 (7), 46–59.

Thomas, J. N., Masci, F., and Love, J. J., 2015. On a Report that the 2012 M 6.0 Earthquake in Italy Was Predicted after Seeing an Unusual Cloud Formation. Nat. Hazards Earth Syst. Sci. 15, 1061–1068. doi:10.5194/nhess-15-1061-2015,

Turner, D.J., 1998. Ball lightning and other meteorological phenomena. Physics Reports, 293 (1), 1-60.

Vescovi, P., 1988. La linea trasversale Passo della Cisa – Val Parma – Bassa Val d'Enza: 1. Sistema trascorrente sinistro nella zona del Passo della Cisa (prov. di Parma). L'Ateneo Parmense, Acta Naturalia, 24, 221-243.

NCGT Journal
New Concepts in Global Tectonics

New Concepts in Global Tectonics Journal
Volume 13, Number 10, December 2025

ISSN number; ISSN 2202-0039

Lunar Periodicities and Earthquakes in Italy

***Stefano Calandra*[1], *Daniele Teti*[2]**

[1]*CEO EqForecast, Venezia, Italy;*
[2] *Senior IT, EqForecast, L'Aquila, Italy.*

Corresponding Author: Stefano Calandra, EqForecast, Venezia, Italy; Email: s.calandra@earthquakesforecast.com

Abstract: The role of external gravitational forces in modulating crustal stress has long been debated in seismology, yet no quantitative study has assessed the possible physical–statistical correlation between lunar cycles and earthquake recurrence in Italy. Here, this relationship is examined using a statistical–quantitative approach interpreted within a tidal-stress framework, applied to 7,948 earthquakes (M≥3) recorded between 1600 and 2024. Results show a systematic concentration of events between the New Moon and First Quarter and at intermediate lunar declinations (±10°–20°), with statistical significance across all magnitude classes. A particularly strong anomaly (exceeding 2σ) is observed for M≥5 earthquakes in the +10° to +20° declination band. In this magnitude range, seismic frequency peaks at the New Moon and decreases progressively in the subsequent phases. Intermediate-magnitude events (M4–4.9) also cluster during the early synodic phases, suggesting that energy release increases with the rate of change of the gravitational potential (|dτ/dt|). A modest asymmetry between New Moon and Full Moon for larger earthquakes likely reflects an interaction between synodic phase and lunar declination. Analysis of the 9.3 and 18.6-year nodal cycles reveals a structured cyclicity in Italian seismicity, indicating a long-term regulatory role of nodal precession. A significant tidal signal is also detected in the hydrothermal microseismicity of Campi Flegrei (68% and 79% of events falling within the most frequent declination and synodic bands), suggesting a tidal modulation distinct from that of tectonic seismicity. Overall, lunar and nodal periodicities modulate seismicity in a statistically predictable way, providing a physically grounded basis for probabilistic forecasting models that can be integrated with local fault-energy estimates from existing methodologies.

Keywords: *Earthquake forecasting; lunar and solar tides; gravitational forces; tidal stress variations; statistical correlation; seismic triggering; nodal precession; probabilistic models.*

1. Introduction

The relationship between astronomical phenomena and seismic activity has become an increasingly relevant topic in geophysics, particularly with regard to the 18.6-year cycle of lunar nodal precession. This cycle, which repeats regularly over time, may influence the spatial and temporal distribution of earthquakes on Earth. Although the direct role of the lunar nodes in triggering seismic events is not yet fully understood, recent studies have identified a statistical correlation, supported by a coherent physical interpretation, linking lunar cyclicity to the recurrence of earthquakes in specific geographic regions. The eight lunar phases and the Moon's declination relative to Earth's equator also appear to show systematic relationships with seismic activity and may serve as useful statistical indicators for estimating earthquake magnitude. Lunar phase is determined by the relative positions of the Earth, Moon, and Sun and describes the visible changes in the Moon's appearance. The eight principal phases comprise the New Moon, First Quarter, Full Moon, and Last Quarter, along with the intermediate waxing and waning stages. Because no comprehensive studies of this kind have previously been carried out specifically for Italy, the present work represents the first quantitative investigation of both the statistical correlation and the physical interpretation

ISSN number; ISSN 2202-0039

linking lunar behavior to Italian seismicity from 1600 to the present. Although this study does not claim the existence of a deterministic relationship, the findings indicate that lunar periodicities modulate the statistical likelihood of earthquake occurrence.

1.1 The Role of the Moon, the Sun, and the Solar System in Earthquake Triggering

A substantial body of research supports the existence of a correlation between lunar phases and earthquake occurrence, although the periodicity detected varies with magnitude, geographic region, and fault type. Most studies indicate that earthquake frequency contains a periodic component linked to the lunar cycle, with maxima occurring when the Moon reaches specific configurations relative to the Earth and the Sun, depending on the region examined. This periodic behavior is most commonly associated with the four principal lunar phases—New Moon, First Quarter, Full Moon, and Last Quarter—and suggests a potential influence of Earth tides on seismicity, particularly during phases in which tidal forces may modify stress conditions along faults [1]. Lunar and solar tidal forces act as an additional stress on faults already close to failure [2], potentially accelerating the fracturing process and advancing the seismic event [3]. A further line of research highlights that earthquake triggering may also result from periodic variations in vertical tidal forces, which can modulate the release of seismic energy accumulated over time [4]. In particular, the vertical component of these tides appears to be influenced by gravitational variations generated by the seven major planets of the Solar System, which act on the fault over a 24–48hour time window and define an instability parameter that may contribute to the triggering of seismic rupture at that location. This topic has already been examined by the Author in a previous study [5].

1.2 Lunar Nodal Precession and Lunar Declination

While the cycle of lunar phases is familiar to most people, the 18.6-year cycle of the lunar nodes is a less widely known astronomical phenomenon that warrants closer examination. It is associated with the geometry and long-term motion of the Moon's orbit around the Earth. The lunar nodes are the two points where the Moon's orbital plane intersects the ecliptic, the imaginary plane defined by Earth's orbit around the Sun. The 18.6-year cycle reflects the periodic variation in the Moon's declination, which oscillates between a maximum of approximately ±28.6° and a minimum of about ±18.3° relative to Earth's equator:

- Maximum northern declination → when the Moon reaches its greatest distance north of the equator (+28.6°).
- Maximum southern declination → when it reaches its greatest distance south (−28.6°).
- Minimum declination → when the Moon is aligned with Earth's equator (0° declination).

Lunar nodal precession refers to the slow backward motion of the two points where the Moon's orbit crosses the ecliptic. These nodes do not remain fixed; instead, they migrate by roughly 19 degrees per year in the direction opposite to the Moon's orbital motion. This gradual shift completes a full revolution along the ecliptic over a period of approximately 18.6 years.

1.3 Precession, Lunar Declination, and Seismicity

This phenomenon produces cyclic effects on astronomical events such as eclipses and tides, and several studies suggest that it may influence the occurrence of earthquakes with M>7 [6] [7] [8] or M>6 [9] [10] every 18.6 years in a non-random manner, with a confidence level exceeding 90%.

Some authors [7] [10] have identified an association between earthquakes and extreme values of lunar declination. Other studies [6] [8] [9] [11] have focused on the 18.6-year cycle without specifically referring to extreme declination values, instead exploring the phenomenon as a global periodicity linked to seismic activity. In particular, Hui & Xiaoming [8] examined the relationship between horizontal tidal forces—maximized for lunar declinations between ±10° and ±28°—and global seismic activity, offering a significant perspective on tidal forcing as a potential triggering factor. *Overall, the body of international research agrees on a correlation between the 18.6-year lunar periodicity and seismicity,* with a prevailing consensus that this periodicity primarily influences moderate-to-large earthquakes (M≥5–6). However, a minority viewpoint—represented by Vidale et al. (1998) [12] who analyzed earthquakes in California with M>5 and in other highly seismic regions, and by Beeler & Lockner (2003) [13], who calculated stress variations applied to faults by Earth tides and compared them with the magnitude of tectonic stress—questions the significant impact of crustal tides on earthquake triggering. These authors suggest that other geodynamic factors, such as pre-existing tectonic stresses and lithospheric rheology, may play a more dominant role in controlling global seismicity, and that the correlations observed in some studies may reflect statistical fluctuations rather than a genuine physical relationship.

1.3 Previous Studies on the Correlation Between Lunar Phases and Earthquakes

The prevailing scientific literature indicates that, although a correlation exists between tidal forces and seismic activity, it is statistically significant mainly for large-magnitude earthquakes (M>5), particularly during Full Moon and New Moon phases. However, a smaller portion of the literature proposes a broader correlation extending to lower-magnitude earthquakes and to a modulation of seismic activity throughout the entire lunar cycle, with more evident effects for shallow and

ISSN number; ISSN 2202-0039

moderate-magnitude events. A number of studies have examined the statistical relationship between lunar phases and earthquakes. In the two studies by Kilston and Knopoff (1983) [9], which analyzed 31 earthquakes in Southern California between 1933 and 1980, and Yanben H., Zhian L., and Hui H. (1998) [14], large earthquakes were found to be more likely during New Moon and Full Moon phases, while in the former study, smaller earthquakes showed no correlation. One of the most recent investigations [2], which analyzed 11,397 earthquakes with Mw>5.5 using data from the Global CMT catalog for the period 1976–2015, provides some of the most convincing evidence of a link between tidal forces and seismic activity—particularly for very large earthquakes (M>8) occurring during Full Moon and New Moon phases. A study on giant earthquakes in subduction zones, based on global data from 1976 to 2015, found [15] a statistically significant correlation between tidal configurations (Spring and Neap tides) and earthquake occurrence, with specific variations depending on the subduction zone. Since these configurations coincide with New/Full Moon and First/Last Quarter phases, *the study suggests a lunar-phase influence operating on a global geodynamic scale.* A broader modulation of lunar phases correlated with earthquakes emerges from a 2010 study [16] that analyzed global seismic data from 1973 to 2008 for all magnitudes. The results indicate a correlation between lunar cycles and seismic activity for earthquakes with M>6, which tend to increase gradually from the First Quarter to the Full Moon, then decrease toward the Third Quarter, across all latitude bands—with more pronounced effects for shallow and moderate-magnitude earthquakes. Some studies, however, report more uncertain data. One investigation [17] based on earthquakes recorded by the Taiwan Telemetered Seismic Network (TTSN) between 1973 and 1991 correlated lunar phases with earthquake magnitudes and found a significant relationship for light earthquakes (<M5) during New and Full Moon phases, but no significant correlation for earthquakes >M5. No correlation between strong earthquakes (M>5) and lunar phases was reported in studies [18] and [19], which analyzed global seismic data downloaded from the USGS (United States Geological Survey). Conversely, another study [20] found that, on a global scale from 1973 to 2011, a correlation with the Full Moon was present but weak. Two Italian studies on the subject reached similar conclusions. The first [1] analyzed seismic events within two earthquake swarms in the Apennines—the 1997 Colfiorito and the 2009 L'Aquila sequences—and found a cycle of about seven days, with maxima occurring roughly three days before the four principal lunar phases. The second [3] concluded that low-magnitude swarms (M≤4.7) tend to occur on the same day, or within 2–3 days before or after, the New or Full Moon phases. Both studies therefore highlight a strong correlation between lunisolar tides and the release of tectonic stress.

2. Materials and Methods

Based on several experiments conducted by the Author in this study (see *infra*, Section 2.2.1), it is hypothesized—and intended to be demonstrated—that lunar cyclicity correlates with the geographic recurrence of earthquake epicenters, following a regular periodicity corresponding to multiples of both 18.6 and 9.3 years. The Author also examined the correlation between the earthquake dataset and specific values of lunar phase and lunar declination, both at the national scale and within each of the 19 defined seismic zones. For the analysis concerning the correlation between earthquakes and lunar phases or declinations, the Author additionally included seismic data from the Campi Flegrei area (Naples), a region with a complex seismic history linked to the presence of a geothermal reservoir [21] that periodically induces vapor upwelling and triggers earthquakes. These Campi Flegrei events appear to show a weak correlation with certain lunar phase and declination (see *infra,* Section 4.1.1). In the present work, four complementary statistical approaches were applied to analyze the distribution of Italian earthquakes with respect to lunar phases, lunar declinations, and nodal periodicities:

1. *Chi-square (χ^2) test for uniformity* – Verifies whether earthquakes are uniformly distributed among lunar phases or declination bands; $p<0.05$ indicates significant deviations.
2. *One-tailed binomial test* – Tests concentration within a priori defined groups (e.g., phases 1, 3, 5, 7 or declinations −20°/−10° and 10°/20°) compared to control groups.
3. *2σ above the mean method* – Identifies anomalous peaks; a value exceeding two standard deviations above the mean is considered significant.
4. *Nodal periodicity analysis (18.6 and 9.3 years)* – Time differences between the last/penultimate and previous earthquakes in each zone were compared to the nodal cycles, divided into nine decimal intervals, and tested using χ^2 and binomial methods. The median of deviation values between earthquake years for each of the 19 zones—close to an integer with an average deviation of ±0.1—was used to verify the existence of a structured periodicity.

The combined use of the χ^2 test, one-tailed binomial test, and 2σ criterion enabled a rigorous analysis of the relationship between astronomical configurations and seismicity at both national and regional scales. This statistical triangulation made it possible to distinguish:

- A general modulation of seismicity associated with lunar phases and declinations (with significant values on a national scale);
- A local predictive cyclicity, more evident in certain zones, where the concentration of events

ISSN number; ISSN 2202-0039

within specific phases or declination ranges exceeded the established significance thresholds.

Regarding the selection of earthquake databases, the Author considered events from 1100 to the present for the analysis of lunar nodal precession, since this calculation requires only the year and hour of each event; precise information on the day is not necessary. Furthermore, historical earthquakes remain compatible with nodal-cycle computations despite discrepancies arising from the use of different calendar systems over time.

For the analyses involving lunar phases and lunar declinations, however, only earthquakes from 1600 onward were included, because the exact date of each event is essential for these calculations. In addition, between October 4 and October 15, 1582, *several days were removed during the transition from the Julian to the Gregorian calendar* [22], making accurate calculations for earlier earthquakes impossible. Therefore, for the study of lunar nodal precession, the ASMI database [23] was used; for lunar phases and declinations, the INGV catalogue [24] was selected, which begins in 1600. This methodological distinction does not affect the results, as both databases are equivalent starting from 1600.

2.1 Details of the 20 Geographical Zones Considered in This Study

For this analysis, 20 Italian seismic areas were identified, defined using empirical criteria and selected on the basis of the historical relevance of seismic events (M≥5) recorded from 1100 to the present. This subdivision does not follow predefined tectonic or administrative zonation's; rather, it was constructed specifically to serve the objective of the study, namely to test, within each area, the cyclic recurrence of seismic events in relation to lunar phases and lunar nodal precession. The delineation of these areas was carried out through a systematic examination of the Italian Macroseismic Historical Archive (ASMI) catalogue [23]. Nineteen of these zones were analyzed in the portion of the study dedicated to nodal precession. A twentieth zone, Campi Flegrei (Naples) — for which only modern seismic data are available—was included exclusively for the analysis of correlations between earthquakes and lunar phases or declinations. For each earthquake with M≥5, the epicentral designation reported in the ASMI catalogue was used as the reference. *A representative polygon was then defined for each epicentral area,* grouping within the same polygon all geographically proximate localities (within several tens of kilometers) that appeared in the catalogue with similar or contiguous names. For example, an event labeled "Alta Valtiberina" was merged with adjacent areas such as Sansepolcro, Casentino, and Montefeltro when these appeared in the ASMI catalogue with significant events. The polygons corresponding to the 20 areas were manually drawn on raster images of the ASMI maps. Polygon vertices were first recorded in pixel coordinates and subsequently converted into geographic coordinates (latitude and longitude) through linear georeferencing [revised term: previously indicated as generic "georeferencing"], using known control points and local degree/pixel scale factors. The maximum estimated error in the geographic position of the vertices is less than ±0.01°. The complete geographic coordinates of all polygons are provided in Table *1 - Calandra, S. (2025). Details of the 19 geographical areas - Lunar cycles and earthquakes in Italy. Zenodo. https://doi.org/10.5281/zenodo.15856560.*

The ASMI portal provides, for each of the geographically defined areas, a list of earthquakes with selectable magnitude thresholds. In this study, only events with M≥5 were considered for the statistical analysis of the correlation between earthquakes and the periodicities associated with the lunar nodes. For the analysis of the correlation between lunar phases, lunar declinations, and seismicity, however, six magnitude classes starting at M3 were used instead, drawing—within the same zonations—from the more recent INGV catalogue. The table referenced below reports, for each of the 20 areas included in this study, the corresponding map, the geographic coordinates of the reference polygon (or circle), and the principal municipalities involved, following the exemplary structure shown here.

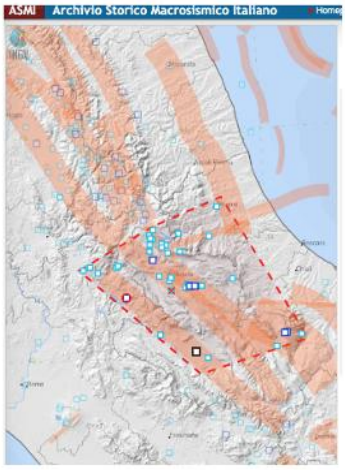

1)
Marsica e Provincia AQ, Gran Sasso, Maiella, Teramano, Reatino.
Polygon vertices:
1. Latitude: 42.414, Longitude: 12.817
2. Latitude: 42.693, Longitude: 13.725
3. Latitude: 42.055, Longitude: 14.228
4. Latitude: 41.923, Longitude: 13.540

Main municipalities involved: L'Aquila, Avezzano, Sulmona, Tagliacozzo, Celano, Pescina, Carsoli, Magliano de' Marsi, Capistrello, Civitella Roveto, Balsorano, Pratola Peligna, Popoli, Castel di Sangro, Scanno, Pescasseroli, Roccaraso, Ovindoli, Castel del Monte, Barisciano, Tornimparte, Accumoli, Amatrice, Cittareale.

Fig. 1 - Geographic polygon defining 1 of the 20 seismic areas used in this study. Vertices were georeferenced from pixel to latitude – longitude coordinates with an estimated positional error <±0.01°. *Full polygon coordinates and area descriptions are provided in Table 1.*

ISSN number; ISSN 2202-0039

2.2 Lunar Nodal Precession

This study explores how the historical analysis of earthquakes in Italy, based on the 9.3- and 18.6-year periodicities, can provide useful clues for forecasting future seismic epicenters. Using the model of lunar nodal precession, tables are constructed that make it possible to determine, year by year, the locations most likely to experience new seismic events. The study draws inspiration from authors who have previously conducted similar research [6] [7] [8] [9] [10] [11], on earthquakes in other regions of the world. The following table provides a summary of the outcomes and characteristics of their work. Table *2 - Calandra, S. (2025). summary table of the bibliography of lunar nodes and declinations [Data set].Zenodo* https://doi.org/10.5281/zenodo.17213937.

All the studies listed in the table recognize a lunar periodicity of 18.6 years as potentially associated with seismic activity, especially for high-magnitude earthquakes (typically M≥6.0 or ≥ 7.0). Most authors also considered lunar declination, either by checking for clustering around extreme values (±28.6°), or, as in the case of Hui & Xiaoming (2001) [8], by identifying significant clusters within intermediate bands (±10° to ±28°) that correspond to maximum horizontal tidal forces. The approach adopted in this study aims to provide a detailed understanding of seismic cyclicity, with potential applications in seismic risk management. Historical epicenters of earthquakes with M≥5 occurring in Italy from the year 1100 to the present [23] were reconstructed in relation to the 9.3- and 18.6-year cycles. These cycles, known as *lunar nodal precession cycles*, were analyzed to identify a possible seismic recurrence law linked to astronomical phenomena, one that may relate past events and potentially allow the forecasting of future seismic episodes on the scale of broad geographic macro-areas. *For this purpose, 19 epicentral zones were identified across Italy,* each of which demonstrated, on an experimental basis, a sufficiently reliable cyclic behavior. Within each of these 19 seismic zones, three complementary analyses were performed:

1. Identification of localities affected by M≥5 earthquakes from 1100 to 2024. Each of the 19 localities was assigned a sequential number, a name, and the complete list of years in which M≥5 earthquakes occurred. These data were compiled in a dedicated Excel worksheet (see Table 3 below).
2. Calculation of the p-value using a one-tailed binomial test, expressed through the corresponding chi-square (χ^2) value in the same worksheet, to evaluate the presence of nodal periodicities (9.3065 and 18.613 years) by assessing the recurrence of the two most recent earthquakes relative to the historical events within each zone.
3. Analysis of median temporal deviations for each zone. For every M≥5 earthquake, the difference in years relative to all preceding M≥5 events within the same zone was computed. The median value for each zone—divided by 18.6 or 9.3 years—was then used to determine whether a structured periodicity was present across the 19 zones considered.

2.2.1 P-value Analysis of Nodal Cyclicity at 9.3065 and 18.613 Years

For each of the 19 Italian seismic zones, the target year was defined as the year of the most recent known M≥5 earthquake (in some cases, the second most recent event was used when the last earthquake did not provide an interpretable result). Beginning from this reference point, temporal differences were calculated with respect to all earlier earthquakes in the same zone. Based on experimental evidence, only events belonging to *sequences without gaps longer than at least 100 years were considered valid for cyclicity analysis*. Each temporal difference (in years) was then normalized by dividing by 18.6 or 9.3 years, corresponding to the periods of the lunar nodal cycle. See file Pvalue_LunarNodes_Italy19zones.xlsx, in: Table *3 - Calandra, S. (2025). Calculation sheet of P-value for lunar node precession in 19 zones in Italy. Zenodo.* https://doi.org/10.5281/zenodo.17215030.

The following criteria were applied:

- Values close to an integer (±0.1) were interpreted as possible indicators of periodic recurrence.
- To quantify the distribution, the normalized values (cycle counts) were grouped into nine decimal intervals (width ≈0.11) to test for clustering near integer multiples (intervals 1 and 9).
- A χ^2 goodness-of-fit test was applied, and in parallel, a one-tailed binomial test was used to compare the observed frequency in intervals 1+9 with the expected count for a random distribution.

A p-value <0.05 was considered statistically significant, suggesting a structured, non-random periodicity compatible with the 18.6- or 9.3-year nodal cycles. The worksheets “chi quadro,” “chi quadro 9,3,” and “chi quadro 18,6” contain the calculations for the one-tailed binomial test, expressed through the χ^2 value, used to verify nodal cyclicity (9.3065 and 18.613 years) and to evaluate the recurrence of the most recent earthquakes relative to earlier events within each zone. The resulting output for each zone is the p-value associated with nodal cyclicity. By entering the earthquake years for any of the 19 zones in column B of the *“chi quadro”* sheet, the p-value is automatically computed in cells S22–U22. *One of the two most recent earthquakes is selected as the target year and entered in cell D1.* The entries “1” in columns G and H are then

ISSN number; ISSN 2202-0039

identified, ensuring that the selected sequence corresponds to the most recent uninterrupted interval relative to the target year. Cells corresponding to prior intervals are removed from columns G–J. If the distribution of temporal deviations relative to the target year exhibits a strong clustering near integer values (±0.1), the resulting p-value may be statistically significant (<0.05), as reported in cells Y5 and S22–T22–U22 of the *"chi quadro"* sheet for each zone. A significant concentration ($p<0.05$) indicates that the seismicity in that zone follows a regular periodicity associated with the lunar nodal cycle.

2.2.2 P-value Analysis for Target Year 2016 (Valnerina – Zone 4)

Let us examine an illustrative example of the p-value calculation for a specific worksheet, namely Zone 4 (Valnerina).

Dataset: historical years from 1941 onwards: 1941, 1943, 1948, 1951, 1962, 1973, 1974, 1979, 1997, 1998 (n=10, (see, *supra*, worksheet "*4-chi quadro",* file *Pvalue_LunarNodes_Italy19zones.xlsx,* Section 2.2.1, Table 3).

Target year: 2016. Cycle: 18.6 years. In-phase threshold: deviation ≤0.111 → p_0 =0.222.

In-phase events observed k=6. Expected count E=n p_0=2.220.

p–value (binomial, P(X≥6))=0.010883

p–value (χ^2 with 1 d.f., from χ^2 total=8.272771)=0.004024.

Interpretation: Both tests indicate statistical significance ($p<0.05$). However, the exact binomial test is preferred when expected counts are small. For each historical date, we compute: Δ years, cycles (Δ/18.6), fractional part, phase error (min(frac, 1 − frac)), and whether the error ≤0.111. The table below summarizes the results.

Historical year	Δ years	Cycles	Fractional	Phase error	In phase?
1941	75	4.032258	0.032258	0.032258	YES
1943	73	3.924731	0.924731	0.075269	YES
1948	68	3.655914	0.655914	0.344086	NO
1951	65	3.494624	0.494624	0.494624	NO
1962	54	2.903226	0.903226	0.096774	YES
1973	43	2.311828	0.311828	0.311828	NO
1974	42	2.258065	0.258065	0.258065	NO
1979	37	1.989247	0.989247	0.010753	YES
1997	19	1.021505	0.021505	0.021505	YES
1998	18	0.967742	0.967742	0.032258	YES

2.2.2.1 Note on binomial vs χ^2 discrepancy.

The binomial test provides the exact probability of obtaining k or more successes in n trials with a success probability p_0. By contrast, the χ^2 test offers an approximation by comparing observed and expected frequencies through squared deviations; when expected counts are small ($E<5$), this approximation becomes less reliable. In this case, $E \approx 2.22$ (<5), making the binomial test the preferred exact method. Numerical results: Binomial p-value=0.010883; χ^2=8.272771 → χ^2 p-value=0.004024. Overall, the agreement between the exact binomial test and the χ^2 statistic—both yielding $p<0.05$—indicates that the historical earthquake sequence in Zone 4 is unlikely to arise from a random process. Instead, it shows a structured recurrence pattern consistent with the 18.6-year lunar nodal cycle. The clustering of phase errors within ±0.111 for six out of ten historical events—most notably the strong alignment of the 1941, 1943, 1962, 1979, 1997, and 1998 earthquakes—further supports the hypothesis that seismicity in this zone is modulated by nodal periodicity. These results, taken together, indicate that the *Valnerina sequence shows a statistically robust phase-locking behavior with the nodal cycle, supporting the broader finding* that several Italian seismic zones display predictable temporal recurrences that are unlikely to arise by chance.

2.2.3 Median Analysis of Temporal Differences Between One M≥5 Earthquake and All Others

The calculation of the median of the temporal differences between the year of an M≥5 earthquake and all other events of the same category—after division by 18.6 or 9.3 years—yields values consistently close to an integer across the different geographic areas. The use of the median, rather than the mean, is particularly appropriate for identifying regular patterns within cyclic phenomena. The median reduces the influence of anomalies or extreme events and highlights the central tendency of the distribution. If the median repeatedly returns values near integers, this indicates that most earthquakes tend to fall within an interval consistent with the hypothesized cycles. This may suggest that the cyclicity associated with the precession of the lunar nodes exerts a measurable influence on seismic recurrence. When the median of the temporal differences between earthquakes—divided by 18.6 or 9.3 years—returns an *integer value for a given zone, this may indicate the presence of a structured periodicity within the seismic dataset,* modulated according to the characteristics of each zone and compatible with nodal periodicity. For example, Zone 1 shows a median temporal difference of 196 years and a median of 21.1 years. See the value in cell D1 of worksheet "1" in the file: *MEDIAN_DIFFERENCE_CALCULATION_19zones.xlsx*, reported in Table 4 - *Calandra, S. (2025). Analysis of the median deviation between the year of an earthquake M>5 and all other years. Zenodo.* https://doi.org/10.5281/zenodo.16419440

2.2.4 Summary of Zone-Specific Calculation Criteria

The 19 worksheets corresponding to the Italian epicentral zones were consolidated into a summary table titled *"Lunar Node Precession M5 – Results"* (see *supra*,

ISSN number; ISSN 2202-0039

Section 2.2.1, Table 3). This table integrates the following key parameters:

- *Nodal periodicity:* For each of the 19 zones, the relevant periodicity (9.3 or 18.6 years) was determined, along with the median residuals (i.e., the deviation between the earthquake year and the expected nodal cycle) and the median number of completed cycles.
- *Consistency with historical cycles:* For each zone, the most recent and second most recent earthquakes that align with the nodal cycles are listed, indicating whether the periodicity is maintained, disrupted, or only partially supported.
- *Type of periodicity:* The table specifies whether the dominant coherence is associated with the short (9.3-year) cycle, the long (18.6-year) cycle, or both.
- *Statistical significance*: A one-tailed binomial p-value was calculated for each zone as a metric for assessing the probability that the observed alignment between seismic sequences and nodal cycles could arise from random variability.

This framework enables *direct comparison across epicentral zones, facilitating an evaluation of the stability and regularity of nodal cyclicity in relation to historical seismicity*. The binomial test provides a quantitative measure of the strength of the correlations, whereas the qualitative assessment of cycle–event correspondence helps distinguish zones exhibiting a well-structured periodic pattern from those where the sequence appears interrupted or less clearly defined.

2.2.5 Forecasting Seismic Risk Zones for 2026–2027 for Events M≥5

In keeping with the methodology used to evaluate nodal cyclicity in past earthquakes across the 19 study zones, the Author also computed p-values for the 9.3- and 18.6-year nodal cycles projected into future years. The same analytical framework applied to assess the historical cyclicity of the last two M≥5 earthquakes in each zone—relative to earlier events—was used to forecast potential future alignments. The table below presents the results obtained from the lunar nodal precession model, identifying the localities that may be at elevated seismic risk for M≥5 events in Italy during the 2026–2027 biennium. Table 5 - *Calandra, S. (2025). Calculation sheets of P-value for lunar node precession in 19 zones in Italy - Prediction 2026 and 2027 [Data set]. Zenodo. https://doi.org/10.5281/zenodo.17242842*.

2.2.6 P-value Analysis for Target Years 2026 and 2027 (Valnerina – Zone 4)

As an illustration, we present the p-value calculation for one specific worksheet—Zone 4 (Valnerina)—following the same procedure used for the last historical target event of 2016 (see *supra*, Section 2.2.2). For the target year 2026, the analysis reveals a clear resonance with the nodal cycles of the historical M≥5 earthquakes in this zone (1730, 1741, 1767, 1791, 1832, 1854, 1873, 1878, 1883, 1898, 1916). The computation was performed using the long nodal cycle (18.6 years). For each historical event, the temporal difference relative to 2026 (Δ years) was calculated, along with the corresponding fraction of the nodal cycle (Δ/18.6). Each case was then evaluated to determine whether its phase error fell within the threshold of ≤ **0.111**, which corresponds to ±1/9 of a full cycle. Out of n=21 historical events considered, k=7 satisfy the "in phase" condition. The theoretical expectation, given by $E=n\cdot p_0$ with $p_0=0.222$, is E=4.66.

Applying the one-tailed binomial test:

$$P(X \geq 7) = \sum_{i=7}^{21} \binom{21}{i} p_0^i (1-p_0)^{21-i} \approx 0.0088$$

The resulting value is p=0.0088.
(see *supra,* worksheet *"4–chi quadro"*, File: *Pvalue_LunarNodes_Italy19zones_prediction_2026.xlsx*, Section 2.2.5, Table 5).

Since p<0.05, the null hypothesis of a random distribution is rejected. This means that the probability of observing 7 or more in-phase events, against an expected count of approximately 5, is very low (less than 1%). The result therefore confirms that *the observed concentration cannot be attributed to chance* and strengthens the hypothesis of a probabilistic seismic forecast for the target year 2026 in the Valnerina area. Moreover, the length of the historical period analyzed exceeds one century, thus fulfilling the preliminary requirement for the reliability of the calculation.

2.3 Lunar Phases, Lunar Declination, and Earthquake Magnitude

International research on the correlation between lunar phases, lunar declination, and earthquakes focuses predominantly on large-magnitude events, while studies that systematically separate seismicity into distinct magnitude classes are relatively rare. This study introduces an innovative approach applied to the Italian context, analyzing lunar influence across five magnitude intervals, from M3 (3 Richter) up to events above M5 (5 Richter). This segmentation—combined with a geographically restricted scale organized into 19 Italian zones for earthquakes M≥5—makes it possible to highlight zone-specific patterns and refine the understanding of the role of tidal forces in the earthquake-triggering process. The study draws inspiration from previous works that have investigated similar correlations, both between lunar declination and earthquakes (see *supra*, Section 1.3), and between lunar phases and earthquakes (see *supra*, Section 1.4) in other regions of the world. The following table provides a summary of the outcomes and characteristics of the studies concerning lunar phases, while the synthesis of the bibliography on lunar declination is reported in the

ISSN number; ISSN 2202-0039

previous Table 2 (see *supra,* Section 2.2). Table *6 - Calandra, S. (2025). Summary table: bibliography on lunar phases and earthquakes. [Data set]. Zenodo. https://doi.org/10.5281/zenodo.17235906*

This study investigates possible correlations between lunar phase, lunar declination, and earthquake magnitude, from the lowest range (M3=3 Richter) to the highest (M≥5). Moreover, it is possible to assess whether this national-scale pattern is consistent with the earthquakes recorded within each of the 20 seismic zones examined. These consist of the same 19 zones analyzed in the section dedicated to lunar nodal precession, plus the Campi Flegrei (Naples) area, for which only modern seismic data are available. For lunar phases and lunar declination, and for each of the five magnitude classes considered, *an internal coherence test of the dataset was performed*: the results obtained for all earthquakes from 1600 to 2024 were compared with those derived from earthquakes of the last 150 years, which are more numerous and reliable due to improvements in detection techniques.

2.3.1 Data Collection by Magnitude Class

The Author analyzed 7,948 earthquakes [24] that occurred in Italy from 1600 to the present, all with M>3, and grouped them into magnitude classes as summarized below:

3-3.6R	**3.7-4R**	**4.1-4.3R**	**4.4-4.9R**	**>5R**	**TOT EQS 1600-2024**
5375	767	580	758	468	**7.948**

The lunar phases number eight [25] [26] , distributed across the 28-day lunar revolution cycle around Earth:

1 → New Moon → 4 days
1 → Waxing Crescent → 3 days
3 → First Quarter → 4 days
2 → Waxing Gibbous → 3 days
3 → Full Moon → 4 days
4 → Waning Gibbous → 3 days
5 → Last Quarter → 4 days
6 → Waning Crescent → 3 days

From the 7,948 earthquakes with M>3, the Author grouped all events into six lunar-declination bands [27]:

-28° / -20°
-20° / -10°
-10° / 0°
0° / 10°
10° / 20°
20° / 28°

For each magnitude class, the Author then investigated whether earthquakes tended to cluster within specific lunar phases or declination intervals. Two worksheets were generated for each of the five magnitude classes (see infra, Table 7), for a total of ten analytical sheets:

- Odd-numbered sheets (1–3–5–7–9): contain all earthquakes in each magnitude class, listed chronologically from the earliest to the most recent and annotated with the corresponding lunar phase and lunar declination.
- Even-numbered sheets (2–4–6–8–10): contain only earthquakes from the last 50–150 years, used to compare the consistency of historical records with more recent and more reliable seismic observations.

Sheet 1 and 2 → M3–3.6
Sheet 3 and 4 → M3.7–4
Sheet 5 and 6 → M4.1–4.3
Sheet 7 and 8 → M4.4–4.9
Sheet 9 and 10 → M5+

Table *7 - Calandra, dr. S. (2025). Moon phases, lunar declinations, and earthquakes by magnitude range [Data set]. Zenodo. https://doi.org/10.5281/zenodo.17237018*.

This framework makes it possible to identify both temporal and spatial patterns of earthquake clustering in relation to lunar phases and lunar declination. *To evaluate the statistical significance of these concentrations, three distinct approaches were applied:*

• *Lunar declination:* because the same two declination bands (–20°/–10° and +10°/+20°) repeatedly emerged as the most active regardless of magnitude, each earthquake was classified as a *"success"* if it fell within one of these two bands, and as a *"failure"* otherwise. A one-tailed exact binomial test was then applied:

$$\text{P-value} = 1 - \text{BINOM.DIST}(N_{obs} - 1,\ N_{tot},\ p_{expected},\ \text{TRUE})$$

where

- N_{obs}= number of earthquakes observed in the two declination bands,
- N_{tot}= total number of events,
- $p_{expected}$= theoretical uniform probability.

• *Lunar phases:* because the phases exhibiting anomalous concentrations change with magnitude class, a dual statistical strategy was adopted:

1. χ^2 goodness-of-fit test applied to the entire eight-phase distribution, to determine whether the overall pattern deviates from uniformity.
2. One-tailed binomial test focused on the most recurrent anomalous phases (e.g., phases 1 and 3, or phases 1, 3, 5, 7), to directly estimate the probability that the observed excess could arise by chance.

• *Mean + 2σ criterion:* for both lunar phase and declination analyses, an additional diagnostic threshold was employed: values exceeding two standard deviations

ISSN number; ISSN 2202-0039

above the mean were flagged as exceptional. This criterion provides a visual and statistical confirmation of the significant patterns revealed by the χ^2 and binomial tests.

2.3.2 Summary of Magnitude-Specific Calculation Criteria

The ten worksheets (two for each of the five magnitude ranges) were compiled into a summary table titled *"1600–2024 distribution of earthquakes in lunar phases and declination by magnitude – Italy"* (see *supra,* Section 2.3.1, Table 7). This table consolidates the following key parameters:

• *Lunar declinations:* for each magnitude class, the percentage concentration of earthquakes falling within the two most relevant declination bands (–20°/–10° and 10°/20°) is reported, along with the overall p-value relative to a uniform distribution and the one-tailed binomial p-value computed specifically for those bands.

• *Lunar phases:* the phases exhibiting above-expected concentrations (typically phases 1, 3, 5, and 7, or phases 1 and 3) are listed, together with the corresponding percentage of earthquakes, the overall χ^2 p-value, and the one-tailed binomial p-values calculated exclusively for those phases.

• *2σ criterion:* for both declination and phase analyses, the study also assessed whether the observed frequencies exceeded the theoretical mean by at least two standard deviations, in order to validate the statistical significance of the detected anomalies.

This framework enables direct comparison—across magnitude classes and across historical versus recent data—of the robustness of the correlations between earthquakes and astronomical parameters. Importantly, the methodological distinction between the binomial test (rigorous, fixed declination bands) and the χ^2 test (general, variable phase distributions) allows systematic and persistent concentrations to be differentiated from more flexible yet still statistically meaningful patterns.

2.3.3 Data Collection by Geographical Zone

Using the same analytical framework and computational procedures adopted for the magnitude classes, the Author then examined the data by geographical zone, focusing exclusively on stronger earthquakes (M≥5). The objective was to evaluate whether a statistically robust correlation existed between specific lunar phases or lunar declination bands and seismicity within one or more of the 19 zones previously defined according to the criteria described above (see *supra*, Section 2.1).

For the Campi Flegrei area, however, the analysis was extended to all earthquakes with M≥3 occurring between 1984 and 4 October 2025, since a long historical record comparable to the other 19 zones is not available due to the hydrothermal, reservoir-driven seismicity characteristic of this region (see *supra*, Section 2). For each geographical zone, the Author assessed whether earthquakes tended to cluster within particular lunar phases or within specific lunar declination intervals. A dedicated calculation sheet was prepared for each of the 20 zones, in which all M≥5 earthquakes were chronologically ordered from the oldest to the most recent and assigned their corresponding lunar phase and lunar declination. Data collection and computational criteria were applied on a zone-by-zone basis, following precisely the same methodology previously described for the magnitude-based analyses (see *supra*, Sections 2.3.1 and 2.3.2). The 20 geographical worksheets (including the Campi Flegrei sheet) were compiled into a summary table titled "*Summary p-value – by area"*. Both the summary table and individual worksheets are available as a dataset in the following reference: Table *8 - Calandra, S. (2025). Moon phases, lunar declinations, and earthquakes by geographical zone [Data set]. Zenodo. https://doi.org/10.5281/zenodo.17244504*.

Since, as shown in the Results (see *infra*, Section 3.2.1), not all p-values computed for the 20 epicentral zones were sufficiently low to reject the null hypothesis, a methodological refinement was required. In particular, the one-tailed binomial test and the "$>2\sigma$" concentration criterion (i.e., a frequency excess greater than two standard deviations above the expected value) applied to the two lunar declination bands already identified (–20°/–10° and 10°/20°) and to the most recurrent lunar phases do not always yield statistically significant results at the individual-zone scale. For this reason, the Author extended the analysis to the entire national dataset, examining whether lunar phases 1 (New Moon) and 3 (First Quarter), as well as the two declination bands –20°/–10° and 10°/20°, occurred more frequently than expected under a uniform distribution. Since their frequencies were systematically higher than the theoretical expectation, four additional summary worksheets were generated, compiling the corresponding p-values at the national scale:

• P-value phase 1 band
• P-value phase 2 bands (phases 1 and 3)
• P-value declination 1 band
• P-value declination 2 bands (–20°/–10° and 10°/20°)

These summary sheets make it possible to evaluate the statistical significance of the observed concentrations in a concise and comparable manner, overcoming the local variability of individual zones and providing a more robust, nationwide assessment.

3. Results

3.1 Nodal Precession (18.6 and 9.3 Years) — Zone-by-Zone Analysis (M≥5)

The analysis of the lunar nodal precession cycles—corresponding to the 18.6-year period and its 9.3-year half-cycle—reveals a clear temporal recurrence of Italian earthquakes with M≥5 across the 19 epicentral zones examined. The one-tailed binomial test (see *supra*, Table

ISSN number; ISSN 2202-0039

3, Section 2.2.1), applied to evaluate whether the temporal intervals follow these cycles, shows that 16 out of 19 zones exhibit p-values below the conventional significance threshold ($p<0.05$). *This indicates that the temporal sequence of earthquakes is inconsistent with a random process and instead reflects a stable periodic structure over time* (see Fig. 2).

Median Lunar frequency (years) for earthquakes M>5, by area					Lunar periodicity (years) and p-value for earthquakes M>5, by area		
Zone n.	Geographic zone	Median of residuals (years)	Nodal periodicity	Median number of cycles	Last/penultimate Eq in resonance with nodal cycle	Type of periodicity	P-value with one-tailed binomial test
1	AQ e Marsica	196	9,3	16,9 ✓	The earthquake of 2009 fits with the recent cycle 1804–1933, but it had been interrupted. The earthquake of 2017 fits with the recent cycle 1905–2009.	18,6 (2009); 9,3 (2017)	0,001 (2009) ✓; 0,016 (2017) ✓
2	Stretto Messina	316	9,3 e 18,6	34 e 17 ✓	The earthquake of 1909 fits with the **long cycle 1499-1908**	9,3	0,042 ✓
3	Garfagnana	120	9,3	12,9 ✓	The earthquake of 2013 fits with the recent cycle 1790–2012.	9,3	0,0061 ✓
4	Valnerina	151	18,6	8,1 ✓	*the calculation of the median starts from 1277. The earthquake of 1997 fits with the short cycles 1791–1838 and 1948–1979; the earthquake of 2016 fits with the recent cycle 1941–1998.	18,6	0,0041 ✓
5	Molise Irpinia Sannio PZ	258	18,6	13,9 ✓	The earthquake of 2013 does not fit (by little) with the cycle 1826–1930. The earthquake of 1990 fits with the **full long cycle 1005–1982.**	9,3	0,011 ✓
6	Fiorentino Mugello	215	9,3	23,1 ✓	The earthquake of 1939 fits with the cycle 1725–1864, but it had been interrupted.	9,3	0,026 ✓
7	Asolano Cansiglio	76,5	18,6	4,1 ✓	The earthquake of 1936 fits with the cycle 1695–1936 → The earthquake of 1943 does not fit with any cycle.	-	✗
8	Milanese Veronese	92,5	9,3 e 18,6	9,9 e 5,0 ✓	*the calculation of the median starts from 1396. The earthquake of 1951 fits with the cycle 1802 - 1932	9,3	0,026 ✓
9	Sicilia	205,5	9,3 e 18,6	22,1 e 11,0 ✓	*the calculation of the median starts from 1169. The earthquake of 1968 (Belice) fits with the **long cycle 1624–1968.**	9,3	0,023 ✓
10	Val di Paglia Val d'Orcia	166	18,6	8,9 ✓	*the calculation of the median starts from 1320; The earthquake of 1911 fits with **the cycle 1558 - 1909.** The earthquakes of 1919 e 1940 do not fit with any cycle.	18,6	0,038 ✓
11	Parma Modena Em Rom	215	9,3	23,1 ✓	The earthquake of 2012 fits with the cycle 1873 - 2003	9,3	0,021 ✓
12	AltaValtiberina	205	9,3 e 18,6	22 e 11 ✓	*the calculation of the median starts from 1458; The earthquake of 1948 fits with the **full cycle 1352–1919.**	18,6	0,0038 ✓
13	Forlivese Riminese	215	9,3	23,1 ✓	The earthquake of 1963 fits with the recent cycle 1768–1935.	9,3	0,003 ✓
14	Basilicata Pollino	58	18,6	3,1 ✓	The earthquake of 2012 does not fit with any cycle.	-	✗
15	Calabria	120	9,3	12,9 ✓	*the calculation of the median starts from 1377; The earthquake of 1947 fits with the interrupted **long cycle 1184–1854.**	9,3	✓0,026
16	Anconetano Ascolano	188	18,6	10,1 ✓	The earthquake of 2013 fits with the **long cycle 1269 - 1873,** but it had been interrupted.	9,3	0,035 ✓
17	Friuli	66	9,3	7,09 ✓	*the calculation of the median starts from 1700; The earthquake of 1977 fits with the short recent cycle 1931–1976 **(45 years).**	9,3	0,011 ✓
18	Gargano	138,5	9,3	14,9 ✓	The earthquake of 2018 fits with the **long cycle 1414–1841,** but it had been interrupted.	9,3	0,016 ✓
19	Torinese	92	9,3 e 18,6	9,9 e 4,9 ✓	no ✗	-	✗

Fig. 2 - Nodal periodicity of M≥5 earthquakes in 19 Italian zones. *The median frequencies of M5+ earthquakes (left table) are close to whole numbers, indicating a cyclical regularity in relation to lunar cycles of 9.3 and 18.6 years. In the right table, p-values <0.05 in 16 out of 19 zones confirm a non-random periodicity of M5+ earthquakes, consistent with lunar nodal cycles.*

The column *"Median of residuals (years)"* in Fig. 2 (left panel; see *supra*, Table 4, Section 2.2.3) reports the median time interval (in years) between each M≥5 earthquake and all preceding events within a given zone, representing the local median recurrence timescale. The column *"Median number of cycles"* in Fig. 1 shows the number of nodal cycles (9.3 or 18.6 years) obtained by dividing the median residual by the nodal periodicity. In almost every zone, *this value is close to an integer (within ±0.1),* indicating that earthquake recurrence tends to synchronize with integer multiples of the lunar nodal cycles. This pattern suggests that most earthquakes occur after an integer or half-integer number of nodal cycles, *pointing to a structured periodicity in the seismic record modulated according to regional tectonic characteristics and consistent with the lunar nodal periodicities.*

The right-hand table in Fig. 2 reports the nodal periodicities and corresponding p-values calculated using the one-tailed binomial test (see *supra,* Section 2.2.1). In 16 of the 19 zones, p-values fall below 0.05, confirming that the distribution of earthquakes is not random but follows cycles compatible with the 9.3- and 18.6-year lunar periodicities. Zones exhibiting the strongest and most persistent periodic signals—according to the "*P-value with one-tailed binomial test*"

ISSN number; ISSN 2202-0039

column (see *supra*, Fig. 2 and file *Lunar_node_precession_M5_results.xlsx*, Table 3, Section 2.2.1)—include AQ and Marsica, Valnerina, Molise–Irpinia–Sannio, Fiorentino–Mugello, and Sicily, where statistical significance is consistently high for one or both cycles. Beyond statistical significance alone, the column *"Last/penultimate Eq in resonance with nodal cycle"* (see *supra*, Fig. 2 and the same dataset) shows that several Italian regions exhibit not just isolated resonant pairs of earthquakes, but rather extended sequences in which multiple consecutive events respect the nodal periodicity over multi-cycle intervals. Zones such as Stretto di Messina, Molise–Irpinia–Sannio–Potenza, Sicily, Val di Paglia–Val d'Orcia, Alta Valtiberina, Calabria, Anconetano–Ascolano, and Gargano display long sequences—spanning 200–300 years—in which multiple earthquakes align with the 9.3- and 18.6-year cycles.

These long, multi-century intervals of temporal coherence substantially *enhance the interpretative value of the p-values computed for individual zones, as they demonstrate that earthquake recurrence follows a regular, non-random pattern.* The presence of consecutive multi-cycle or even tri-cycle nodal sequences suggests the existence of a gravitational synchronization mechanism linking lunar nodal precession to local seismic dynamics. Conversely, the three areas Asolano–Cansiglio, Basilicata–Pollino, and the Turin area do not show statistically significant periodicity, likely due to limited historical data or highly fragmented seismic sequences. A special case is Friuli–Venezia Giulia, where the last resonant earthquake falls within a shorter sequence (~45 years), representing the minimum interval considered in this study for identifying a structured recurrence.

Overall, the convergence between statistical significance and the multi-century duration of nodal cycles reinforces the *hypothesis that Italian earthquake periodicity is modulated by a repeating astronomical mechanism linked to lunar nodal precession.* The combined use of the binomial test, the median-residual analysis, and the verification of multi-cycle resonances provides a coherent picture of astronomically modulated seismic periodicity, with direct implications for the understanding and long-term forecasting of major seismic events.

3.2 Lunar Phases — National Analysis by Magnitude

The analysis of 7,948 Italian earthquakes recorded between 1600 and 2024 shows that event distribution across the synodic cycle is not uniform. A one-tailed binomial test (see *supra,* "*Summary of p-values by magnitude*", column "*One-tailed binomial test on phases 1,3,5,7 p-value <0.05*", Table 7, Section 2.3.1), applied to four a priori selected lunar phases (1=New Moon, 3=First Quarter, 5=Full Moon, 7=Last Quarter), returns $p<0.05$ for all magnitude classes examined (M3–3.6, M3.7–4, M4.1–4.3, M4.4–4.9, M≥5). This confirms a systematic and statistically significant concentration of earthquakes during the four principal synodic phases. The effect is even stronger for M4.1–4.3 earthquakes in the last 150 years: 62% of all events fall within the four predefined phases (1, 3, 5, 7); 37% fall within phases 1 and 3 alone, with a particularly marked excess at the New Moon (phase 1). For magnitudes <M5, phase 1 exceeds the expected uniform value by 1.9–2σ, indicating that the probability of such concentrations arising from randomness is negligible. In contrast, intermediate control phases (2, 4, 6) show no significant deviations ($p>0.05$), reinforcing the interpretation that the observed association specifically concerns the four principal lunar phases. Overall, the national-scale results show *a robust and persistent statistical link between earthquake occurrence and the major synodic phases, with the New Moon playing a particularly prominent role.*

3.2.1 Regional Analysis by Geographic Zone (M≥5)

When the analysis is restricted to magnitude ≥M5 earthquakes and carried out at the regional scale, the pattern becomes more selective but remains consistent with national findings. The global χ^2 test indicates deviations from uniformity in 13 of the 19 epicentral zones, although this method tends to be sensitive to fragmented time series and may overestimate local signals (see *supra,* Table 7, Section 2.3.1). A more stringent approach is provided by the one-tailed binomial test applied to the same a priori phases (1, 3, 5, 7). According to this criterion (see *supra*, column "*One-tailed binomial test on predefined phases (lunar phases 1, 3, 5, 7)"* in "*Summary of p-values by area*", Table 8, Section 2.3.3), only 5 of the 19 zones reach statistical significance ($p<0.05$): AQ e Marsica ($p=0,0008$), Valnerina ($p=0,0427$), Molise–Irpinia–Sannio ($p=0,0320$), Fiorentino–Mugello ($p=0,0021$) and Sicilia ($p=0,0207$). In all these regions, the significant concentration involves the full set of the four main synodic phases. However, as also observed nationally, phases 1 (New Moon) and 3 (First Quarter) are the most frequently associated with excess seismicity and often return lower p-values than the combined 1–3–5–7 group (see *supra,* Section 3.2). A complementary indirect analysis, based on counting the number of zones in which each phase exceeds its expected frequency (see *supra,* "*P-value phase 2 bands*", Table 8, Section 2.3.3), confirms this pattern. Phases 1 (New Moon) and 3 (First Quarter) exceed expected values in 14 out of 19 zones each. Phases 4 (Waxing Gibbous), 5 (Full Moon), and 7 (Last Quarter) exceed expectations in 10 zones each. All remaining phases show lower occurrences. A binomial test applied to this distribution yields $p=0.0236$, indicating that the excess observed in phases 1 and 3 is unlikely to be due to chance. Taken together*, the regional-scale results reinforce the national conclusions: the occurrence of Italian earthquakes is*

ISSN number; ISSN 2202-0039

significantly associated with the principal synodic phases, with New Moon and First Quarter consistently emerging as the phases most strongly linked to seismicity ≥M5, followed by Full Moon and Last Quarter. The *coherence between the two analytical levels—by magnitude and by geographic zone*—supports the interpretation that lunar modulation of M≥5 seismicity in Italy is most pronounced during the early synodic phases and the First Quarter.

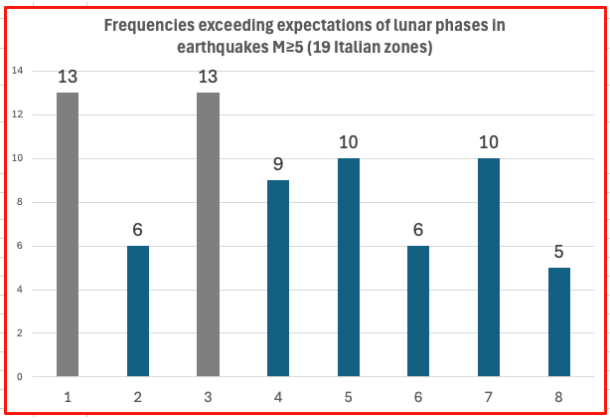

Fig. 3 – Frequencies exceeding expected values for the eight lunar phases in M≥5 earthquakes across the 19 Italian seismic zones. *Phases 1 (New Moon) and 3 (First Quarter) are the most recurrent, each occurring in 13 out of 19 zones (13 occurrences out of 72 total; p=0.0236), confirming the statistical significance of their prevalence relative to the other phases.*

3.3 Lunar Declinations — National Analysis by Magnitude

Considering the six declination bands (−28°/−20°, −20°/−10°, −10°/0°, 0°/10°, 10°/20°, 20°/28°) and stratifying the data by magnitude (M3–3.6, M3.7–4, M4.1–4.3, M4.4–4.9, M≥5), the one-tailed binomial test (see *supra,* "Summary of p-values by magnitude," column "*One-tailed binomial test on bands −20°/−10°, 10°/20°, p-value <0.05*", Table 7, Section 2.3.1), applied with "success" defined as membership in the −20°/−10° or 10°/20° bands, yields p<0.05 for every magnitude class. These two bands therefore constitute the only declination ranges showing consistent, cross-magnitude statistical significance, forming the most robust core of the national-scale signal. Alongside this stable core, some magnitude classes show additional excesses in other bands (e.g., 20°/28° for M3.7–4 earthquakes), but these anomalies are not persistent across all classes and do not weaken the *systematic prominence of the two central bands (−20°/−10° and 10°/20°). These two intervals represent a clear domain of statistical anomaly for all magnitudes and, in particular, for M≥5 events,* which exhibit concentrations exceeding 2σ relative to a uniform distribution. As an internal consistency check, counting the number of bands that exceed the expected uniform value within each magnitude class (regardless of which bands they are) shows that, on average, approximately *45% of earthquakes across magnitude classes fall within the −20°/−10° and 10°/20° bands.* This confirms the presence of a diffuse national signal; however, the decisive methodological result remains that of the targeted binomial test*: the concentration of earthquakes of all magnitudes in the −20°/−10° and 10°/20° declination bands is significant (p<0.05)* and represents the *dominant national-scale declination pattern* associated with seismic triggering.

3.3.1 Regional Analysis by Geographic Zone (M≥5)

While at the national scale the −20°/−10° and 10°/20° declination bands are systematically significant across all magnitude classes, the analysis conducted at the level of individual epicentral zones for the strongest events (M≥5) yields a more selective and less uniform pattern. The strength of the signal decreases as the number of available events diminishes, and not all areas exhibit statistically meaningful behavior Applying the one-tailed binomial test (see *supra*, "*Summary p-value – by area*", column "*One-tailed binomial test on predefined belt 10°/20°*", Table 8, Section 2.3.3) to the predefined 10°/20° band, *only 2 of the 19 zones exceed the significance threshold (p<0.05): Valnerina and Molise–Irpinia–Sannio*, both showing a clear excess of earthquakes within the same central band identified at the national level. Aggregating data across all 19 zones yields 15 zones (compared to an expected ~9 under uniformity) in which the 10°/20° declination band contains more M≥5 earthquakes than expected. The binomial test (see *supra*, "*P-value declination 1 band*", Table 8, Section 2.3.3) confirms that this concentration is statistically significant (p=0.0199) for the 10°/20° band alone. A similar result is obtained for the combined −20°/−10° and 10°/20° bands (see *supra*, "*P-value declination 2 bands*", Table 8, Section 2.3.3), with 9 and 15 zones, respectively, exceeding expected counts (p=0.037). Although these findings reinforce *the central role of the −20°/−10° and 10°/20°* bands, not all zones replicate the same pattern. In several local contexts, other bands also emerge: for example, the 20°/28° interval shows an excess in the Milanese–Veronese area (see *supra*, "*Summary p-value – by area," column "Concentration 1.9/2σ*", Table 8, Section 2.3.3). In other zones, the observed frequency reaches or exceeds the 2σ threshold, though not always within the same declination range. This indicates that magnitude-based statistics and zone-based statistics are not perfectly superimposable, even though they share a common core of coherence. It should also be noted that several areas—such as Torinese, Anconetano, and Alta Valtiberina—do not exhibit statistically significant concentrations in any declination band (see *supra*, "*Summary p-value – by area*", column "*P-value (ranges with observed >expected) Relevant lunar declinations*", Table 8, Section 2.3.3). In these cases, the signal may be obscured by the limited number of historical earthquakes, although

ISSN number; ISSN 2202-0039

a genuine absence of local correlation cannot be ruled out. *Overall, 78% (15/19) of the Italian epicentral zones show a higher-than-expected concentration of M≥5 earthquakes in the 10°/20° lunar declination band.*

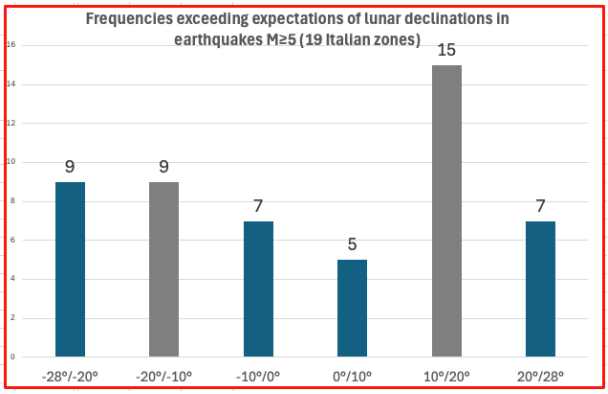

Fig. 4 – Frequencies exceeding the expected values for the six lunar declination bands in M≥5 earthquakes across the 19 Italian seismic zones. *The 10°/20° band is the most recurrent, appearing in 15 out of 19 zones of Italy (p=0.0199), confirming the statistical significance of its predominance.*

Although the detailed behavior varies from zone to zone, the general tendency confirms that intermediate declinations represent the astronomical conditions most frequently associated with seismic triggering—fully consistent with the patterns observed at the national scale. The agreement between the two perspectives—by magnitude and by zone—supports the interpretation that lunar modulation of strong earthquakes (M≥5) in Italy operates preferentially through intermediate declinations, *particularly within the −20°/−10° and 10°/20° bands, which emerge as statistically significant domains both nationally and in several individual epicentral areas.*

3.4 Marginal Distribution of Earthquakes by Lunar Phase and Magnitude

Building on the dataset described in the Methods (see supra, Section 2.3.1), the Author conducted two complementary analyses to identify additional relationships between lunar phase and the occurrence of *7,948 Italian earthquakes (1600–2024)*, grouped into magnitude classes.

3.4.1 Excess Percentages — Analysis by Lunar Phase

For each lunar phase, the percentage distribution of earthquakes within each magnitude interval was calculated, isolating only those magnitude classes whose seismic frequency exceeded the average distribution for that same lunar phase. This approach highlights the phases in which seismicity is statistically elevated for specific magnitude ranges. The 468 strongest earthquakes (M≥5) cluster primarily in phases 3, 5, 6, 7, and 8, with corresponding excesses of +2.3%, +2.7%, +1.0%, +1.1%, and +1.3% above the expected mean. These findings indicate an increased occurrence of high-magnitude events during the *First Quarter, Full Moon, and Last Quarter*—periods of the synodic cycle associated with strong variations or maxima in the tidal potential. See Fig. 5 and Table 9.

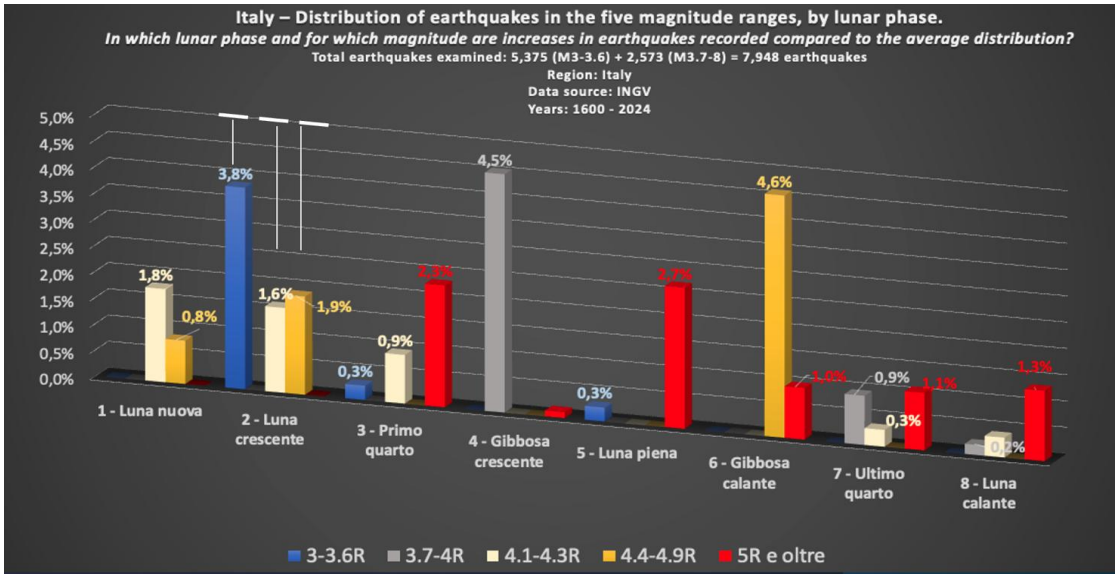

Fig. 5 – **Percentage distribution of Italian earthquakes (1600–2024) by magnitude and lunar phase.** *The figure shows the excess frequency of earthquakes in each magnitude range relative to the expected mean distribution for each lunar phase.*

Table *9 - Calandra, . dr S. (2025). Percentages of excess - Analysis by lunar phase [Data set]. Zenodo. https://doi.org/10.5281/zenodo.17427852*

3.4.2 Excess Percentages — Analysis by Magnitude

For each magnitude class, the distribution of

ISSN number; ISSN 2202-0039

earthquakes across the eight lunar phases was computed, identifying only the phases in which the observed frequency exceeded the overall mean frequency of that magnitude class across the synodic cycle. The resulting figure reports the percentage excess above the expected value, allowing identification of the most recurrent phases for each energy level. For the 468 strongest earthquakes (M≥5), a clear concentration emerges in phases 1, 3, 5, and 7, with increases of +4.6%, +3.3%, +2.2%, and +1.8%, respectively, confirming the predominance of the *New Moon, First Quarter, Full Moon, and Last Quarter.* See Fig. 6 and Table 10.

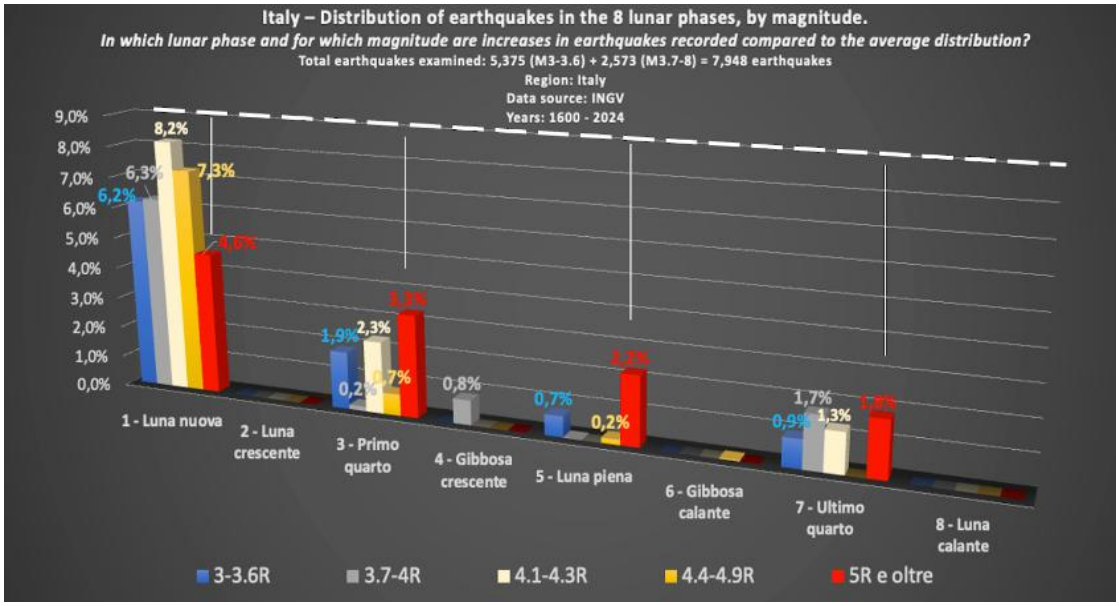

Fig. 6 – **Percentage distribution of Italian earthquakes (1600–2024) by magnitude and lunar phase.** *The figure shows the excess frequency of earthquakes in each magnitude class relative to the mean distribution across the eight lunar phases.*

Table *10 - Calandra, dr S. (2025). Percentages of excess - Analysis by magnitude [Data set]. Zenodo. https://doi.org/10.5281/zenodo.17427882*

3.4.3 Excess Percentages — Combined Analysis

A direct comparison of the two figures reveals the lunar phases in which excesses appear simultaneously in the two analytical frameworks:

- M≥5 earthquakes show parallel increases in phases 3 (First Quarter), 5 (Full Moon), and 7 (Last Quarter).
- Magnitude 4.4–4.9 shows concurrent increases in phases 1 (New Moon) and 3 (First Quarter).
- Magnitude 4.1–4.3 presents enhanced frequencies in phases 1, 3, and 7, consistent with the trend observed for higher magnitudes.
- For M3.0–3.6, phase 2 (Waxing Crescent) exhibits an excess of approximately +3.8% in Fig. 5, indicating a distinct behavior: during this phase—corresponding to a minimum in the tidal-stress gradient between conjunction and the first quadrature—seismicity is lower in magnitude but more recurrent, consistent with low-amplitude, high-frequency tidal-stress oscillations.

These recurrent patterns, stable over more than four centuries, indicate a statistically structured behavior unlikely to arise by chance and point to the existence of temporal windows of elevated seismic probability.

These findings are consistent with physical analyses of the tidal-stress gradient, according to which the New Moon, First Quarter, and Full Moon correspond to intervals of maximal variation in the gravitational potential [2] [8] [9]. By contrast, phase 2 (Waxing Crescent), where the gradient reaches a relative minimum, exhibits lower-magnitude yet more recurrent seismicity, consistent with low-intensity tidal-stress oscillations. This relationship between tidal forcing and seismic response is further explored (see *infra*, Section 4.2).

3.5 Forecasting Seismic Risk Zones for 2026–2027 (M≥5)

Using the same methodology previously outlined (see *supra*, Section 2.2.6), the Author applied the nodal-cycle calculation scheme in forward projection, taking 2026 and 2027 as target years. For each of the 19 Italian epicentral zones, the historical M≥5 earthquakes were compared with the two target years, examining whether their temporal separations corresponded to integer or half-integer multiples of the lunar nodal cycles. The one-tailed binomial p-value quantifies the probability that the observed alignments with the 9.3- and 18.6-year cycles occurred by chance. Values of $p<0.05$ indicate a statistically significant periodicity, and hence a potential nodal resonance for the target year. The summary table (see *supra,* file *Lunar_node_precession_summary_M5_prediction_202*

ISSN number; ISSN 2202-0039

6-2027.xlsx, Section 2.2.5, Table 5), also visualized in Fig. 7, reports for each zone:

- whether a significant nodal resonance is present ($p<0.05$);
- the type of periodicity detected (9.3 or 18.6 years);
- the historical reference cycle (ancient, recent, complete, or fragmentary);
- and the predictive indicator (yellow marker for ancient or short cycles; bold for long, recent, or well-established cycle.

Lunar node precession - forecast for 2026 M≥5

Zone n.	geographical area	Possible EQ 2026 M>5	resonance with a cycle of at least 100 years	type of periodicity	P-value
1	AQ e Marsica	si	recent cycle 1804–2017	9,3	0,026
2	Stretto Messina	no			×
3	Garfagnana	no			×
4	Valnerina	si	long cycle 1730–1916	18,6	0,0088
5	Molise Irpinia Sannio PZ	no			×
6	Fiorentino Mugello	yes	ancient cycle 1504–1804	18,6	0,035
7	Asolano Cansiglio	no			×
8	Milanese Veronese	yes	ancient and short cycle 1693–1876	18,6	0,0019
9	Sicilia	no			×
10	Val di Paglia Val d'Orcia	no			×
11	Parma Modena Em Rom	no			×
12	AltaValtiberina	yes	ancient and short cycle 1504–1689	18,6	0,011
13	Forlivese Riminese	no			×
14	Basilicata Pollino	yes	ancient cycle 1693–1894	18,6	0,016
15	Calabria	yes	short ancient cycle 1767–1821	18,6	0,009
16	Anconetano Ascolano	yes	recent short cycle 1951–2013	18,6	0,011
17	Friuli	no			×
18	Gargano	no			×
19	Torinese	no			×

Lunar node precession - forecast for 2027 M≥5

Zone n.	geographical area	Possible EQ 2027 M>5	resonance with a cycle of at least 100 years	type of periodicity	P-value
1	AQ e Marsica	yes	recent cycle 1804–2017	9,3	0,0002
2	Stretto Messina	no			×
3	Garfagnana	no			×
4	Valnerina	yes	**FULL CYCLE 1246 - 2016**	9,3	0,045
5	Molise Irpinia Sannio PZ	yes	long cycle 1561–2013	9,3	0,046
6	Fiorentino Mugello	yes	ancient cycle 1470–1812	18,6	0,021
7	Asolano Cansiglio	no			×
8	Milanese Veronese	yes	**FULL CYCLE 1065 - 1951**	18,6	0,023
9	Sicilia	no			×
10	Val di Paglia Val d'Orcia	yes	ancient and short cycle 1802–1861	18,6	0,011
11	Parma Modena Em Rom	yes	ancient cycle 1411–1600	18,6	0,035
12	AltaValtiberina	yes	ancient and short cycle 1489–1694	18,6	0,088
13	Forlivese Riminese	no			×
14	Basilicata Pollino	no			×
15	Calabria	yes	short ancient cycle 1767–1824	18,6	0,017
16	Anconetano Ascolano	no			×
17	Friuli	no			×
18	Gargano	yes	ancient cycle 1627–1841	9,3	0,05
19	Torinese	no			×

Fig. 7 – Lunar node precession: forecast of seismic zones M≥5 for the years 2026–2027. *Summary of the one-tailed binomial test ($p<0.05$) applied to the 19 Italian epicentral zones, showing areas in nodal resonance with the lunar precession cycles of 9.3 and 18.6 years.*

Forecast for 2026: the zones showing statistically significant periodicity ($p<0.05$) and resonance with either the 9.3- or 18.6-year cycles are: AQ and Marsica, Valnerina, Fiorentino–Mugello, Alta Valtiberina, Basilicata–Pollino, Calabria, Anconetano–Ascolano, and Milanese–Veronese.

Among these, *AQ and Marsica, Valnerina, Fiorentino–Mugello, and Basilicata–Pollino* exhibit resonance with long or complete nodal cycles, active for more than a century, providing the strongest predictive reliability. The remaining zones—Alta Valtiberina, Milanese–Veronese, Anconetano–Ascolano, and Calabria—display resonance with older or partial cycles (yellow symbols in Fig. 7), suggesting a lower likelihood of reactivation during 2026–2027 under this astronomical model.

Forecast for 2027: the zones most consistent with significant nodal cycles are: AQ and Marsica, Valnerina, Molise–Irpinia–Sannio, Fiorentino–Mugello, Milanese–Veronese, Val di Paglia–Val d'Orcia, Parma–Modena–Emilia, Alta Valtiberina, and Calabria. Among these, the strongest candidates—those aligned with long, well-established nodal cycles—are: *AQ and Marsica, Valnerina, Molise–Irpinia–Sannio, Fiorentino–Mugello, and Milanese–Veronese*. These zones present the most robust evidence of potential reactivation in 2027, according to the nodal-precession model. The remaining zones show resonance with older or incomplete cycles and should therefore be considered *secondary* or *lower-significance* candidates.

Applying the nodal-precession model to the two target years 2026–2027 identifies, through a uniform and statistically verifiable procedure, *a restricted set of*

ISSN number; ISSN 2202-0039

Italian zones with potential for M≥5 seismic reactivation during the 2026–2027 biennium. These zones are concentrated *primarily along the central and southern Apennines*, where resonance with the 9.3- and 18.6-year lunar nodal cycles appears most stable and persistent for the forecast years.

3.6 Lunar Declination and Lunar Phases — Campi Flegrei Analysis by Magnitude

The Campi Flegrei area (Zone 20), which lacks the historical depth available for the other 19 zones, was analyzed separately by including all earthquakes with M≥3 recorded between 1984 and 4 October 2025 (see *supra*, Section 2.3.3). Applying the same one-tailed binomial methodology used in the national analysis (see supra, Sections 3.2–3.3), the Author evaluated which lunar declination bands and lunar phases exhibit frequencies exceeding those expected under a uniform distribution.

For lunar declinations, the three most populated bands (−28°/−20°, −20°/−10°, and 20°/28°) account for 68% of all events. The one-tailed binomial test (see *supra*, "Summary of p-values by area", Table 8, Section 2.3.3) yields a significant result (p=0.014), indicating that the observed excess is incompatible with a random distribution. Although this declination pattern does not coincide with the two central bands (±10°–20°) that dominate the national behavior, the statistical significance nonetheless suggests the presence of a non-random local modulation consistent with a tidal influence acting on the shallow geothermal system of the area.

Regarding lunar phases, the five most frequent ones—3 (First Quarter), 4 (Waxing Gibbous), 5 (Full Moon), 6 (Waning Gibbous), and 7 (Last Quarter)—collectively account for 79% of all M≥3 earthquakes. Here too, the one-tailed binomial test is significant (p=0.013), confirming that the distribution of events along the synodic cycle is not uniform. Unlike the national-scale pattern, which is dominated by the four cardinal phases (1, 3, 5, 7) and in particular by the New Moon, the Campi Flegrei anomaly extends across the interval from First Quarter to Last Quarter, indicating a broader local response that is plausibly influenced by the high sensitivity of the hydrothermal system to periodic variations in the stress field. Overall, the Campi Flegrei area exhibits statistically anomalous behavior for both lunar declinations and lunar phases, with p<0.05 in both cases, confirming the presence of a robust local tidal signal that is distinct from the national pattern.

4. Discussion

4.1 Methodological Coherence and Analytical Criteria

This study examined the temporal and spatial distribution of Italian seismicity from 1600 to 2024, structuring the investigation across three complementary analytical levels, each defined by its spatial scale and magnitude threshold (see *supra*, Sections 2.2 and 2.3).

1. *The first level concerns lunar-phase analysis* at the national scale for events with M≥3. A total of 7,948 earthquakes were evaluated to determine whether the synodic cycle of 29.53 days modulates seismic frequency and whether the eight lunar phases—partitioned proportionally according to their astronomical durations—correspond to statistically significant variations in seismic rate. This approach specifically focuses on identifying phases associated with the largest tidal-stress gradients (phases 1, 3, 5, 7) and possible intervals of relative stability (phases 2, 6).

2. *The second analytical level investigates lunar declination*, carried out both nationally and zonally, and applied to earthquakes with M≥3 and M≥5. At the national scale, all M≥3 events were analyzed to determine whether seismicity congregates within specific declination bands (−28°/−20°, −20°/−10°, −10°/0°, 0°/10°, 10°/20°, 20°/28°). At the zonal scale, only M≥5 earthquakes were considered across the 20 epicentral areas (the 19 historical zones plus the experimental Campi Flegrei zone) to test whether the declination preferences observed nationally persist within individual geotectonic contexts. This two-tiered analysis makes it possible to explore how the Moon's position relative to Earth's equator influences local and regional seismic responses, particularly during periods when the vertical component of the tidal vector undergoes rapid variation.

3. *The third analytical level concerns nodal precession at long temporal scales*, applied exclusively to M≥5 events within the 19 historical zones (excluding Campi Flegrei, which lacks an adequate historical series). The recurrence of strong earthquakes was examined with respect to the 9.3- and 18.6-year lunar nodal cycles. Periodicity was assessed through one-tailed binomial testing and comparison with random distributions, with the aim of detecting non-random cyclic behavior in the historical earthquake sequences.

An integrated analysis subsequently compared the results across the three scales—synodic (lunar phase), declinational (lunar position), and nodal (precession)—to evaluate the internal coherence of the model and possible convergence among seismic-frequency maxima. *This tripartite methodological framework allows short-term effects associated with synodic and declination dynamics to be distinguished from long-term modulations imposed by nodal precession*, producing a gravitational model that, while complex, remains statistically consistent. The subdivision of the synodic month into eight lunar phases follows an astronomically grounded scheme based on the phase durations reported by NASA lunar calendars [25] (2019) and the computational algorithms of Meeus [26] (1998) and Pander [28] (2020). Rather than adopting only the four cardinal phases—or, conversely, excessively fine partitions lacking physical meaning—the use of eight

ISSN number; ISSN 2202-0039

phases provides a higher-resolution representation of the dynamic transitions between tidal-stress maxima and minima, enhancing the ability to detect seismic modulation associated with rapid changes in gravitational gradients.

4.2 Physical Interpretation: Tidal Forces, Lunar Phases, Lunar Declination, and Nodal Cyclicity

In 13 of the 19 geographic zones examined, the results (see supra, Section 3.2.1) show that M≥5 earthquakes cluster systematically around the New Moon and First Quarter, indicating that periods of maximum synodic tidal-stress gradient correspond to times of heightened seismic probability. At the national scale, lower-magnitude earthquakes (M 3–4.9) display a more complex pattern but still exhibit modulation along the synodic cycle: Phase 1 shows >2σ concentrations (see *supra*, Section 3.2) for intermediate magnitudes (<M5), whereas phases 3, 5, and 7 show decreasing contributions for M≥5 events (see *supra*, Section 3.4.3). Similarly, this study demonstrates that the intermediate lunar-declination band (−20°/−10° e 10°/20°) represents a strong and persistent statistical anomaly across all magnitudes—and especially for M≥5 earthquakes (see *supra*, Section 3.3)—with concentrations exceeding 2σ relative to a uniform distribution ($p<0.05$). At the zonal level, the central declination band (−20°/−10° e 10°/20°) remains prominent, with 15 of 19 zones exhibiting M≥5 frequencies above expectation, even though not all regions show the same pattern (see *supra,* Section 3.3.1). Finally, nodal-precession analysis reveals that the temporal sequence of strong earthquakes cannot be explained as random, but reflects a stable, long-term periodic structure (see *supra*, Section 3.1). In 16 of the 19 zones, p-values for the 9.3- and 18.6-year cycles fall below 0.05, confirming that seismic recurrence aligns with lunar nodal periodicities. Some areas display particularly clear multi-cycle coherence. Taken together, these findings indicate a physically grounded statistical correlation, in which the significance of the observed patterns is consistent with a physical model governed by the rate of change of the tidal potential ($|d\tau/dt|$), a dynamic parameter widely recognized in the literature as relevant to crustal stress response.

4.2.1 Tidal Forces and Lunar Phases

This regularity confirms the presence of a stable and structured statistical signal, consistent with international findings and with what several authors have already proposed [2] [8] [9], namely, that *the gravitational modulation induced by the Moon—rather than its instantaneous position—is the dynamic factor most directly associated with earthquake triggering processes. The physically relevant parameter is therefore not the lunar altitude or declination at the moment of the earthquake, but the temporal variation of the tidal force*, that is, the time derivative of the gravitational stress acting on the crust. The New Moon, First Quarter, and Full Moon phases correspond to the periods of maximum tidal-potential gradient, when the resultant vector of solar and lunar forces undergoes rapid changes either in magnitude (syzygies) or in direction (quadratures). These variations exert their influence not through absolute force levels, but through the gravitational destabilization they impose on the Earth–Moon–Sun system. In this regard, the hypothesis previously advanced by the Author [5]—that earthquakes tend to occur during phases of extreme stability or instability of the gravitational field—proves consistent with the observation that rapid changes in the tidal potential coincide with increased probability of seismic release.

TIDAL STATES AND CORRESPONDENCE WITH LUNAR PHASES

TIDAL STATE	ASSOCIATED LUNAR PHASES	DYNAMIC BEHAVIOUR	OBSERVED SEISMIC CORRELATION
INSTANTANEOUS GRAVITATIONAL STASIS ($d\tau/dt = 0$)	Phase 1 – New Moon Phase 5 – Full Moon	Momentary inversion points of the tidal potential (maxima and minima). The total tide-generating potential reaches its highest and lowest values.	Transition between opposite stress polarities; both sizygies correspond to maximum tidal amplitude.
DYNAMIC TRANSITION ($\|d\tau/dt\|$ maximum)	Phase 3 – First Quarter Phase 7 – Last Quarter	Rapid temporal and directional variation of the lunisolar tidal field between two potential extrema.	Highest probability of stress activation and energy release.
INTERMEDIATE METASTABILITY	Phase 2 – Waxing Crescent Phase 6 – Waning Gibbous	Gradual vector inversion between consecutive sizygies; micro-oscillations of tidal stress.	Recurrent low-magnitude seismicity associated with slow stress modulation.

Fig. 8 – Tidal dynamics and lunar phases. *Relation between the temporal derivative of the tidal potential ($d\tau/dt$), lunar phases, and the observed seismic response. Syzygies (New and Full Moon) mark instantaneous gravitational stasis ($d\tau/dt=0$); quadratures correspond to dynamic transitions ($\|d\tau/dt\|$ maximum); phases 2 and 6 represent intermediate metastable states.*

The results show that seismic likelihood rises both when the standard deviation of the resultant gravitational force (σ^{Rf}) is very low (stasis) and when it is very high (dynamic turbulence) over 24–48 hour windows [5]. *These two extreme conditions—gravitational stasis ($d\tau/dt\approx0$) and dynamic turbulence ($|d\tau/dt|$ at*

maximum)—constitute complementary configurations of crustal instability [2] [7] [29] [30], as illustrated in Fig. 8. The tidal gradient ($d\tau/dt$) represents the time derivative of the lunisolar traction potential, quantifying how rapidly gravitational stress varies across the Earth's crust. The largest values of $|d\tau/dt|$ occur during the quadratures (First and Last Quarter), when the direction of the Sun–Moon resultant changes most rapidly, generating dynamic transitions in the stress field. In contrast, during syzygies (New Moon and Full Moon), the gradient tends toward zero ($d\tau/dt \approx 0$): the system passes through instantaneous points of gravitational stasis corresponding to the maxima and minima of the tidal potential. Both conditions—stasis and transition—define metastable configurations of the crust, in which seismic release may be triggered by minimal variations in the gravitational field or by local perturbations.

"Syzygies and quadratures therefore represent periods of maximal dynamic instability: the former due to gradient inversion, the latter due to maximal gradient change. The brief near-equilibrium intervals preceding or following these transitions may correspond to metastable mechanical states of the crust, conceptually analogous to metastable shear-zone regimes observed in granular systems under cyclic loading [31]. Under such conditions, even small oscillatory perturbations in phase or declination may facilitate earthquake triggering. The statistical asymmetry observed in this study — specifically, the higher concentration of earthquakes in the early synodic phases (see supra, Section 3.4.2—does not imply an intrinsic difference between the two syzygies, but may reflect contingent orbital factors, such as the frequent coincidence of perigee with the New Moon, which temporarily amplifies tidal traction [16] [32] or declination effects (see infra, Section 4.3). In this context, even modest stress variations ($\approx 10^3$ Pa) may become significant relative to tectonic loading rates [33], enabling elastic energy release on faults close to failure. This behavior is consistent with the metastable nature of crustal stress and with the 9.3- and 18.6-year lunar nodal cycles, which modulate long-term conditions of gravitational equilibrium and Earth–Moon resonance, enhancing the regularity of seismic triggering cycles."

4.2.2 Tidal Forces and Lunar Declination

The results indicate that strong earthquakes respond not only to synodic-phase variations but also to horizontal tidal modulation. This behavior is consistent with Dong-Shan et al. (2021) [7], who show that nodal tidal effects and declination oscillations modulate the global stress field, producing dynamically unstable equilibrium conditions at intermediate declinations. Similarly, Hui & Xiaoming (2001) [8] identify these belts (±10°–20°) as the regions of maximum variation in the horizontal gravitational potential, where the combined action of solar and lunar traction reaches its highest degree of directional tidal instability. Observationally, two coherent but distinct seismic response regimes emerge:

1. *Dynamic-turbulence regime ($|d\tau/dt|$ maximum):* This regime characterizes phases 1 (New Moon) and 3 (First Quarter), where rapid variation of both the vertical and horizontal tidal gradients produces a condition of dynamic instability—an effect that is particularly relevant for M≥5 earthquakes.
2. *Gravitational metastability regime ($d\tau/dt \approx 0$):* This regime is associated with intermediate declinations (±10°–20°) and, to a lesser extent, with phases 5 (Full Moon) and 7 (Last Quarter), where the tidal system enters a temporary equilibrium between the components of the tidal vector, making it highly sensitive to small perturbations and favoring the release of moderate-magnitude seismic events.

Tidal States and Correspondence with Lunar Declinations

LUNAR DECLINATION	ORIENTATION OF TIDAL VECTOR	PREDOMINANT COMPONENT	FIELD STABILITY	EXPECTED SEISMIC EFFECT
0° (EQUATORIAL)	Mainly horizontal, parallel to the Earth's equator	Tangential force, symmetric between hemispheres	Stable and balanced	Low seismic activity
±10° – 20° (INTERMEDIATE)	Inclined, rapid directional variation	Comparable horizontal and vertical components	**Metastable (directionally unstable)**	High sensitivity to perturbations; significant clustering of **M ≥ 5** earthquakes
±28° (MAXIMUM)	Nearly vertical	Vertical uplifting force dominant	Stable but asymmetric	Secondary or reduced activity

Fig. 9 – Tidal dynamics and lunar declination. *Summary of how lunar declinations relate to tidal-vector orientation and seismic response. Intermediate declinations (±10°–20°) correspond to metastable gravitational states and show the highest recurrence of strong earthquakes (M≥5)*

The present study shows that *intermediate lunar declinations (±10°–20°)—where the vertical and horizontal components of the tidal vector balance and its direction changes rapidly—represent the most critical*

ISSN number; ISSN 2202-0039

configurations for earthquake triggering. Both regimes are consistent with observational data: M≥5 earthquakes concentrate statistically within the ±10°–20° belts, while lower-magnitude seismicity (<M5) reflects the same tidal modulation in a more diffuse but regular form, confirming the cyclic and metastable nature of the crustal response to lunisolar forcing. Horizontal tidal forcing reaches its maximum when the Moon is at intermediate altitudes above the horizon (roughly 45°–135° zenith distance), corresponding to lunar declinations between ±10° and ±28°. Under these conditions, the tangential component of gravitational stress acting on the crust is maximized.

4.2.3 Tidal Forcing and Lunar Nodal Precession

While both lunar phases and lunar declination follow monthly rhythms—the former describing variations in visible illumination (~29.5 days), the latter describing the oscillation of the Moon with respect to the terrestrial equator—these two cycles are near-synchronous but not perfectly aligned. Their superposition produces a regular alternation of tidal forces that periodically modulates gravitational stress on the Earth's crust. In contrast, lunar nodal precession does not act as an instantaneous factor; rather, it represents a long-term gravitational modulation that controls the amplitude of the monthly declination oscillations and, consequently, the effectiveness of tidal forces in promoting seismic release. Previous studies (see *supra*, Section 2.2) examining the relationship between seismicity and lunar nodal cycles focused mainly on global or regional scales, primarily involving large earthquakes (≥M7) and very long time series. These works identified statistical recurrences at 18.6 and 9.3 years but generally did not disentangle the respective influences of nodal position, declination, and synodic phase. In many cases, the three components—node, declination, and phase—were treated as manifestations of a single tidal periodicity. In the present study, however, they are deliberately analyzed as distinct but interdependent physical phenomena, each characterized by its own timescale and its own degree of influence on crustal stress.

The analysis conducted here (see *supra*, Section 3.1), based on 19 Italian epicentral regions, confirms that in more than 80% of the areas examined (16 out of 19), the temporal recurrence of M≥5 earthquakes is statistically consistent with the 18.6-year nodal cycle, with p-values <0.05. This result suggests that tidal forces do not act randomly but instead follow a multi-decadal gravitational rhythm capable of influencing the long-term average rate of seismic release. In particular, *the regular distribution of the median temporal deviations within each zone, lying close to integer multiples of the nodal cycle, indicates (see infra, Section 4.4) that the crustal response to the lunisolar traction field possesses a stable periodic component linked to the geometry of lunar orbital precession.*

4.2.4 Connection Between Monthly and Nodal Timescales

Compared with previous work, *the methodological advantage of this approach lies in separating the multi-decadal timescale of nodal precession from the monthly cycles of phases and declination.* This distinction makes it possible to identify more clearly the hierarchical levels through which seismic modulation operates. Taken together, the integrated analysis of lunar phases, lunar declination, and nodal precession outlines a gravitational model that remains coherent across multiple temporal scales. The first two components—the synodic and declinational cycles—modulate seismicity on short timescales, producing cyclical variations in crustal stress and in the likelihood of earthquake triggering; the third component, the nodal cycle, governs long-term recurrence by modulating the frequency and amplitude of seismic activation, effectively synchronizing the Earth's seismic response with the gravitational rhythms of the Earth–Moon system. This distinction between monthly and multi-decadal scales is not an artificial separation but the expression of a single multicomponent physical process in which the tidal gradient and nodal precession act as complementary forcings within the same stress field. It is from this interaction that the dual periodicity observed in the present study emerges: a short-term, cyclic, locally modulating pattern, and a long-term, regular, structuring pattern—both ultimately linked to a common gravitational mechanism.

Monthly-scale information (synodic phases) and multi-decadal/century-scale information (nodal precession) therefore appear coherent and mutually reinforcing. Phases 1–3–5–7 identify intra-monthly windows of elevated probability (driven by variations in the tidal gradient), whereas the 9.3-/18.6-year nodal periodicity identifies inter-annual windows in which the temporal recurrence for a given seismic zone is highest. Where the two signals converge—e.g., when an M≥5 earthquake occurs in a zone that shows p<0.05 in the nodal test for the target year and simultaneously shows statistical significance in phases 1–3–5–7 under the one-tailed binomial phase test—the confidence level increases, suggesting the potential for probabilistic forecasting models grounded in physically connected but temporally distinct scales. Where all three astronomical signals converge—i.e., when an M≥5 earthquake occurs in a zone with p<0.05 in the nodal test for the target year, within statistically significant lunar phases (1–3–5–7), and within the most recurrent declination belts (±10°–20°)—the confidence level increases further, *indicating the feasibility of developing multi-parameter probabilistic forecasting approaches* based on physically related but scale-separated temporal drivers.

A representative example is the Valnerina earthquake of 24 August 2016 (M6.0, 01:36:32), which occurred simultaneously in lunar phase 7 (Last Quarter) and within the 10°–20° declination band—the two most frequent intervals for that area (see *supra*, "Summary p-value – by area", column "One-tailed binomial test on predefined

phases (lunar phases 1, 3, 5, 7)", Table 8, Section 2.3.3). Furthermore, the same event is in nodal resonance (p=0.004024) with the Valnerina 1941–1998 cycle (see *supra,* Section 2.2.2), confirming the coherence between the 18.6-year periodicity and the observed triggering conditions. This triple convergence—synodic, declinational, and nodal—constitutes strong evidence for an astronomical modulation of the crustal stress field, where short-, medium-, and long-term contributions interact to transiently amplify the likelihood of seismic release. This multiscale coherence—from monthly modulation by lunar phases and declination to the multi-decadal cyclicity of nodal precession—finds additional support at even shorter scales in the author's previously published results [5]. That study demonstrated that the overall gravitational configuration of the Solar System, including the Sun, Moon, and planets, produces brief but critical temporal windows (24–48 hours) characterized by extreme stability or instability in the resultant gravitational field (σ^{Rf}). These intervals, corresponding to the maxima and minima of the tidal gradient ($|d\tau/dt|$), statistically coincide with the occurrence of energetic earthquakes. This confirms that *seismic triggering is governed by a hierarchy of gravitational resonances operating across nested temporal scales:*

- long-term: 18.6- and 9.3-year nodal precession cycles,
- medium-term: monthly synodic and declinational cycles,
- short-term: daily or multi-day planetary and lunar configurations.

All operate through the same physical mechanism—the alternation between phases of gravitational turbulence and gravitational stasis—which modulates the crustal stress field and shapes the temporal windows of highest seismic probability.

4.3 Interpretation of Results and Statistical Relevance of Critical Lunar Phases

The analyses performed at national and regional scales (see supra, Section 3.2), together with the magnitude- and phase-resolved examination (see supra, Section 3.4), converge in showing that the seismic distribution across the synodic cycle is not uniform but is systematically modulated in accordance with the phases that exhibit the strongest tidal-stress variations. The two sections differ, however, in scope and magnitude threshold:

– Section 3.2 considers both the full national seismic archive (1600–2024, M≥3) and a regional assessment limited to M≥5 events, useful for identifying the most responsive epicentral zones;

– Section 3.4 examines the entire national archive (1600–2024, M≥3), focusing on the percentage distribution of earthquakes by magnitude class and lunar phase.

By evaluating deviations above the expected mean, the study compensates for unequal sample sizes and highlights systematic departures for each phase. In this way, Figures 5 and 6 provide two complementary perspectives:

– the first (*phase-based analysis*) identifies the lunar phases in which seismicity clusters for each magnitude range;

– the second (*magnitude-based analysis*) identifies the energy levels that recur most frequently within each lunar phase.

Across both representations, phases 1 (New Moon) and 3 (First Quarter) consistently emerge as the intervals of strongest positive deviation relative to expectation, with $p<0.05$ in all magnitude classes but with >1.9–2σ excesses only for magnitudes <M5 (see *supra*, Section 3.2). For magnitudes ≥5, the regional analysis (see *supra*, Section 3.2.1) shows that phases 1 and 3 are the most recurrent, each appearing in 13 of 19 zones (13 occurrences out of 72 total, p=0.0236), confirming the statistical relevance of their predominance. In addition, the one-tailed binomial test on the predefined phases (1,3,5,7) yields $p<0.05$ in five zones (Abruzzo–Marsica, Valnerina, Molise–Irpinia–Sannio, Fiorentino–Mugello, Sicily). These two results are distinct but complementary: *the first documents how often phases 1 and 3 recur across different seismic areas, while the second quantifies their statistical significance relative to a uniform distribution of the four principal phases.* A key methodological aspect concerns the joint interpretation of the two symmetrical representations in Figures 5 and 6 (see *supra*, Section 3.4.3), both derived from the entire national archive (1600–2024, M≥3). Although they mirror each other in construction, neither reports absolute counts; instead, they show percent deviations from the expected mean of a theoretically uniform distribution. Under random conditions, each of the eight lunar phases would account for 12.5% of events, and each of the five magnitude classes for 20%. Each bar therefore represents the extent to which the observed frequency departs from those baselines, either by phase (Fig. 6) or by magnitude (Fig. 5). Figure 6 highlights, for each magnitude class, the lunar phases where seismicity exceeds the mean expected over the synodic month; conversely, Figure 5 shows the magnitude classes that exceed the expected proportion within each lunar phase. This dual normalization—by phase and by magnitude—*removes biases due to sample size* and reveals structural variations in tidal modulation independent of the absolute number of events. As a result, the adopted method isolates genuine structural patterns in the tidal modulation of seismicity, separating them from fluctuations attributable to sampling. The comparison of Figures 5 and 6 reveals a complex synodic dynamic: intermediate-magnitude earthquakes (M4–4.9) cluster in the early phases of the cycle (1–3, New Moon and First Quarter), whereas stronger events (M≥5) show an initial excess followed by a progressive decrease in frequency toward the Last Quarter (phase 7). In this sense, Figure 5 depicts the overall behavior of the system—the excess above the statistical mean along the synodic month—while Figure 6 captures the transient energetic response of the crust, characterized by an initial peak followed by relaxation (see Fig. 10).

NCGT Journal
New Concepts in Global Tectonics
New Concepts in Global Tectonics Journal
Volume 13, Number 10, December 2025
ISSN number; ISSN 2202-0039

Interpretive Framework for Figures 4 and 5: Statistical and Physical Meaning

Figure	Description of Representation	Physical Interpretation
Fig. 5 – Excess by lunar phase	Shows the percentage excess of earthquakes (of all magnitudes) relative to the mean in each lunar phase.	Highlights the most *statistically active* phases — those with the highest overall seismic occurrence along the synodic month.
Fig. 6 – Excess by magnitude	Shows which lunar phases exhibit a relative over-frequency for a given magnitude class.	Highlights the most *energetically responsive* phases — those where stronger events occur more frequently relative to weaker ones.

Fig. 10 – Summary table comparing the statistical meaning of Figures 5 and 6 (see *supra*, Section 3.4.2). *Figure 5 illustrates overall seismic activity across the lunar month; Figure 6 reflects the energy response of the crust, emphasizing phases associated with relatively stronger events*

The regular sequence 1→3→5→7 (New Moon → First Quarter → Full Moon → Last Quarter) describes a complete cycle of tidal modulation, during which the crust alternates between dynamic-transition phases (quadratures, $|d\tau/dt|$ maxima) and gravitational-stasis phases (syzygies, $d\tau/dt \approx 0$). The statistical asymmetry observed between New Moon and Full Moon (see *supra*, Section 4.2.1) for stronger events M≥4.4 (see *supra*, Section 3.4.2) appears to reflect the interaction of multiple astronomical cycles. *New Moon configurations coincide more frequently with intermediate lunar declinations (±10°–20°),* which (see *supra,* Section 4.2.2) correspond to positions where the horizontal component of tidal traction is maximal and where the temporal gradient $|d\tau/dt|$ undergoes its most rapid changes. Under such conditions, the frequency of stronger earthquakes may increase [7] [8], reflecting higher tangential tidal stress capable of enhancing triggering probability. The data from this study confirm this: within the declination belts −20°/−10° and +10°/20°, New Moon systematically exhibits more events than Full Moon. For intermediate magnitudes (M4.4–4.9), the counts (see *supra*, "decl. phase M4.4" and "decl. phase M5+", Table 10, Section 3.4.2) show 38 and 25 earthquakes in phase 1 versus 16 and 20 in phase 5, with p-values between 0.11 and 0.41 (χ^2 test, 1 df). For M≥5, the corresponding p-values are 0.096 and 0.116, indicating a similar but weaker trend. Although these values do not reach formal significance (α=0.05), *they indicate a consistent prevalence of intermediate declinations (±10°–20°) during New Moon configurations, supporting the hypothesis of a combined effect of synodic phase and declination on tidal gradients and triggering probability.* Overall, the synodic response of the Italian seismic system aligns with tidal theory (see *supra*, Section 4.2.1): *the rate of change of the gravitational potential ($|d\tau/dt|$)—rather than its absolute amplitude—emerges as the dominant physical factor associated with the probability of seismic release.* Triggering probability peaks during phases of rapid tidal-gradient variation and weakens thereafter, reflecting a cyclical modulation of crustal behavior driven by the gravitational forcing of the Sun–Moon system.

4.4 Nodal Precession (9.3 and 18.6 Years) in the 19 Zones

The long-term temporal component further reinforces the overall framework. To assess whether M≥5 earthquakes display a periodicity consistent with the lunar nodal cycles (18.613 and 9.3065 years), a one-tailed binomial test was applied to the distribution of temporal offsets between the most recent earthquakes and the historical events within each zone. A p-value<0.05 indicates a statistically significant, non-random recurrence. Using this test on the temporal differences between the latest (or penultimate) M≥5 event and the historical earthquakes in the same zone, *16 out of 19 areas yielded p<0.05, indicating that the recurrence is not attributable to chance and that nodal periodicity constitutes a robust regional-scale signal.* In several zones—such as AQ and Marsica, Valnerina, Sicily, Molise–Irpinia–Sannio, and Fiorentino–Mugello—the significance is particularly strong, with recurrences matching integer or half-integer multiples of the 9.3/18.6-year cycles. Further validation comes from the analysis of the median of the temporal residuals (normalized to nodal cycles). In nearly all zones, the "median number of cycles" falls within ±0.1 of an integer—an outcome that is difficult to reproduce with random data and that supports the presence of structured periodicity (see *supra*, Section 3.1). In contrast, when events from geographically unrelated areas are aggregated—such as the four synthetic zones constructed using randomization techniques (see *supra,* "Random" sheets, Table 4, Section 2.2.3)—nodal periodicity loses coherence. Using data from 1200–2024, the chronological randomization yields nodal periodicities far from unity (see *supra,* Section 3.1), demonstrating that *artificially merging heterogeneous regions eliminates the cyclic behavior that emerges within individual zones. This*

ISSN number; ISSN 2202-0039

evidence supports the internal coherence of the empirically defined 19 Italian zones, which preserve lunar nodal significance only when analyzed separately, confirming that nodal periodicity is a local, geologically coherent phenomenon rather than a sampling artefact. In several areas—including the Messina Strait, Sicily, Val di Paglia–Val d'Orcia, Alta Valtiberina, Calabria, Gargano, and Molise–Irpinia–Sannio—long temporal cycles (on the order of 200–300 years) or sequences of multiple events satisfying the 9.3/18.6-year periodicity can be identified, indicating a secular persistence of the nodal signal. At the opposite end of the spectrum, Friuli–Venezia Giulia displays a shorter periodicity (~45 years), which represents the lower bound of temporal validity for the model used here: significance remains detectable, but within a more limited temporal window.

4.5 Methodological Differences Between Lunar Phases and Lunar Declination

A relevant methodological distinction concerns the different tests applied to lunar phases and lunar declinations (see *supra,* Section 2). For declinations, the significant belts (−20°/−10° and 10°/20°) remain stable across all magnitude classes, allowing the use of a one-tailed binomial test that yields exact and rigorous p-values. For lunar phases, however, the categories showing significant excess vary with magnitude, requiring the use of the χ^2 test—a more flexible but less stringent approach. The additional mean + 2σ criterion provided an independent visual and numerical check supporting the anomalies detected by both methods. In both cases, *phase 1 (New Moon) and the declination belts ±10° to ±20° emerge as configurations of maximum gravitational instability, reinforcing the coherence of the tidal model across different analytical scales.*

4.6 Methodological Note on Zone 20 – Campi Flegrei

Although the Campi Flegrei area does not contain a classical active fault, it was included experimentally as a 20th zone (see *supra*, Section 2.1) to examine whether hydrothermal microseismicity exhibits statistical correlations with the astronomical parameters analyzed (lunar phases and declinations). Seismicity in Campi Flegrei is dominated by hydrothermal pressurization and shallow volcano-tectonic processes [21]; however, variations in the tidal field can modulate fluid pressures and influence the frequency of minor events. Consistent with this rationale, only the analyses concerning lunar phases and declinations were conducted for this zone, whereas the 18.6-year nodal cycle assessment was not applied due to the absence of a historical time series comparable to that available for the other 19 zones. The results (see *supra*, Section 3.6) show significant p-values for both declinations and synodic phases, with 68% and 79% of events falling within the most populated declination belts and lunar phases, respectively. These findings suggest a potential modulating effect of the tidal cycle on hydrothermal-induced microseismicity, even though the underlying physics differs from tectonic stress accumulation. Consequently, Zone 20 was included as an ancillary case to assess tidal sensitivity in an active hydrothermal system without interfering with the nodal-cycle modelling applied to the 19 tectonic zones. This distinction preserves the separation between the two physical regimes and ensures methodological consistency throughout the study.

4.7 Validation and Predictive Implications of the Nodal Model

Applying the nodal-precession model to both historical and forward-looking datasets confirms that Italian seismicity exhibits a structured cyclic behavior aligned with the gravitational rhythms of the Earth–Moon system. A first indication of internal coherence emerges from the behavior of the median temporal deviations among M≥5 earthquakes within each zone: in all 19 areas, the ratio between these intervals and the 9.3- or 18.6-year cycles lies within ±0.1 of an integer (see *supra*, Section 3.1). This indicates that, regardless of the number or distribution of local earthquakes, most events tend to occur at regular multiples of the lunar nodal cycles. Such regularity—observed in 100% of the zones—suggests *a structural periodicity in Italian seismicity that cannot be explained by randomness and is instead consistent with the lunar nodal cycle. The 18.6-year precession (and its 9.3-year half-cycle) appears to modulate recurring windows of crustal instability and the probability of seismic release.* A second line of validation comes from the one-tailed binomial test, which provides a quantitative measure of statistical significance: 16 of the 19 zones display p-values <0.05, indicating that earthquake recurrence patterns are compatible with a periodic model rather than with a random distribution. The convergence of these two indicators—the median deviations (which reflect the geometric stability of the cycle) and the p-values (which quantify its statistical significance)—provides *dual confirmation of the nodal method and supports its use in forward projections.*

4.7.1 From Nodal Cyclicity to Seismic Forecasting

In this framework, the forecasts for 2026–2027 (see *supra*, Section 3.5) are not a purely theoretical exercise but a natural extension of a temporal structure already verified in historical data. Not all resonances, however, carry the same predictive weight: recent and complete cycles extending over more than a century and confirmed by multiple phase-coherent events offer higher reliability, whereas older or fragmentary cycles (marked with a yellow symbol in Fig. 7) correspond to weaker or historically interesting correlations with limited predictive relevance. Zones in resonance with long and recent cycles—particularly *AQ–Marsica, Valnerina, Calabria, and Fiorentino–Mugello*—can therefore be considered higher-priority areas for the biennium.

Overall, the evidence that Italian seismic sequences conform to regular multiples of the 9.3- and 18.6-year cycles confirms that crustal behavior is modulated by a *repetitive gravitational mechanism* capable of synchronizing, over time, the phases of energy

ISSN number; ISSN 2202-0039

accumulation and release. This behavior—verified across multiple centuries—provides a *physical basis for probabilistic forecasting models* grounded in measurable astronomical laws and in a statistically coherent relationship between nodal cyclicity and historical seismicity. Although the model does not specify exact dates, identifying 24-month windows for individual areas yields useful information for applications such as:

- territorial planning and earthquake engineering
- risk assessment and insurance modeling
- preventive management of critical infrastructure (transport networks, dams, energy systems).

Importantly, the term "risk zone" does not imply that an event is imminent, but that the gravitational configuration is in resonance with past cycles of seismic release. *The actual occurrence of an earthquake also depends on the accumulated elastic strain on a fault*—an energy parameter for which systematic and direct indicators are still lacking. Giulio Riga's Previsio model [34] attempts precisely to estimate this energetic component—the seismic charge state of Italian faults—yet it does not currently allow the critical threshold to be determined with certainty.

In this context, nodal resonance provides an astronomical probability framework that can be integrated with local physical models (such as Previsio) to construct a dynamic and probabilistic assessment of seismic risk. Integrating these two layers—gravitational periodicity and local energy state—represents a key step toward developing future probabilistic forecasting models with a physical basis, capable of describing seismic behavior in a coherent and testable way. The methodological robustness of the nodal-precession model, already supported by randomization tests (see *supra,* Section 4.4) that yielded non-significant medians (indicating the absence of spurious periodicity), strengthens the validity of the proposed forecasts. The empirical verification of the 2026–2027 outcomes will serve as a practical benchmark for evaluating the predictive capability of the nodal model for M>5 earthquakes, thereby contributing to the consolidation of an astronomical, probabilistic approach to seismic forecasting.

4.8 Interpretative Synthesis – Toward an Integrated Predictive Model

The analyses conducted in the previous chapters show that the three principal astronomical signals—lunar phases, declination, and nodal precession—describe distinct yet coherent hierarchical levels of tidal modulation acting on terrestrial seismicity. Synodic phases regulate the monthly distribution of earthquakes; lunar declinations introduce a monthly modulation related to orbital inclination, with a north–south alternation roughly every two weeks; and nodal precession acts as a long-term synchronizing force, governing the recurrence times of major earthquakes. Their interaction defines a multiscale system of gravitational forcings in which seismic probability increases when synodic, declinational, and nodal components align.

This multiscale coherence—from monthly modulation by phases and declination to the multidecadal periodicity of nodal precession—finds further confirmation at even shorter timescales in the author's previous work [5]. That study demonstrated that the global gravitational configuration of the Solar System—including the Sun, Moon, and planets—produces short but critical 24–48-hour windows of extreme stability or instability in the resultant gravitational field (σ^{Rf}). These windows, which may or may not coincide with extrema in the tidal gradient ($|d\tau/dt|$), show statistical correlation with the occurrence of energetic earthquakes. This supports the idea that, on daily scales, *dynamical interactions among the Sun–Moon–planet system can generate transient variations in crustal stress that are independent of the regular lunar cycles, acting as short-term forcings capable of triggering or amplifying seismic release* even outside the main synodic or declinational phases.

Consistent with the *notion that earthquake triggering is governed by a hierarchy of gravitational resonances,* distinct temporal scales emerge:

- *long-term* — nodal precession at 18.6 and 9.3 years, determining secular cyclicity and regional synchronization of major earthquakes;
- *medium-term* — monthly synodic and declinational cycles, modulating the frequency and amplitude of ordinary seismicity;
- *short-term* — daily or multiday planetary and luni-solar configurations defining windows of maximal gravitational instability or stasis.

All these temporal scales act through the same physical mechanism: the alternation of gravitational turbulence and stasis, which transiently modulates the crustal stress field and establishes the critical conditions for triggering. On this basis, it becomes possible to outline an integrated predictive model that combines:

- astronomical dynamics (phase, declination, nodal cycles, and planetary configurations);
- the energetic state of faults, estimated through models such as Previsio;
- continuous statistical verification of the observed recurrences.

Such a multiparametric approach, grounded in verifiable physical relationships, would make it possible to identify future time windows of elevated seismic probability on hourly, monthly, multiyear, and secular scales, while maintaining a quantitatively assessable level of uncertainty. The convergence between historical evidence and the statistical structure identified in this study suggests that tidal and nodal modulations of the Sun–Moon–Earth system constitute a persistent and physically motivated component of regional seismic variability, providing a coherent framework for interpreting the observed cyclic behavior and for developing more rigorous predictive approaches.

5. Conclusions

5.1. Summary of the Main Findings

This study presents the first systematic analysis of Italian seismicity (1100–2024) in relation to the principal

ISSN number; ISSN 2202-0039

lunar astronomical cycles—synodic phases, declination, and nodal precession—using a dataset of 7,948 historical and instrumental earthquakes (M≥3). The results show that earthquake occurrence does not follow a random pattern but instead reflects a regular modulation associated with the tidal rhythms of the Earth–Moon system. At the monthly scale, earthquakes cluster preferentially in the early synodic phases, between New Moon and First Quarter, and in the intermediate declination bands (±10°–20°), which are statistically significant across all magnitude classes. For the most energetic earthquakes (M≥5), this modulation becomes even more pronounced: the +10°/+20° declination band exceeds the 2σ threshold, and New Moon exhibits a marked peak in seismic frequency, followed by a progressive decline through the subsequent phases. These findings are consistent with the physical interpretation adopted in this work: the dynamic parameter most closely associated with seismic release is not the absolute amplitude of the tidal force but *the rate of change in the gravitational potential (|dτ/dt|), which reaches its maximum precisely in the early synodic phases.* In this framework, Italian seismicity appears to be governed by an alternating pattern of enhanced dynamic instability (New Moon → First Quarter) and progressive gravitational re-equilibration (Full Moon → Last Quarter), yielding a physically and statistically coherent modulation across all magnitude classes.

5.2. Physical Meaning of the New Moon / Full Moon Asymmetry

The statistical asymmetry observed between New Moon and Full Moon does not imply an intrinsic difference in tidal amplitude between the two syzygies, which physically generate equivalent forces. Rather, *the asymmetry arises from the combined effect of synodic phase and lunar declination.* The analysis shows that, over the historical period considered, New Moon more frequently coincides with intermediate declinations (±10°–20°)—positions where the tangential component of tidal traction and the temporal variability of the gravitational potential (|dτ/dt|) reach their highest values. Under these conditions, the crust enters a state of dynamic metastability, becoming more sensitive to local perturbations and more prone to seismic release. The observed modulation—an initial peak in seismic frequency at New Moon followed by a gradual attenuation during the subsequent phases—thus reflects not a physical difference between the two syzygies, but *the contingent interaction between the synodic maximum and critical declination bands.* In this sense, the synodic behavior of Italian seismicity represents the periodic response of the crust to the rhythm of the tidal gradient: strongest at the start of the cycle and progressively diminished toward Full Moon and Last Quarter.

5.3. Nodal Cyclicity and Structural Seismic Behavior

At multidecadal scales, the analysis of Italian seismicity reveals a stable cyclicity associated with lunar nodal precession, with periods of 9.3 and 18.6 years. Examination of historical M≥5 earthquake sequences shows that, in 16 of the 19 epicentral zones analyzed, nodal cycles are statistically significant ($p<0.05$), and the median time intervals between consecutive events tend to align with integer multiples of the nodal periods. This recurring structure suggests that *seismic release in Italy is synchronized with the orbital geometry of the Moon and responds to a long-term gravitational rhythm* that modulates—without strict determinism—the probability of occurrence of the most energetic events. Nodal cyclicity thus emerges as a physical–statistical marker of national tectonic periodicity, consistent with global models that identify long-period tidal oscillations as a meaningful component of crustal stress modulation.

5.4. A Hierarchy of Gravitational Resonances

The body of evidence gathered in this study indicates that seismic triggering does not respond to a single tidal cycle, but rather to a hierarchy of gravitational resonances operating across multiple, mutually coherent temporal scales. Daily variations in the combined planetary gravitational force *[5], the monthly oscillations associated with the lunar synodic and declination cycles, and the multidecadal modulation imposed by nodal precession together form an integrated system of tidal influences that synchronize the seismic response of the Earth's crust.* Although these resonances act with different amplitudes and on different timescales, they appear governed by a common physical principle: *the crust responds not primarily to the absolute magnitude of the lunisolar traction, but to the rate of change in the gravitational potential (|dτ/dt|), which determines the prevailing state of dynamic turbulence or stability in the stress field*. When several gravitational cycles — planetary, synodic, and nodal — enter constructive phase, the Earth system approaches a state of critical metastability in which even minor perturbations may trigger seismic release. In this perspective, seismicity emerges as the periodic expression of a broader, multilevel gravitational dynamics that links the Earth to the larger planetary system.

5.5. The Case of the Campi Flegrei

The supplementary analysis performed on the microseismicity of the Campi Flegrei caldera—although representing a geophysical system distinct from tectonic seismicity—shows *that active hydrothermal systems can also respond to tidal modulation.* Earthquakes of M≥3 recorded within the caldera exhibit significant clustering in the most frequent declination bands (68%) and in the most recurrent synodic phases (79%). These results suggest that *variations in the tidal field may modulate the instability of the hydrothermal system* when the internal pressure of the caldera is elevated, creating preferential temporal windows for microfracturing within the porous medium.

However, due to the non-tectonic nature of the phenomenon and the short duration of the available time series, this behavior cannot be interpreted in terms of nodal cyclicity and does not influence the validation of the

predictive model applied to the 19 tectonic zones. The Campi Flegrei case therefore serves as an ancillary application of the methodology, illustrating how complex geothermal systems may also exhibit tidal sensitivity, while maintaining physical dynamics that are fundamentally independent from tectonic faulting.

5.6. Implications for Probabilistic Forecasting

Lunar and nodal periodicities modulate seismicity in a statistically predictable manner, providing a physical–statistical foundation for developing multiscale probabilistic forecasting models. When integrated with local estimates of fault energy state (as in Giulio Riga's *Previsio* model [34]) these results could support the construction of dynamic risk maps that identify time windows of elevated seismic instability without implying deterministic predictions of date or hour. Looking ahead, the combination of measurable astronomical parameters, GNSS data, and geophysical stress indicators (radon emissions, magnetic variations, slow deformation signals) may form the basis of a new applied "terrestrial astro-seismology," capable of quantitatively describing the relationship between external gravitational dynamics and the internal seismic response of the crust.

5.7. Limitations and Research Outlook

This study does not propose a deterministic causal mechanism; rather, it demonstrates a robust physical–statistical correlation: the recurring astronomical statistical signals (phases, declinations, nodes) are physically justified by the behavior of the tidal gradient and its capacity to modulate states of crustal instability or relaxation. Although the results are statistically strong, the model requires further testing at both local and global scales, integrating independent datasets (GNSS, radar interferometry, crustal deformation, geoelectrical variations). *The next step is the development of an operational multiscale model* that incorporates external gravitational oscillations alongside the internal dynamics of the regional stress field. From an applied perspective, these findings open the possibility of creating real-time probabilistic seismic risk maps that quantify the temporal criticality level of major Italian faults. Such tools would complement—rather than replace—traditional energetic and seismological models, offering a physically grounded temporal dimension for seismic hazard evaluation.

Acknowledgement

We thank for the support to this Research, provided with numerous suggestions, especially: Carlo Doglioni (former president of INGV), Paolo Gasperini (Department of Physics, Geophysics Sector, University of Bologna), Luigi Cavaleri (ISMAR - CNR, Venice, Italy), Francesco Celani, (INFN, Frascati, Italy), Daniele Cataldi, LTPA Observer Project group. We thank for meticulous checking of the text Roberto Pigro (MD, PhD Università degli Studi di Udine, Cipro). Finally, we thank for supporting my public interventions the mathematician Claudio Pace (Terni, Italy).

Funding Information

This study was not financially supported by any institution.

Author's Contributions

All authors read and approved the final manuscript.

References

[1] M. Caputo and G. Sebastiani, "Time and space analysis of two earthquakes in the Appennines (Italy)," *NS*, vol. 03, no. 09, pp. 768–774, 2011, doi: 10.4236/ns.2011.39101.

[2] S. Ide, S. Yabe, and Y. Tanaka, "Earthquake potential revealed by tidal influence on earthquake size–frequency statistics," *Nature Geosci*, vol. 9, no. 11, pp. 834–837, Nov. 2016, doi: 10.1038/ngeo2796.

[3] A. Carpinteri and O. Borla, "Acoustic, electromagnetic, and neutron emissions as seismic precursors: The lunar periodicity of low-magnitude seismic swarms," *Engineering Fracture Mechanics*, vol. 210, pp. 29–41, Apr. 2019, doi: 10.1016/j.engfracmech.2018.04.021.

[4] D. Zaccagnino, F. Vespe, and C. Doglioni, "Tidal modulation of plate motions," *Earth-Science Reviews*, vol. 205, p. 103179, June 2020, doi: 10.1016/j.earscirev.2020.103179.

[5] Stefano Calandra and Daniele Teti, "Correlation Study: Triggering and Magnitude of Earthquakes in Italy (≥M4.3) in Relation to the Positions and Gravitational Forces of the Sun, Moon, and Planets Relative to Earth," pp. 25–62, Mar. 2024, doi: 10.5281/ZENODO.17726553.

[6] A. A. Gusev, "On the reality of the 56-year cycle and the increased probability of large earthquakes for Petropavlovsk-Kamchatskii during the period 2008–2011 according to lunar cyclicity," *J. Volcanolog. Seismol.*, vol. 2, no. 6, pp. 424–434, Dec. 2008, doi: 10.1134/S0742046308060043.

[7] Dong-Shan, Y., Yu-Ping, G. & Hu, H. Correlation between lunar node tide and great earthquakes. Appl. Geophys. 18, 1–8 (2021). https://doi.org/10.1007/s11770-020-0834-, "Correlation between lunar node tide and great earthquakes", doi: https://doi.org/10.1007/s11770-020-0834-6.

[8] H. Hui and L. Xiaoming, "Research on Correlation of Positions of Celestial Objects with Earthquakes," *Natural Hazards*, vol. 23, no. 2/3, pp. 339–348, 2001, doi: 10.1023/A:1011115708096.

[9] S. Kilston and L. Knopoff, "Lunar–solar periodicities of large earthquakes in southern California," *Nature*, vol. 304, no. 5921, pp. 21–25, July 1983, doi: 10.1038/304021a0.

[10] I. N. Huda and J. Souchay, "Study of the relation between luni-solar periodicities and earthquake

events," Apr. 10, 2021, *arXiv*: arXiv:2104.04872. doi: 10.48550/arXiv.2104.04872.

[11] Shirokov, V.A, "The 18.6-Year Lunar Cycle and Earthquake Forecasting," *Mörner, N.A. (Ed.), Earthquake Prediction and Precursors. Springer-Verlag, pp. 232-245.*.

[12] J. E. Vidale, D. C. Agnew, M. J. S. Johnston, and D. H. Oppenheimer, "Absence of earthquake correlation with Earth tides: An indication of high preseismic fault stress rate," *J. Geophys. Res.*, vol. 103, no. B10, pp. 24567–24572, Oct. 1998, doi: 10.1029/98JB00594.

[13] N. M. Beeler and D. A. Lockner, "Why earthquakes correlate weakly with the solid Earth tides: Effects of periodic stress on the rate and probability of earthquake occurrence," *J. Geophys. Res.*, vol. 108, no. B8, p. 2001JB001518, Aug. 2003, doi: 10.1029/2001JB001518.

[14] H. Yanben, L. Zhian, and H. Hui, "Interdisciplinary Studies of Astronomical Factors and Earthquakes in China," in *Geodesy on the Move*, vol. 119, R. Forsberg, M. Feissel, and R. Dietrich, Eds., in International Association of Geodesy Symposia, vol. 119. , Berlin, Heidelberg: Springer Berlin Heidelberg, 1998, pp. 465–471. doi: 10.1007/978-3-642-72245-5_77.

[15] Y. Fujii, J. Kodama, and D. Fukuda, "Giant Earthquakes are Occurring at Lunar Phases Specific to each Subduction Zone," presented at the 13th ISRM International Congress of Rock Mechanics, May 2015, p. ISRM-13CONGRESS-2015-206.

[16] Kolvankar, VKolvankar, Vinayak G., et al.inayak G., et al., "Lunar periodicities and earthquakes," *NCGT Newsletter 56 (2010)*, pp. 32–49.

[17] C.-H. Lin, Y.-H. Yeh, Y.-I. Chen, J.-Y. Liu, and K.-J. Chen, "Earthquake Clustering Relative to Lunar Phases in Taiwan," *Terr. Atmos. Ocean. Sci.*, vol. 14, no. 3, p. 289, 2003, doi: 10.3319/TAO.2003.14.3.289(T).

[18] Z. Zhang, S. Wu, and J. Li, "The solar and lunar effect of earthquake duration and distribution," *Earthq Sci*, vol. 26, no. 2, pp. 117–124, Apr. 2013, doi: 10.1007/s11589-013-0023-2.

[19] S. E. Hough, "Do Large (Magnitude ≥8) Global Earthquakes Occur on Preferred Days of the Calendar Year or Lunar Cycle?," *Seismological Research Letters*, vol. 89, no. 2A, pp. 577–581, Mar. 2018, doi: 10.1785/0220170154.

[20] L. Chiou, "The Association of the Moon and the Sun with Large Earthquakes," 2012, *arXiv*. doi: 10.48550/ARXIV.1210.2695.

[21] T. Vanorio, D. Geremia, G. De Landro, and T. Guo, "The recurrence of geophysical manifestations at the Campi Flegrei caldera," *Sci. Adv.*, vol. 11, no. 18, p. eadt2067, May 2025, doi: 10.1126/sciadv.adt2067.

[22] "The Gregorian Reformation of the Calendar," *Nature*, vol. 130, no. 3284, pp. 535–535, Oct. 1932, doi: 10.1038/130535c0.

[23] A. Rovida, M. Locati, A. Antonucci, and R. Camassi, "Archivio Storico Macrosismico Italiano (ASMI)," p. 6000 earthquakes, 670 data sources, 30000 macroseismic intensity data points, June 2017, doi: 10.13127/ASMI.

[24] Istituto Nazionale di Geofisica e Vulcanologia (INGV), "Rete Sismica Nazionale (RSN)." Istituto Nazionale di Geofisica e Vulcanologia (INGV), p. approx. 27 GB per day of new waveform data, approx. 415 active seismic stations, the archive totals to more than 600 distinct seismic stations, Dec. 13, 2005. doi: 10.13127/SD/X0FXNH7QFY.

[25] *NASA Scientific Visualization Studio. (2019, December 2). Moon Phase and Libration, 2020. NASA Goddard Space Flight Center. Retrieved April 13, 2025, from https://svs.gsfc.nasa.gov/4768*.

[26] J. Meeus, *Astronomical algorithms*, 2nd ed. Richmond, Va: Willmann-Bell, 1998.

[27] P. Bretagnon and G. Francou, "VizieR Online Data Catalog: Planetary Solutions VSOP87 (Bretagnon+, 1988)," *VizieR Online Data Catalog*, p. VI/81, May 1995.

[28] * *Pander, J. (2020). Lunar Phase Calendar Generator. GitHub repository: https://github.com/PanderMusubi/lunar-phase-calendar*.

[29] T. H. Heaton, "Tidal Triggering of Earthquakes," *Geophysical Journal International*, vol. 43, no. 2, pp. 307–326, Nov. 1975, doi: 10.1111/j.1365-246X.1975.tb00637.x.

[30] L. Métivier, O. de Viron, C. P. Conrad, S. Renault, M. Diament, and G. Patau, "Evidence of earthquake triggering by the solid earth tides," *Earth and Planetary Science Letters*, vol. 278, no. 3–4, pp. 370–375, Feb. 2009, doi: 10.1016/j.epsl.2008.12.024.

[31] Y. Li, W. Hu, Q. Xu, H. Luo, C. Chang, and X. Jia, "Metastable state preceding shear zone instability: Implications for earthquake-accelerated landslides and dynamic triggering," *Proc. Natl. Acad. Sci. U.S.A.*, vol. 122, no. 1, p. e2417840121, Jan. 2025, doi: 10.1073/pnas.2417840121.

[32] John Essington Sanders, "Sanders, John Essington, 'THE LUNAR PERIGEE-SYZYGY CYCLE FOR 1998: IMPLICATIONS FOR ASTRONOMIC TIDAL HEIGHTS' (2010). Long Island Geologists' Abstracts. 310. https://commons.library.stonybrook.edu/long-island-geologists-abstracts/310/

[33] S. Tanaka, M. Ohtake, and H. Sato, "Evidence for tidal triggering of earthquakes as revealed from statistical analysis of global data," *J. Geophys. Res.*, vol. 107, no. B10, Oct. 2002, doi: 10.1029/2001JB001577.

[34] G. Riga and P. Balocchi, "Information and Predictive Oscillators of Energy Earthquakes," *OJER*, vol. 08, no. 03, pp. 201–222, 2019, doi: 10.4236/ojer.2019.83012.

NCGT Journal
New Concepts in Global Tectonics

New Concepts in Global Tectonics Journal
Volume 13, Number 10, December 2025

ISSN number; ISSN 2202-0039

Local Electromagnetic Precursors: Mechanisms and Pre-Seismic Monitoring through Low Frequency Bands

Valentino Straser[1], Gabriele Cataldi[2], Daniele Cataldi[2-3]

[1]*University of Makeni (Sierra Leone),*
[2]*Radio Emissions Project (I),*
[3]*LTPA Observer Project (I),*

Corresponding Author:
Valentino Straser, University of Makeni (Sierra Leone).
valentino.straser@gmail.com

Abstract: Earthquake prediction is one of the major challenges of modern geophysics, and research on electromagnetic seismic precursors has opened new perspectives for the early detection of seismic events. Local electromagnetic precursors, generated directly within the Earth's crust, occur mainly in the low-frequency bands, such as SELF (Super Extremely Low Frequency), ELF (Extremely Low Frequency) and VLF (Very Low Frequency). These signals can be produced by a variety of physical processes, including rock fracturing, the piezoelectric effect and the movement of fluids in rock pores, all of which can be found in the preparation zone of an earthquake. Unlike non-local seismic precursors, associated with solar and interplanetary phenomena, local pre-seismic radio sources provide direct information on seismo-generative processes occurring in the Earth's crust.

Keywords: Seismic Electromagnetic Precursor, Earthquake Prevision, Geomagnetic Activity, Solar Activity. Electromagnetic Monitoring.

Introduction

Earthquake prediction is one of the most difficult and important challenges in the field of geophysics and seismology. Despite significant progress in understanding tectonic processes, the identification of reliable warning signals remains complex and the subject of numerous research. In this context, the study of electromagnetic seismic precursors has gained attention as a possible tool to improve the ability to detect impending seismic activity.

Among the different types of seismic precursors, electromagnetic precursors offer a unique advantage because they can be detected before the seismic event occurs, potentially providing early warning that could be decisive in mitigating seismic risk. Pre-seismic electromagnetic signals, which occur in the low-frequency bands, can be the result of a variety of physical phenomena, including rock fracturing, piezoelectric effect, and fluid movement in rock pores, all of which occur in the preparation zone of an earthquake.

In this work, some of the main characteristics of local electromagnetic seismic precursors will be examined, with particular attention to the mechanisms of signal generation, propagation and detection. These precursors, generated directly within the Earth's crust, offer new opportunities to better understand pre-seismic processes and improve the prediction capabilities of seismic events.

Characteristics of local pre-seismic radio signals

During the new millennium, numerous studies have been conducted on the correlation between seismic phenomena and electromagnetic signals, in particular in the ELF (Extremely Low Frequency, 3-30 Hz) and VLF (Very Low Frequency, 3-30 kHz) bands. One of the major contributions that scientific research has been able to provide has been the development of the concept of "lithosphere-atmosphere-ionosphere coupling", which explores how electromagnetic signals generated by tectonic faults can propagate up to the ionosphere and create measurable anomalies [1-5].

The most important aspects of these studies are represented by the detection of electromagnetic signals in the ELF/VLF frequencies before seismic events (the so-called Seismic Electromagnetic Precursors or SEPs), supporting the idea that rock fracturing and tectonic movement can generate anisotropic radio sources. These signals, if correctly detected, could be used as seismic precursors. It has now been established that there are ionospheric perturbations induced by earthquakes that cause modifications in the propagation of radio waves in the VLF band. These ionospheric perturbations are caused by processes that occur below the Earth's surface, confirming the link between tectonic activity and electromagnetic disturbances [5]. One of the proposed models is the idea of an interaction between the lithosphere and the ionosphere (a mechanism also known

ISSN number; ISSN 2202-0039

as “Lithosphere-ionosphere coupling”), where tectonic forces generate electric fields that are then reflected in the ionosphere, creating perturbations measurable with monitoring networks tuned in the SELF-VLF band (0<f≤30 kHz).

The main mechanisms that could explain the formation of local pre-seismic radio sources, and why these electromagnetic emissions can have non-isotropic characteristics are:

- **Piezoelectric effect**

  some rocks, such as quartz, generate electric fields when subjected to mechanical stress, such as in the case of tectonic faults. This phenomenon is known as the piezoelectric effect. Deformation of rocks can create electric fields and electromagnetic signals that propagate non-uniformly, influenced by the composition of the rocks and the geometries of the faults, which causes the radio signal to propagate non-isotropically.

- **Rock Fracture**

  When rocks under stress fracture (creating macro and micro-fractures), electrical charges are released. This phenomenon generates electromagnetic fields, which in turn manifest themselves as local emissions. Fracturing does not occur uniformly, so electromagnetic signals propagate in preferential directions, linked to the structure of the rock.

- **Triboelectric and chemical effects**

  The breaking of chemical bonds and the rubbing between rocks during the fracturing process can generate free electrons and electrical charges, creating electromagnetic fields. These signals are not isotropic because the fracturing process occurs along preferential lines.

- **Waveguide effect along faults**

  Faults can act as a kind of waveguide for electromagnetic signals. This means that electromagnetic signals produced by rocks under stress do not propagate uniformly in all directions, but follow specific paths along the faults, creating signals with anisotropic characteristics.

- **Fluid Currents**

  The movements of fluids in the pores of rocks, induced by tectonic stress, can generate electric fields. Also in this case, the electromagnetic signal generated tends to propagate along the preferential lines dictated by the structure of the Earth's crust, creating non-isotropic emissions.

In other words, electromagnetic signals that are generated before an earthquake have non-isotropic characteristics because the propagation is influenced by the structure of rocks and faults. Phenomena such as the piezoelectric effect, rock fracturing and fluid movement all contribute to the formation of these pre-seismic radio sources, which have an anisotropic behavior related to the irregular and complex nature of the terrain [3] [6-10].

Monitoring of Electromagnetic Seismic Precursors (SEPs).

As far as electromagnetic monitoring is concerned, a big step forward has been made thanks to the studies of the authors who have focused on the SELF-VLF band (SELF = Super Extremely Low Frequency; VLF = Very Low Frequency) (**Fig. 1**). Focusing on the monitoring of natural radio sources that are observed in these bands is fundamental in the study of electromagnetic seismic precursors for a series of reasons that concern their unique propagation capabilities, their physical origins, and their relationship with seismic phenomena.

It is useful to remember here that the acronym "SELF" was introduced in the research on possible precursor signals by the authors in 2014 [17] because before 2014 there was no clear classification of the radio band with frequency between 0 and 3 Hz (**Fig. 1**).

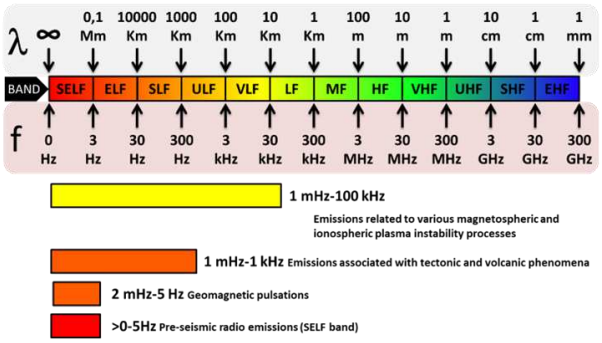

Fig. 1 – Radio Bands. In the image above you can see the electromagnetic spectrum between 0 and 300 GHz divided into radio bands. Credits: Radio Emissions Project.

In fact, for many years, the ULF band (0.3-3kHz) was usually used to refer to electromagnetic signals in the SELF band or was even associated with the ELF band (3-30Hz). The acronym ULF, in fact, was used to refer to radio emissions with the lowest frequency detectable with a radio receiver designed, for example, to work in

ISSN number; ISSN 2202-0039

the geomagnetic band below 1 Hz. Why this happened is not clear, but it should be remembered that the ITU-R designation, defined by recommendation V.431 [18], had already clarified for some time that the ULF (Ultra Low Frequancy) band is between 300 Hz and 3 kHz, and the ELF (Extremely Low Frequency) band between 3 and 30 Hz.

What was missing from the ITU-R designation was the radio band between 0 and 3 Hz: a band in which the authors observed both signals attributable to the geomagnetic band and those associated with local pre-seismic radio frequencies. For this reason, in 2014, the authors began to use the acronym SELF (Super Extremely Low Frequency) to refer to the band with frequency $0<f<3$ Hz (**Fig. 1**) in the context of environmental electromagnetic monitoring.

Thanks to the "Radio Emissions Project" that the authors created to analyze the pre-seismic radio frequency in the SELF-VLF band, it was possible to detect local pre-seismic radio emissions related to seismic events of medium and strong intensity mainly in Italy but also in other regions of the world [11-16], taking advantage of the physical characteristics of radio waves that have a frequency not exceeding 1kHz.

The main reasons why it is convenient to monitor pre-seismic radio emissions in the SELF-VLF band are the following:

- **Greater penetration depth into the Earth's crust**

  Electromagnetic waves in the SELF-VLF band ($0<f\leq30$ kHz) have a very high penetration capacity compared to higher frequency waves. This means that they can propagate through deep layers of the Earth's crust and tectonic faults. Therefore, they can reveal information about processes that occur at depth and that are linked to the movement of faults, fractures of rocks and release of energy before an earthquake [1] [29] [30] [33] [34].

- **Long-range propagation**

  Electromagnetic waves in the SELF-VLF band have an exceptional ability to propagate over large distances through the Earth's crust and atmosphere: this property of radio waves follows a certain proportionality with the wavelength: the longer the wavelength of an electromagnetic source, the greater its ability to propagate in different propagation media without undergoing significant attenuation. This phenomenon allows to monitor large geographic areas with few detection stations, increasing the probability of detecting pre-seismic signals from different tectonic zones. Radio sources in the SELF-ELF band, therefore, can cross large distances with minimal energy losses, making them the ideal focus for study projects dedicated to pre-seismic radio frequency [1] [29-32].

- **Sensitivity to electromagnetic processes generated by tectonic stresses**

  Electromagnetic waves in the SELF-VLF band are generated by physical processes such as:

  - **Piezoelectric effect**: When rocks rich in quartz crystals are subjected to stress, they produce detectable electric fields in the SELF-VLF band [6] [8] [10] [23] [27] [28].
  - **Rock fracturing**: When rocks fracture (macro and micro-fractures) under tectonic pressure, electric charges are released that generate electromagnetic fields in the SELF-VLF band [22-26].
  - **Movement of fluids in the pores of rocks**: This movement can induce electric currents that produce electromagnetic emissions [8] [10] [19-21].

  Monitoring these bands allows us to detect electromagnetic signals associated with processes that precede an earthquake, helping to identify seismic precursors.

- **Lithosphere-ionosphere coupling**

  The SELF-ELF and VLF bands are useful for detecting coupling phenomena between the lithosphere and the ionosphere. Before an earthquake, electromagnetic variations caused by faults can propagate up to the ionosphere, modifying its properties. These changes can be detected by radio receivers working in the VLF band, which reflect ionospheric perturbations related to seismic events [1] [28] [34-36].

- **Interaction with the Schumann resonance**

  Radio waves in the ELF band are relevant because they fall within the range of Schumann resonances, a global phenomenon caused by electromagnetic waves trapped in the cavity between the Earth's surface and the ionosphere. Variations in this resonance can be influenced by perturbations caused by seismic activity, thus allowing indirect monitoring of seismic activity on a global scale [28] [37-40].

- **Measurable anomalies before seismic events**

  As previously stated, pre-seismic radio frequency research has shown that the SELF-

New Concepts in Global Tectonics Journal
Volume 13, Number 10, December 2025
ISSN number; ISSN 2202-0039

VLF band is often subject to anomalies that precede earthquakes, making it an ideal target for seismic precursor monitoring. The ability to detect signals that occur hours to days before a seismic event makes this band particularly useful for seismic forecasting.

- **Greater immunity to local disturbances**

Higher frequencies, such as those used for other radio communications, are often subject to local interference from infrastructure and electrical equipment. The SELF-VLF band, on the other hand, is less vulnerable to such disturbances, meaning that the detected signals may be more reliable and actually originate from geophysical processes, rather than artificial sources [29] [30] [38] [39] [41].

Monitoring the SELF-VLF band is crucial because these frequencies can provide unique and reliable information on deep geophysical phenomena, allowing to identify pre-seismic electromagnetic signals that may not be detectable on other frequency bands. This band allows to obtain a complete picture of the electromagnetic dynamics associated with seismogenic processes and is essential for the development of seismic forecasting methods based on electromagnetic data [16].

The importance of Fourier transform spectrography applied to the study of pre-seismic radio emissions

Before the studies conducted by the authors, high-quality data on local seismic precursors were lacking. Thanks to the Radio Emissions Project, it was possible, for the first time, to obtain detailed spectrographic data on the signatures of pre-seismic radio signals, both local and non-local, allowing to greatly simplify the identification of anthropogenic signals (generally characterized by a narrow bandwidth) from natural ones (usually characterized by a wide bandwidth).

This project allowed to identify and characterize with greater precision the electromagnetic emissions related to seismic events, thus offering a significant contribution to the understanding of local pre-seismic radio emissions also developing innovative considerations and theories on their genesis mechanism [11-17]. The developed approach also allowed to reformulate the classification of electromagnetic seismic precursors in general, distinguishing two main categories:

Non-local seismic precursors (**Fig. 2**; because they are not general within the Earth's crust):

- **SSPs** (Solar Seismic Precursors): electromagnetic phenomena visible on the solar surface, such as solar flares, magnetic loops above sunspots and coronal mass emissions (CMEs), which represent the electromagnetic substrate from which dense emissions of the solar ion flux originate.

- **ISPs** (Interplanetary Seismic Precursors): dense solar ion fluxes present in interplanetary space, directed towards the Earth, which include proton, electronic, velocity and dynamic pressure increases of the solar wind, perturbations of the interplanetary magnetic field (IMF). These fluxes will have an interaction with the Earth's magnetosphere.

- **SGPs** (Seismic Geomagnetic Precursors): result of the interaction between ISPs and the Earth's magnetosphere, generating geomagnetic perturbations such as increases in geomagnetic indices, auroral indices, hemispheric power, and perturbations of the Earth's magnetic and geomagnetic field, such as ELF storms and geomagnetic micropulses.

Local seismic precursors (because they are general within the Earth's crust):

- **SEPs** (Seismic Electromagnetic Precursors): radio emissions generated in the earthquake preparation zone. Triboelectric and chemical effects and formation of electric currents generated by the movement of fluids in the pores of rocks, radio frequency induced through the piezoelectric effect following tectonic stress.

Fig. 2 – **Modulation of non-local seismic precursors.** In the image above you can see the close relationship between the "non-local" seismic precursors. Credits: Radio Emissions Project.

This "reformulation" was achieved by analyzing the spectrographic signature of non-local seismic precursors (Fig. 3) and local ones by analyzing radio signals with FFT technology. The impulsive characteristics of local radio emissions allowed the authors to understand that in the SELF band it was possible to observe pre-seismic radio emissions that could not be associated with terrestrial geomagnetic activity. In other words, we can say that the use of Fourier transform spectrography is essential for analyzing pre-seismic signals generated by both local and non-local sources.

NCGT Journal
New Concepts in Global Tectonics
New Concepts in Global Tectonics Journal
Volume 13, Number 10, December 2025
ISSN number; ISSN 2202-0039

The Fourier transform (FFT) is a mathematical operation that allows to convert a signal from the time domain to the frequency domain, breaking it down into a sum of sinusoids (pure waves) of various frequencies. In other words, the FFT allows to analyze the "composition" of a complex signal in terms of its frequency components, making it possible to identify characteristics that would not be visible by observing the signal in time alone.

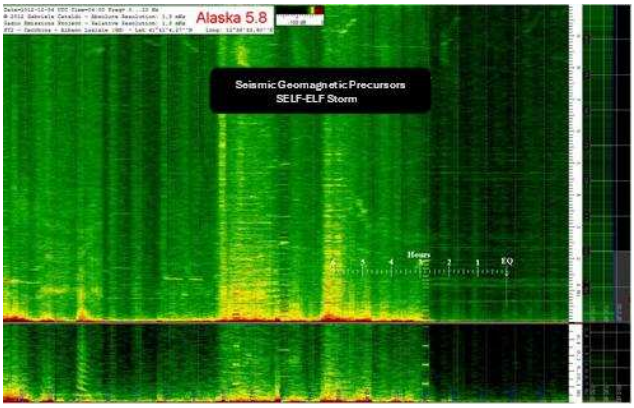

Fig. 3 – Seismic Geomagnetic Precursor (SGP). In the spectrogram above, the typical spectrographic imprint of a SGP can be observed: the very long duration combined with the intensity that increases with the increase of the wavelength of the natural electromagnetic background, are the main characteristics of a geomagnetic perturbation that precedes a seismic event of strong or medium-strong intensity. In this specific case, this SELF-ELF storm preceded the M5.8 earthquake that was recorded in Alaska on December 4, 2012. This geomagnetic seismic precursor was captured using a coil antenna containing about 500,000 turns. The electromagnetic monitoring station was located in the southern outskirts of Albano Laziale (Italy). Credits: Gabriele Cataldi, Radio Emissions Project.

In the context of pre-seismic signals, this ability to decompose signals into frequency components allows the authors to isolate and study electromagnetic phenomena related to seismicity, thus improving the understanding of pre-seismic dynamics. The Fourier transform is particularly useful when dealing with complex signals such as electromagnetic emissions, which may contain critical information but are difficult to detect without frequency analysis.

This multidisciplinary approach, integrating FFT analysis with the study of classified seismic precursors (SSP, ISP, SGP and SEP), represents a major step forward in seismic research. The ability to detect, characterize and understand pre-seismic electromagnetic signals could open new possibilities for seismic forecasting on a global scale, offering a significant contribution to seismic risk mitigation.

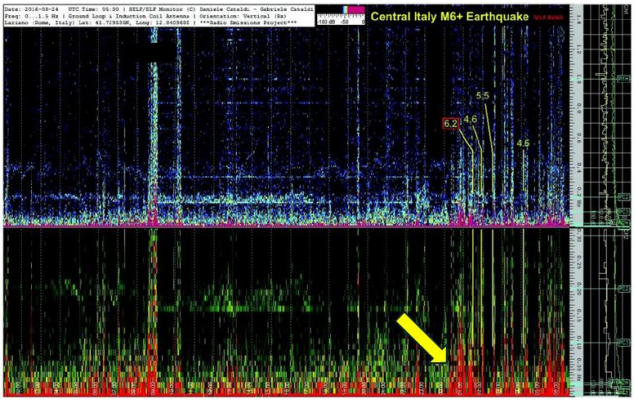

Fig. 4 – Seismic Electromagnetic Precursor (SEP). The image represents the dynamic spectrogram of the Earth's electromagnetic field recorded between 02:00 UTC, August 23, 2016 and 06:30 UTC, August 24, 2016 by the environmental electromagnetic monitoring station of Radio Emissions Project, located in Lariano, Italy. On the right side of the spectrogram there are a series of impulsive increments that occurred during and after the Italian earthquake, each of which occurred during seismic events whose magnitude is observed in the upper portion of the spectrogram. The time marker of the Italian earthquake M6.2 has been identified by a red line that outlines the edge of the magnitude. Before the Italian seismic event M6.2 a series of impulsive increments (yellow arrow) are visible that preceded the earthquake in the SELF band. These increments started about 90 minutes before the M6.2 earthquake. Credits: Radio Emissions Project.

In **Fig. 3-4** it is possible to observe the difference in the spectral signature between a SGP and a SEP. SGPs have a very long-time duration and a very slow intensity variation since they follow the solar activity and, more precisely, the variation of the solar ion flux density. SEPs, on the other hand, have a very short duration and an impulsive aspect [42] since they do not follow the variation of the Earth's geomagnetic field but are generated through piezoelectric, triboelectric or chemical phenomena that occur in the earthquake preparation zone due to tectonic stress. The FFT technology, therefore, allows to quickly recognize whether the pre-seismic electromagnetic source is local or non-local.

Hypothesis on the coupling mechanism between the increase in the proton density of the solar wind and seismogenesis

Over the last ten years the authors have proposed some hypotheses able to explain the mechanism of connection between the increase of the proton density of the solar wind and the resumption of the global seismic activity M6+, but the most plausible theory they believe can be explained only by involving the variations of the Earth's geomagnetic field; variations that often precede the seismic activity M6+.

There is evidence that suggests that the interactions

ISSN number; ISSN 2202-0039

between the solar wind and the Earth's magnetosphere could influence deep geophysical processes, especially considering the global scale of seismic events:

- **Piezoelectric effect amplified by geomagnetic disturbances**: The piezoelectric effect is well known in materials physics and occurs when certain types of crystals, such as quartz and other silica-rich rocks, generate an electric field when they are compressed, stretched, or fractured. In fault zones, rocks deforming due to tectonic stress can generate electric fields through this effect. However, geomagnetic disturbances induced by interaction with the solar wind could not only affect the surface charges generated by the fractured rocks, but also amplify the production of electric fields in the fault zones, creating a sort of "amplified local electromagnetic response". This could trigger or accelerate processes already underway in the Earth's crust, leading to a more rapid destabilization of faults on a global scale.

  More specifically, when there is an increase in the proton density of the solar wind, this flow of charged particles comes into contact with the Earth's magnetosphere, generating electric currents in the ionosphere and causing geomagnetic disturbances. These disturbances, especially during geomagnetic storms, can alter the local geomagnetic field and interact with local electric fields created through the piezoelectric effect in fault zones, amplifying their intensity or dynamic effect. In practice, rocks under tectonic stress would not only be subjected to internal mechanical pressures but would also be externally influenced by the interaction between piezoelectrically generated electric charges and the disturbed magnetic fields [59-61]. This type of amplification can occur in different ways:

  - **Strengthening of local electric charges**: Geomagnetic disturbances could amplify the electric fields generated by fractured rocks, leading to a greater accumulation of electromagnetic energy in the fault zones. This amplified electromagnetic field could further destabilize the already stressed faults, reducing the threshold necessary to trigger a seismic event. In fact, one could imagine that, when the magnetosphere is perturbed, the piezoelectric electric charges in the faults "are pushed" towards a higher state of excitation, accelerating micro fracturing.

  - **Modification of electrical conduction conditions**: During an increase in proton density, the Earth's geomagnetic field changes, also influencing the electrical conductivity of rocks near the surface. Some research has shown that the electrical conductivity of the Earth's crust can change depending on the external magnetic field [43] [44]. In this context, piezoelectric rocks could become temporarily more conductive or could propagate the accumulated charges more easily, leading to increased electromagnetic reactivity in the faults.

  - **Dynamic effect of the Lorentz force**: Piezoelectric electric charges already present in the rocks could be subjected to a stronger Lorentz force during geomagnetic storms. The Lorentz force is the force exerted on an electric charge moving in a magnetic field. In conditions of strong geomagnetic perturbation, this force could become strong enough to directly influence the movement of electric charges present in the faults and favor the accumulation of mechanical stress, accelerating the release of energy in the form of seismic events.

  Possible methods of verifying this hypothesis are represented by:

  - **Simultaneous monitoring of the Earth's geomagnetic field and local electromagnetic emissions**: It would be possible to correlate data from electromagnetic monitoring stations (SELF-VLF) implemented with RDF (Radio Direction Finding) technology with real-time geomagnetic data, detecting the possible presence of increases in local electromagnetic activity coming from faults during geomagnetic storms or immediately after proton increases. The detection of a local pre-seismic electromagnetic peak could support the hypothesis that geomagnetic perturbations can amplify local pre-seismic radio sources.

  - **Experimental measurements of electrical conductivity in the laboratory**: Simulate in the laboratory the tectonic stress on piezoelectric rocks, applying a variable magnetic field similar to geomagnetic perturbations. This would allow to see if the variations of the magnetic field influence the production of electric charges or the conductivity of rocks under stress.

  - **Terrestrial Magnetohydrodynamic Simulations**: Using computational models, the interaction between piezoelectric charges and geomagnetic perturbations induced by the solar wind could be simulated. This type of modeling could help verify whether the

ISSN number; ISSN 2202-0039

hypothesized amplified effect is actually feasible on a global scale.

- **Inverse Piezoelectric Effect Applied in Seismic Context**: The inverse piezoelectric effect occurs when an electric field applied to a piezoelectric material causes mechanical deformation in the material itself. In this specific case, it is hypothesized that electric charges induced by geomagnetic perturbations or interactions with the solar wind can, through this mechanism [52] [53], directly influence rocks in fault zones [54].

  In fault zones, many of the rocks (such as quartz or other piezoelectric materials) are already subjected to mechanical stress due to tectonic forces. When solar activity causes an increase in the proton density that interacts with the magnetosphere, electromagnetic fields are generated that could, in theory, influence rocks through the inverse piezoelectric effect.

  In this scenario, rocks under mechanical stress could undergo additional mechanical deformations induced by electric charges that accumulate following geomagnetic perturbations. Depending on the direction and intensity of the electric or magnetic field, shortening or lengthening phenomena of the rocks could occur that could alter or contribute, together with other phenomena, to destabilize the static equilibrium of the faults.

  An interesting concept that is linked to this hypothesis is magnetostriction, which occurs when a material deforms in response to a magnetic field. Although piezoelectric materials respond primarily to electric fields, magneto-strictive materials respond to magnetic fields. In a tectonically active environment, where rocks that generate electric fields (piezoelectric effect) already exist, a disturbed external magnetic field (such as that induced by proton increases) could trigger deformations even in materials sensitive to magnetostriction. If piezoelectric or magneto-strictive rocks present in the faults undergo these induced deformations, they could contribute to reducing or increasing the mechanical load in the fault zones, accelerating the process of fracturing and release of seismic energy. In a sense, this would represent a synergy between electromagnetic and mechanical phenomena: tectonic stress acts on a long-time scale, but when a significant electromagnetic pulse, such as that associated with proton increases, arrives, it could "push" these rocks beyond their breaking point.

  This phenomenon could manifest itself in the following ways:

a) **Accelerated micro fracturing**: In rocks already under great pressure, additional deformation induced by the inverse piezoelectric effect could cause microfractures that rapidly evolve into macrofractures. This would accelerate the fracturing of the fault and could lead to the triggering of an earthquake.

b) **Modification of the mechanical behavior of faults**: Mechanical deformation of rocks could modify the behavior of the fault, making it more or less resistant. In some cases, it could "release" stored energy slowly, leading to a release of low-magnitude seismic energy, while in other cases it could cause a sudden release of energy, causing stronger earthquakes.

c) **Local and global effects**: Since this phenomenon involves interaction with the geomagnetic field, which has a global impact, it is possible that the inverse piezoelectric effect will not only manifest itself in a single fault zone, but in multiple fault zones around the world simultaneously, thus increasing global seismic activity. This would explain why the increase in proton density correlates with a resumption of seismic activity on a global scale, as observed by the authors.

To experimentally verify this hypothesis, it could be useful to conduct small-scale experiments that simulate the conditions of the Earth's crust in the laboratory:

- **Experiments with piezoelectric and magnetostrictive materials**: Subjecting rocks such as quartz or magneto-strictive materials to varying electric and magnetic fields, simulating the geomagnetic perturbations induced by proton boosts, could prove the existence of significant mechanical deformation.

- **Field measurements**: Measuring the change in mechanical properties of rocks in an active fault zone during and after a major geomagnetic event. A measurable change in rock deformation or an increase in local seismic activity could suggest a link between the geomagnetic perturbations and the inverse piezoelectric effect.

The inverse piezoelectric effect, combined with geomagnetic perturbations, offers an interesting

ISSN number; ISSN 2202-0039

explanation for the activation of global seismic phenomena during proton surges. Rocks subjected to mechanical stress in faults could further deform due to this effect [45] [46], accelerating the fracturing process and triggering earthquakes. This mechanism could also act on a global scale, if multiple fault zones are simultaneously influenced by geomagnetic perturbations.

- **Schumann Resonance and pressure on the tectonic system**: Another hypothesis concerns the Schumann resonance, which is influenced by variations in the geomagnetic field. An increase in proton activity could alter the frequencies of Schumann waves [47-51], causing small but constant variations in the ionosphere. These variations could generate a constant pressure on tectonic plates at a global level, contributing to their release of energy. Although this phenomenon would not be directly causal in terms of seismic triggering, it could act as an additional stress factor on faults already close to the point of rupture.

- **Magnetohydrodynamics and lithospheric instability**: From the magnetohydrodynamics point of view, the flow of charged particles of the solar wind interacting with the magnetosphere generates electric currents in the upper atmosphere and in the lithosphere. The energy of these currents could, in some cases, penetrate into the more superficial fault zones, modifying the loading conditions of the rocks. This magnetic energy could cause microfractures in the faults and facilitate their sliding or reactivation. In this context, the link between the proton density and the geomagnetic perturbations could not be linear but modulated by factors such as the local geological composition and the arrangement of the faults [55-58].

- **Lorentz forces in fault regions**: Continuing the idea of the Lorentz force, one could explore a more detailed model of how these forces act within fault zones. It is possible that in highly stressed areas, where natural electric fields (such as piezoelectric ones) already exist, Lorentz forces can act on charges already present, accelerating their motion and facilitating the propagation of fractures. This could explain why proton increases seem to correlate well with earthquakes of higher magnitude, where tectonic stress is already high.

- **Long-term effects of solar storms on tectonic plates**: One aspect that could be explored in the coming years through targeted studies is whether solar storms, in addition to their immediate effects, have a long-term influence on tectonic plates. Repeated proton surges could accumulate energy in the Earth's crust, or change the electrical conductivity of faults over time, progressively increasing their instability. This could explain not only large earthquakes, but also an overall increase in seismic activity on a global scale.

The electromagnetic monitoring station

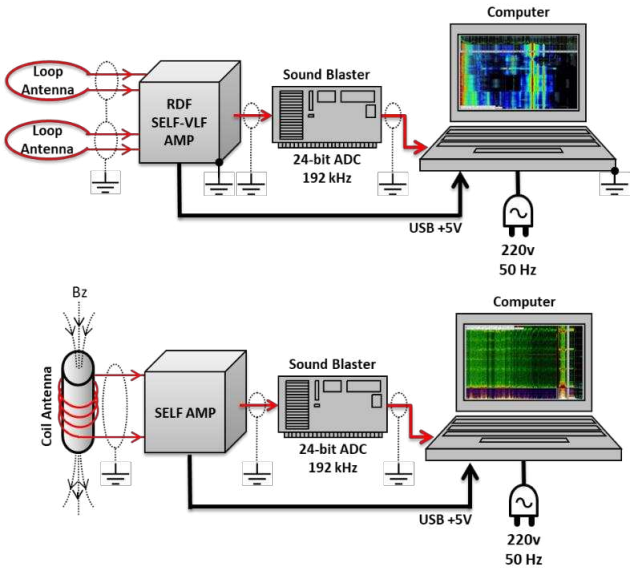

Fig. 5 – Simplified diagram of electromagnetic monitoring stations. Above you can see a simplified diagram of the electromagnetic monitoring station implemented with RDF (Radio Direction Finding) system able to operate in the SELF-VLF band. Below you can see the simplified diagram of a monitoring station designated to monitor the SELF band. Credits: Gabriele Cataldi, Radio Emissions Project.

The studies conducted by the authors on local pre-seismic electromagnetic sources (Seismic Electromagnetic Precursors or SEPs), were carried out through electromagnetic monitoring stations designed to work efficiently in the SELF-ELF band ($0<f\leq30$ kHz). The design of the radio receivers (**Fig. 5**) was carried out by Gabriele Cataldi considering the filtering of anthropogenic radio sources present in the SLF band (interference produced by domestic power lines at 50 Hz) and in the HF band (radio-amateur communications). The use of very low noise operational amplifiers and USB power supply systems have allowed to considerably reduce the electronic noise of the entire electromagnetic monitoring system.

ISSN number; ISSN 2202-0039

The hardware part of the monitoring stations (radio receiver), being powered via USB, could be connected to a notebook computer to operate even during a power outage in the home. This solution allowed not only to use software to analyze the captured radio sources and create spectrograms, but also to keep each individual monitoring station always operational during blackouts lasting 1 or 2 hours. This autonomy could be increased by connecting UPS to the notebook computers.

This electromagnetic monitoring project dedicated to seismic precursors was born in February 2007 with the name “Radio Emissions Project”. Currently, this project does not only include the monitoring of natural radio sources (geomagnetic and tectonic), but also the monitoring of solar activity: more precisely the electromagnetic phenomena observed on the solar surface (sunspots, magnetic loops, solar flares, coronal holes, solar coronal mass ejections or CMEs; defined Solar Seismic Precursors or SSPs) and in interplanetary space (density of solar ion fluxes, interplanetary magnetic field; defined Interplanetary Seismic Precursors or ISPs); also including parameters such as the speed and dynamic pressure of the solar wind.

At the beginning of the Radio Emissions Project, monitoring was mainly oriented to the analysis of pre-seismic radio frequency through the use of coil antennas containing tens of thousands of vertically oriented coils and through single loop antennas with a diameter of 1 meter east according to the horizontal geomagnetic component "H" of the Earth's geomagnetic field, which is the one oriented towards the magnetic North Pole. These configurations were used by the authors to monitor and analyze mainly the variations of the Earth's geomagnetic field to verify whether there was a correlation with potentially destructive seismic activity [16] [17] [62-81]. Only later, in 2017, the electromagnetic monitoring stations were implemented with the RDF (Radio Direction Finding) system which allowed the first studies on local pre-seismic radio sources (Seismic Electromagneic Precursors or SEPs) to be carried out and the first encouraging results to be obtained using a new approach to predict earthquakes: crustal diagnosis [16] [82-108]. The innovative detection technique developed by the authors does not only consist in using quality electronic components and reducing the overall componentry to a minimum, but it also stands out from other electromagnetic monitoring projects created since the 1980s, especially for the quality of the data obtained: using a computerized recording system with a temporal resolution of 1 minute, the Radio Emissions Project allows for evaluations of variations in the electromagnetic field that are on average shorter than other projects. This feature allows for easy observation of impulsive spectral characteristics: a distinctive feature of local pre-seismic radio sources (SEPs). Many projects that in the past have been dedicated to electromagnetic monitoring for the study of SEPs used hourly or even daily averages of the environmental electromagnetic field, drastically compromising the ability to observe local pre-seismic electromagnetic sources. Another fundamental characteristic of electromagnetic monitoring dedicated to SEPs consists in the creation of spectrograms: this type of technology allows to graphically represent many characteristics of the monitored radio frequency: intensity, frequency, bandwidth, time of appearance and disappearance of the signals; all essential characteristics to determine whether a radio signal captured by the monitoring station is of anthropogenic or natural nature. The RDF technology has also allowed the authors to obtain data on the azimuth of the radio signals captured by each individual electromagnetic monitoring station, significantly expanding the diagnostic capacity of the monitoring method.

More precisely, the monitoring stations implemented with RDF technology are currently equipped with dual-channel radio receivers, designed by Gabriele Cataldi and conceived to work with two orthogonally aligned loop antennas: this configuration allows to understand the azimuth of each single electromagnetic emission that is captured within 30kHz. The use of two or more stations simultaneously allows to triangulate local pre-seismic electromagnetic sources (SEPs): the precision of the system therefore increases as the electromagnetic monitoring stations of this type of increase. Currently the RDF monitoring network is made up of monitoring stations present in Italy and Malaysia, but the idea is to extend it to other parts of the globe by finding partners interested in this type of research which, although pioneering, has allowed the authors to obtain notable results on local pre-seismic radio frequency and not only.

Following studies carried out in 2020 [88] [89], in 2024 the authors started working to create a new prototype of radio receiver, this time of digital type, capable of working also in the DC band and able to be connected to multiple types of antennas simultaneously. This new receiver will also be equipped with a Geiger and gas detector (CO2 and H2S). When this new receiver will be ready, the monitoring network will undergo an upgrade becoming the first multi-parametric monitoring network in the world dedicated to the study of electromagnetic seismic precursors.

Discussion

The studies conducted by the authors on local electromagnetic seismic precursors have highlighted aspects relevant to the understanding of seismogenesis and potential predictive applications of pre-seismic radio emissions. The electromagnetic monitoring stations, designed to operate mainly in the SELF-ELF band ($0<f\leq30$ kHz), have proven to be fundamental tools for the detection of signals associated with deep tectonic processes. The results obtained during the research have

ISSN number; ISSN 2202-0039

provided concrete evidence of the existence of electromagnetic signals preceding seismic events, in particular those of medium-high magnitude, contributing significantly to the scientific debate on this topic.

One of the main contributions of the study was the identification of localized electromagnetic emissions that show a repetitive correlation with seismic events. The mechanisms proposed to explain these emissions, such as the piezoelectric effect and rock fracturing, indicate that mechanical deformations caused by tectonic stress and the movement of fluids in the pores of rocks can generate detectable electromagnetic signals. These signals represent an indicator of geophysical processes taking place in the earthquake preparation zone, offering a new perspective for monitoring seismic activity.

The use of monitoring stations capable of detecting signals in the SELF band has allowed the authors to access highly relevant information, thanks to the greater penetration depth of low-frequency electromagnetic waves compared to higher frequencies. This characteristic has allowed the detection of signals propagating through deep layers of the Earth's crust, revealing processes otherwise difficult to observe with other methodologies. Furthermore, the ability of low-frequency radio emissions to propagate over large distances without undergoing significant attenuation has allowed the authors to monitor large geographical areas, broadening the scope of the analysis.

Although the results obtained are promising, the authors maintain a cautious approach in declaring that they have developed a widely tested and accurate seismic forecasting method. However, the observations collected so far indicate that electromagnetic monitoring stations can provide useful preliminary indications of impending seismic activity. The variations in intensity and the impulsive nature of emissions detected before some seismic events have demonstrated the potential of these technologies in crustal diagnosis and in the possible identification of warning signals.

Another important aspect discussed by the authors concerns the difference between local and non-local seismic precursors. Non-local signals, such as those related to solar and interplanetary activity, tend to have a longer duration and a wider spatial distribution, resulting less specific than local signals, which present impulsive characteristics related to regional geophysical phenomena. This has led to the development of a more sophisticated classification of seismic precursors, distinguishing between local signals that provide direct information on tectonic processes and non-local signals that offer more general indications. The authors also highlight the importance of future research perspectives, in particular the implementation of a new digital radio receiver that will be able to operate also in the DC band. This technological evolution will allow the integration of different environmental and geophysical parameters, such as gas detection (CO2 and H2S) and geomagnetic activity. These developments will allow multi-parameter monitoring, significantly improving the quality and resolution of the collected data and opening new perspectives for seismic forecasting based on electromagnetic signals.

Despite the evident progress, the authors reiterate the need for further studies and validations to consolidate the findings. The scientific community, traditionally skeptical about seismic forecasting capabilities, may require further evidence to fully accept the electromagnetic approach as a predictive tool. However, the results obtained so far clearly demonstrate that electromagnetic monitoring can significantly contribute to seismic risk mitigation, integrating traditional seismological techniques with new analysis methods.

Conclusions

The studies presented in this work provide a significant contribution to the understanding of local pre-seismic radio emissions and their potential role as seismic precursors. Through the implementation of a network of electromagnetic monitoring stations, it was possible to identify signals related to seismic activity, particularly in the SELF-ELF band, which proved useful in detecting deep geophysical phenomena associated with tectonic stress.

The results obtained highlighted the validity of the approach based on the detection of local electromagnetic emissions to monitor crustal deformation processes, with potential implications for the prediction of seismic events. The observations indicate a significant correlation between the electromagnetic emissions detected by the stations and seismic events of medium and high magnitude, confirming the possibility of using these signals to identify the preparatory phases of an earthquake.

Although the authors maintain a cautious perspective regarding the predictive capacity of the system, the initial results are encouraging and open new avenues for research in the field of electromagnetic seismic precursors. The technologies employed, although still being refined, show significant potential to improve the understanding of seismogenic mechanisms and to develop more effective tools for seismic risk mitigation. The work has also highlighted the need to develop additional detection tools, including the planned implementation of digital radio receivers, which will allow more accurate and multi-parametric monitoring. The integration of these new tools will allow not only to detect electromagnetic signals, but also to combine data from other sources, such as crustal gas measurements and geomagnetic variations, further improving the analysis capabilities.

ISSN number; ISSN 2202-0039

In conclusion, the studies conducted provide a solid basis for the development of a new seismic monitoring paradigm based on electromagnetic emissions. The authors believe that, with continued technological development and the expansion of the monitoring network, it will be possible to obtain greater precision in identifying areas at seismic risk and, with further validation, improve the prediction capacity of seismic events on a global scale. However, the authors emphasize that seismic forecasting remains a complex scientific challenge and urge caution in interpreting the results. Future studies will be essential to consolidate these findings and broaden the understanding of pre-seismic radio emissions as a crustal monitoring tool.

References

[1] M. Hayakawa, O. A. Molchanov. (2002). Seismo Electromagnetics: Lithosphere-Atmosphere-Ionosphere Coupling. Tokyo: TERRAPUB.

[2] M. Hayakawa, K. Ohta, A. P. Nickolaenko, Y. Ando. (2005). Anomalous Effects in Schumann Resonance Phenomena Observed in Japan, Possibly Associated with the Chi-Chi Earthquake in Taiwan. International Workshop on Seismo Electromagnetics (IWSE), 1999-2000.

[3] M. Hayakawa. (2009). Electromagnetic Phenomena Associated with Earthquakes. Trivandrum: Transworld Research Network.

[4] M. Hayakawa, Y. Hobara. (2010). Current Status of Seismo-electromagnetics for Short-term Earthquake Prediction. Geomatics, Natural Hazards and Risk, 1(2), 115-155.

[5] M. Hayakawa. (2011). Lower Ionosphere Perturbations Associated with Earthquakes, as Detected by Subionospheric VLF/LF Radio Signals. In Electromagnetic Phenomena Associated with Earthquakes (pp. 137-185). Trivandrum: Transworld Research Network.

[6] F. T. Freund. (2007). Pre-earthquake signals: Underlying physical processes. Journal of Asian Earth Sciences, 29(3-4), 481-499.

[7] O. A. Molchanov, M. Hayakawa. (2008). Seismo Electromagnetics and Related Phenomena: History and Latest Results. Terrapub.

[8] E. I. Parkhomenko. (2012). Electrical Properties of Rocks. Springer Science & Business Media.

[9] D. Ouzounov, S. Pulinets, F. Freund. (2011). Lithosphere-Atmosphere-Ionosphere Coupling (LAIC) model – An unified concept for earthquake precursors validation. Journal of Asian Earth Sciences, 41(4-5), 371-382.

[10] M. J. S. Johnston. (1997). Review of electric and magnetic fields accompanying seismic and volcanic activity. Surveys in Geophysics, 18(4), 441-476.

[11] V. Straser, G. Cataldi, D. Cataldi. (2016). SELF and VLF electromagnetic signal variations that preceded the Central Italy earthquake on August 24, 2016. New Concepts in Global Tectonics Journal, V. 4, No. 3, September 2016. pp473-477.

[12] D. Cataldi, G. Cataldi, V. Straser. (2017). SELF and VLF electromagnetic emissions that preceded the M6.2 Central Italy earthquake occurred on August 24, 2016. European Geosciences Union (EGU), General Assembly 2017. Geophysical Research Abstracts Vol. 19, EGU2017-3675, 2017.

[13] G. Cataldi, D. Cataldi, R. Rossi, V. Straser. (2017). SELF-ELF Electromagnetic signals correlated to M5+ Italian Earthquakes occurred on August 24, 2016 and January 18, 2017. New Concepts in Global Tectonics Journal, V. 5, No. 1, March 2017. pp134-143.

[14] V. Straser, G. Cataldi, D. Cataldi. (2017). Seismic signals detected in Italy before the Nikol'skoye (off Kamchatka) earthquake in July 2017. New Concepts in Global Tectonics Journal, v. 5, no. 3, September 2017. pp391-396.

[15] D. Cataldi, E. Cavina, G. Cataldi, V. Straser. (2022). Reverse Migration of the Wood Pigeons and electromagnetic emissions, before the Mw 3.7 earthquake occurred in Visso-Macerata, Central Italy on October 18, 2021. iJournals: International Journal of Social Relevance & Concern (IJSRC), ISSN-2347-9698, Volume 10, Issue 1 January 2022. pp. 24-40.

[16] G. Cataldi. (2020). Precursori Sismici – Monitoraggio Elettromagnetico. Kindle-Amazon,

ISNB: 9798664537970. ASIN Code: B08CPDBGX9.

[17] V. Straser. (2014). Precursori Sismici Elettromagnetici . LTPA Observer Project – Radio Emissions Project: una sperimentazione italiana. Sismicità. FESN – Friuli Experimental Seismic Network; Regione Autonoma Friuli Venezia Giulia Protezione Civile. Comune di Pozuolo Del Friuli. Gas Radon – Elettromagnetismo – Radioattività. Reti di Monitoraggio Ufficiali e Amatoriali. Stato dell'arte nella ricerca di segnali possibili precursori.. Pp45-47.

[18] ITU-R Recommendation V.431 – Nomenclature of the frequency and wavelength bands used in telecommunications, International Telecommunication Union.

[19] F. T. Freund. (2002). "Charge generation and propagation in rocks." Journal of Geodynamics, 33(4), 545-572.

[20] J. R. Bishop. (1981). Pore fluid effects in stress distribution and mechanical behavior of rocks. Pure and Applied Geophysics, 119(4), 913-928.

[21] A. Revil, P. Leroy. (2004). Constitutive equations for ionic transport in porous shales. Journal of Geophysical Research: Solid Earth, 109(B3).

[22] F. T. Freund. (2000). Time-resolved study of charge generation and propagation in igneous rocks. Journal of Geophysical Research: Solid Earth, 105(B5), 11001-11019.

[23] A. Takeuchi, H. Nagahama. (2001). Piezoelectricity generated by fault movements. Tectonophysics, 337(3-4), 223-232.

[24] O. A. Molchanov. M. Hayakawa. (1995). Seismo-electromagnetic phenomena. Izvestiya Physics of the Solid Earth, 31, 81-90.

[25] M. J. S. Johnston. M. Parrot. (2000). Electromagnetic emissions generated by earthquakes. Physics of the Earth and Planetary Interiors, 105(1-2), 159-170.

[26] A. Revil, T. Ané. (2008). Seismicity-induced electromagnetic fields. Journal of Geophysical Research: Solid Earth, 113(B11).

[27] E. I. Parkhomenko. (1971). Electrical Properties of Rocks. Plenum Press.

[28] O. A. Molchanov, M. Hayakawa. (2008). Seismo-electromagnetic phenomena: A study of mechanisms for earthquake preparation. Physics and Chemistry of the Earth, Parts A/B/C, 33(1-2), 77-88.

[29] R. Barr, D. L. Jones, C. J. Rodger. (2000). ELF and VLF radio waves. Journal of Atmospheric and Solar-Terrestrial Physics, 62(17-18), 1689-1718.

[30] J. R. Wait. (1996). Electromagnetic Waves in Stratified Media. Pergamon Press.

[31] K. G. Budden. (1988). The Propagation of Radio Waves: The Theory of Radio Waves of Low Power in the Ionosphere and Magnetosphere. Cambridge University Press.

[32] R. A. Helliwell. (2006). Whistlers and Related Ionospheric Phenomena. Dover Publications.

[33] M. B. Gokhberg, V. A. Morgounov, T. Yoshino. (1995). Earthquake Prediction: Seismo-Electromagnetic Phenomena. Gordon and Breach Publishers.

[34] A. V. Guglielmi, O. D. Zotov. (2012). Electromagnetic Precursors of Earthquakes in the VLF and ELF Ranges. Physics of the Solid Earth, 48(6), 441-448.

[35] M. Parrot. (1994). Statistical studies of ELF/VLF emissions recorded by a low-altitude satellite during seismic events. Journal of Geophysical Research: Space Physics, 99(A12), 23339-23347.

[36] S. A. Pulinets, K. A. Boyarchuk. (2004). Ionospheric Precursors of Earthquakes. Springer.

[37] D. D. Sentman. (1995). Schumann Resonances. Handbook of Atmospheric Electrodynamics, Volume I, 267-295.

ISSN number; ISSN 2202-0039

[38] M. Hayakawa, H. Sato. (1994). Earthquake-related Electromagnetic Waves and Fields (Review). Physics of the Earth and Planetary Interiors, 77(1-2), 127-137.

[39] A. P. Nickolaenko, M. Hayakawa. (2002). Schumann Resonance for Tyros: Essentials of Global Electromagnetic Resonance in the Earth-Ionosphere Cavity. Springer.

[40] A. Kulak, J. Mlynarczyk, K. Zietara, A. Michalec. (2003). A method of detecting the influence of seismic activity on Schumann resonance intensity. Journal of Atmospheric and Solar-Terrestrial Physics, 65(5), 591-596.

[41] O. A. Molchanov, M. Hayakawa. (1998). Subionospheric VLF signal perturbations possibly related to earthquakes. Journal of Geophysical Research: Space Physics, 103(A8), 17489-17504.

[42] V. Straser, G. Cataldi, D. Cataldi. (2016). SELF and VLF electromagnetic signal variations that preceded the Central Italy earthquake on August 24, 2016. New Concepts in Global Tectonics Journal, V. 4, No. 3, September 2016. pp473-477.

[43] N. Bagdassarov. (2021). Electric Resistivity. Cambridge University Press: 19 November 2021. Fundamentals of Rock Physics , pp. 292 – 360.

[44] J. H. Scott. (1983). Electrical and magnetic properties of rock and soil. USGS Publications Warehouse. Series Number: 83-915. DOI: 10.3133/ofr83915.

[45] L. Eppelbaum. (2017). Quantitative Examination of Piezoelectric/Seismoelectric Anomalies from Near-Surface Targets. Geosciences 2017, 7(3), 90.

[46] M. Boudouh, B. El K. Hachi, M. Haboussi, S. H. Habib. (2024). Application of the Finite Element Method (FEM) to Analyze the Mechanical Behavior of Piezoelectric Materials When an Electric Field Is Applied to a Piezoelectric Structure (Inverse Piezoelectricity). Eng. Proc. 2024, 67(1), 13.

[47] M. Sanfui, D. Biswas. (2017), Changes of the first Schumann resonance frequency during relativistic solar proton events. Annales Geophysicae. Pp 1241-1249.

[48] J. Shukla, S. L. Bougher. (2016). Impact of Solar Activity on the Earth's Electromagnetic Environment. urveys in Geophysics. Pp559-690.

[49] V. A. Rakov, M. A. Uman. (2018). The Role of Schumann Resonance in Solar-Terrestrial Physics. Journal of Geophysical Research. Pp 234-245.

[50] O. Santolík, M. Parrot. (2015). Solar Wind Influence on Earth's Ionospheric Conductivity and Schumann Resonances. Journal of Atmospheric and Solar-Terrestrial Physics. Pp 137-145.

[51] A. Greifinger, C. Greifinger. (2012). Effects of Solar Proton Events on Extremely Low Frequency (ELF) Waves in the Ionosphere. Journal of Atmospheric and Terrestrial Physics. Pp 1052-1060.

[52] F. Del Corpo, M. Pezzopane, B. Zolesi. (2021). Space Weather Effects Observed in the Northern Hemisphere during November 2021 Geomagnetic Storm: The Impacts on Plasmasphere, Ionosphere and Thermosphere Systems. MDPI Atmosphere. Pp 1-20.

[53] A. Nilam, T. K. Tulasi Ram. (2022). Statistical Analysis of Equatorial Electrojet Responses to the Transient Changes of Solar Wind Conditions. Frontiers in Astronomy and Space Sciences. Pp 45-60.

[54] S. Samsonov, A. Petrukovich, M. Kubyshkin. (2020). Geomagnetic Storm Effects on the Earth's Surface and Magnetosphere. Springer. Pp 97-114.

[55] M. Forster, S. Namgaladze, M. Hausler, M. Lühr. (2012). Numerical modeling of solar wind influences on the dynamics of the high-latitude upper atmosphere. Advances in Radio Science. Pp 299-312.

[56] A. Tsurutani, M. Buzulukova. (2022). The effects of solar wind interaction with Earth's magnetosphere: Auroras and space weather impacts. Frontiers in Astronomy and Space Sciences. Pp 1-15.

[57] E. Siscoe, J. Siebert. (2006). Magnetospheric currents and the transmission of solar wind energy to the Earth's upper atmosphere. Journal of Geophysical Research. Pp. 1045-1058.

ISSN number; ISSN 2202-0039

[58] V. Vasyliunas. (2007). Mechanisms of energy transfer from the solar wind to the Earth's atmosphere. Space Weather Journal. Pp. 401-418.

[59] H. Chen, P. Han, K. Hattori. (2022). Recent Advances and Challenges in the Seismo-Electromagnetic Study: A Brief Review. Remote Sensing. Pp. 5893-5915.

[60] L. Liu, T. Zhang, H. Geng. (2023). Ionospheric-Thermospheric Responses to Geomagnetic Storms from Multi-Instrument Space Weather Data. Remote Sensing. Pp. 2687-2705.

[61] M. Li, T. Zhang, H. Geng. (2023). Effects of Strong Geomagnetic Storms on the Ionosphere and Degradation of Precise Point Positioning Accuracy during the 25th Solar Cycle. Remote Sensing. Pp. 5512-5530.

[62] G. Cataldi, D. Cataldi. (2013). Reception of Natural Radio Emissions in the ELF Band. The INSPIRE Journal, Volume 20, Spring/Summer 2013. pp12-16.

[63] G. Cataldi, D. Cataldi, V. Straser. (2013). Variations Of Terrestrial Geomagnetic Activity Correlated To M6+ Global Seismic Activity. EGU (European Geosciences Union) 2013, General Assembly, Geophysical Research Abstracts, Vol. 15. EGU2013-2617, Vienna, Austria.

[64] G. Cataldi, D. Cataldi and V. Straser. (2014). Earth's magnetic field anomalies that precede the M6+ global seismic activity. European Geosciences Union (EGU) General Assembly 2014, Geophysical Research Abstract, Vol. 16, EGU2014-1068, Vienna, Austria.

[65] T. Rabeh, G. Cataldi, V. Straser. (2014). Possibility of coupling the magnetosphere–ionosphere during the time of earthquakes. European Geosciences Union (EGU) General Assembly 2014, Geophysical Research Abstract, Vol. 16, EGU2014-1067, Vienna, Austria.

[66] V. Straser, G. Cataldi. (2014). Solar wind proton density increase and geomagnetic background anomalies before strong M6+ earthquakes. Space Research Institute of Moscow, Russian Academy of Sciences, MSS-14. 2014. Moscow, Russia. pp280-286.

[67] V. Straser, G. Cataldi, D. Cataldi. (2015). Solar wind ionic and geomagnetic variations preceding the Md8.3 Chile Earthquake. New Concepts in Global Tectonics Journal, V. 3, No. 3, September 2015, Australia. P.394-399.

[68] G. Cataldi, D. Cataldi, V. Straser. (2016). Tsunami related to solar and geomagnetic activity. European Geosciences Union (EGU) General Assembly 2016, Geophysical Research Abstract, Vol. 18, EGU2016-9626, Vienna, Austria.

[69] G. Cataldi, D. Cataldi, V. Straser. (2017). Solar and Geomagnetic Activity Variations Correlated to Italian M6+ Earthquakes Occurred in 2016. EGU General Assembly 2017. EGU2017-3681, Vol. 19. Vienna, Austria.

[70] G. Cataldi, D. Cataldi, V. Straser. (2021). Space weather and geomagnetic activity related to the Japan M7.1 earthquake recorded on February 13, 2021. New Concepts in Global Tectonics Journal, Vol. 9, No. 1, pp16-23. March 2021.

[71] G. Cataldi, D. Cataldi, V. Straser. (2021). Space weather and geomagnetic activity related to the Chilean M6.7 earthquake recorded on February 3, 2021. New Concepts in Global Tectonics Journal, Vol. 9, No. 1, pp3-9. March 2021.

[72] G. Cataldi, D. Cataldi, V. Straser. (2021). Space weather and geomagnetic activity related to M6+ global seismic activity recorded on February 7, 2021. New Concepts in Global Tectonics Journal, Vol. 9, No. 1, pp24-30. March 2021.

[73] G. Cataldi, D. Cataldi, V. Straser. (2021). Space Weather and geomagnetic activity related to Ecuadorean M7.5 earthquake recorded on February 22, 2019. New Concepts in Global Tectonics Journal, Vol. 9, No. 2, pp79-86. June 2021.

[74] G. Cataldi, D. Cataldi, V. Straser. (2021). Solar Activity and geomagnetic activity related to M6+ global seismic activity recorded on March 20, 2021. New Concepts in Global Tectonics Journal, Vol. 9, No. 2, pp87-93. June 2021.

ISSN number; ISSN 2202-0039

[75] G. Cataldi, D. Cataldi, V. Straser. (2021). Space weather and geomagnetic activity related to M6+ global seismic activity recorded on 3-4 March 2021. New Concepts in Global Tectonics Journal, Vol. 9, No. 2, pp94-98. June 2021.

[76] G. Cataldi, D. Cataldi, V. Straser. (2021). Solar activity and geomagnetic activity related to M6.0 South Sandwich Islands region earthquake recorded March 14, 2021. New Concepts in Global Tectonics Journal, Vol. 9, No. 2, pp99-105. June 2021.

[77] G. Cataldi, D. Cataldi, V. Straser. (2021). Space weather and geomagnetic activity related to the Vanuatu M6.3 earthquake recorded on March 20, 2019. New Concepts in Global Tectonics Journal, Vol. 9, No. 2, pp106-111. June 2021.

[78] G. Cataldi, D. Cataldi, V. Straser. (2021). Space weather and geomagnetic activity related to M6+ earthquakes recorded between 7 and 20 November 2017. New Concepts in Global Tectonics Journal, Volume 9, Number 3, September 2021. pp137-144. ISSN 2202-0039.

[79] G. Cataldi, D. Cataldi, V. Straser. (2021). Space weather and geomagnetic activity related to M6+ earthquakes recorded between 12 and 15 April 2012. New Concepts in Global Tectonics Journal, Volume 9, Number 3, September 2021. Pp145-154. ISSN 2202-0039.

[80] G. Cataldi, D. Cataldi, V. Straser. (2021). Space weather and geomagnetic activity related to M6+ earthquakes recorded between 13 and 16 April 2016. New Concepts in Global Tectonics Journal, Volume 9, Number 3, September 2021. pp158-163. ISSN 2202-0039.

[81] G. Cataldi, D. Cataldi, V. Straser. (2021). Space weather and geomagnetic activity related to M6+ earthquakes recorded between 17 and 19 July 2017. New Concepts in Global Tectonics Journal, Volume 9, Number 3, September 2021. pp164-169. ISSN 2202-0039.

[82] V. Straser, D. Cataldi, G. Cataldi. (2018). Radio Direction Finding System, a new perspective for global crust diagnosis. New Concepts in Global Tectonics Journal, V. 6, No. 2, June 2018. pp203-211.

[83] D. Cataldi, G. Cataldi, V. Straser. (2019). Radio Direction Finding (RDF) - Pre-seismic signals recorded before the earthquake in central Italy on 1/1/2019 west of (AQ). European Geosciences Union (EGU) General Assembly 2019. Geophysical Research Abstract, Vol. 21, EGU2019-3124, 2019, Vienna, Austria.

[84] V. Straser, D. Cataldi, G. Cataldi. (2019). Registration of Pre-Seismic Signals Related to the Mediterranean Area with the RDF System Developed by the Radio Emissions Project. International Journal of Engineering Science Invention (IJESI), www.ijesi.org. Volume 8 Issue 03 Series. March 2019. PP 26-35. ISSN (Online): 2319 – 6734, ISSN (Print): 2319 – 6726.2019.

[85] V. Straser, D. Cataldi, G. Cataldi. (2019). Radio Direction Finding (RDF) - Geomagnetic Monitoring Study of the Himalaya Area in Search of Pre-Seismic Electromagnetic Signals. Asian Review of Environmental and Earth Sciences, v. 6, n. 1, pp16-27, 14 jun. 2019.

[86] V. Straser, D. Cataldi, G. Cataldi. (2019). Electromagnetic monitoring of the New Madrid fault us area with the RDF system - Radio Direction Finding of the radio emissions project. New Concepts in Global Tectonics Journal, V7 N1, March 2019. pp43-62.

[87] V. Straser, G. Cataldi, D. Cataldi. (2019). Namazu's Tail – RDF: a new perspective for the study of seismic precursors of Japan. Lulu Editore, 2019.

[88] V. Straser, G. G. Giuliani, D. Cataldi, G. Cataldi. (2020). Multi-parametric investigation of pre-seismic origin phenomena through the use of RDF technology (Radio Direction Finding) and the monitoring of Radon gas stream (RN222). An international journal for New Concepts in Geoplasma Tectonics, Volume 8, Number 1, May 2020, pp11-27.

[89] D. Cataldi, G. G. Giuliani, V. Straser, G. Cataldi. (2020). Radio signals and changes of flow of Radon gas (Rn222) which led the seismic sequence and the earthquake of magnitude Mw 4.4 that has been recorded in central Italy (Balsorano, L'Aquila) on November 7, 2019. An international journal for New

Concepts in Geoplasma Tectonics, Volume 8, Number 1, May 2020, pp32-42.

[90] V. Straser, G. Cataldi, D. Cataldi. (2020). Radio direction finding for short-term crustal diagnosis and pre-seismic signals. The case of the Colonna earthquake, Rome (Italy). European Journal of Advances in Engineering and Technology, 2020, 7(7):46-59.

[91] V. Straser, D. Cataldi, G. Cataldi. (2020). Radio Direction Finding (RDF) - Geomagnetic monitoring study of the Japanese area related to pre-seismic electromagnetic signals. New Concepts in Geoplasma Tectonics Journal. Vol. 8, No. 2, August 2020. pp119-141.

[92] T. Rabeh, D. Cataldi, Z. Z. Adibin, G. Cataldi, V. Straser. (2020). International study Italy-Malaysia pre-seismic signals recorded by RDF – Radio Direction Finding monitoring network, before earthquakes: Mw 6.3, occurred at 111 km SW of Puerto Madero in Mexico and Mw 6.3, occurred at 267 km NW of Ozernovskiy in Russia, November 20, 2019. New Concept in Geoplasma Tectonics. Vol. 8, No. 2, pp105-118. August 2020.

[93] D. Cataldi, V. Straser, G. Cataldi, G. G. Giuliani, Z. Z. Adibin. (2020). Registration of Pre-Seismic Radio Signals Related To The Russian And Jamaican Earthquakes With The RDF System Developed By The Radio Emissions Project. International Advance Journal of Engineering Research (IAJER), Volume 3, Issue 9 (September – 2020), PP 01-30; ISSN 2360-819X.

[94] V. Straser, D. Cataldi, G. Cataldi, G. G. Giuliani, J. R. Wright. (2020). Effects Of Hurricane Laura On The New Madrid Fault Area - Results Of Electromagnetic Monitoring Through The RDF Network - Radio Direction-Finding And Arkansas Electromagnetic Monitoring Station. New Concepts in Global Tectonics Journal. Vol.8, No.3, pp187-218, December 2020. ISSN 2202-0039.

[95] V. Straser, D. Cataldi, G. Cataldi, G. G. Giuliani. (2021). Pre-Seismic Signals Recorded By The Italian RDF Network Before The Occurrence Of Some Earthquakes In Northern Italy. International Journal of Software & Hardware Research in Engineering (IJSHRE), ISSN-2347-4890, Volume 9, Issue 1, pp63-76. January 2021.

[96] V. Straser, D. Cataldi, G. Cataldi. (2021). Radio Direction Finding, A New Method For The Investigation Of Presismic Phenomena. The Case Of Japan. International Journal Of Engineering Sciences & Research Technology (IJESRT). ISSN: 2277-9655, CODEN: IJESS7. 10(2): February, 2021, pp10-18..

[97] V. Straser, D. Cataldi, G. Cataldi, G. G. Giuliani. (2021). Electromagnetic monitoring of Italian volcanoes with the RDF Network, developed by the Radio Emissions Project. iJournals: International Journal of Social Relevance & Concern (IJSRC). ISSN-2347-9698, Volume 9 Issue 7 July 2021. pp92-136. DOI: 10.26821/IJSRC.9.7.2021.9710.

[98] D. Cataldi, V. Straser, G. Cataldi. (2021). Crustal relaxing - a new seismogenesis phenomenon associated with seismic trigger on a global scale. iJournals: International Journal of Social Relevance & Concern (IJSRC). ISSN-2347-9698, Volume 9 Issue 7 July 2021. pp137-163. DOI: 10.26821/IJSRC.9.7.2021.9711.

[99] V. Straser, D. Cataldi, G. Cataldi. (2022). Pre-seismic phenomena that preceded the M7.0 earthquake recorded in Acapulco (Mexico) on September 8, 2021. iJournals: International Journal of Social Relevance & Concern (IJSRC), ISSN-2347-9698, Volume 10, Issue 1 January 2022. pp. 41-57.

[100] D. Cataldi, V. Straser, G. Cataldi. (2022). "Terrestrial Flares" and presismic monitoring of the Radio Direction Finding network. Results of the experimentation carried out in Italy from 18 to 31 September 2021. iJournals: International Journal of Social Relevance & Concern (IJSRC), ISSN-2347-9698, Volume 10, Issue 4 April 2022. pp. 72-90.

[101] V. Straser, D. Cataldi, G. Cataldi, G. G. Giuliani. (2021). Electromagnetic Monitoring of Italian Volcanoes With the RDF Network. Journal Emerging Environmental Technologies and Health Protection (JEETHP), vol. 4, issue 1, pp. 32-40, ISSN 2623-4874, e-ISSN 2623-4882.

[102] D. Cataldi, G. Cataldi, V. Straser. (2023). Experimentation of The Italian RDF - Radio Direction Finding - Network, In The Search For Electromagnetic Seismic Precursors. iJournals:

International Journal of Social Relevance & Concern (IJSRC). Volume 11 Issue 1 January 2023. ISSN-2347-9698. Pp 1-9.

[103] V. Straser, D. Cataldi, G. Cataldi. (2023). Radio Direction Finder Method to Mitigate Tsunami Risk in Sierra Leone. Advances in Geological and Geotechnical Engineering Research. Volume 05, Issue 02, pp 64-75. April 2023.

[104] V. Straser. G. Cataldi, D. Cataldi. (2023). Analysis of possible electromagnetic seismic precursors related to the Turkish seismic sequence recorded on february 6, 2023. New Concepts In Global Tectonics Journal Vol 11, N 3, September 2023. Pp 213-232.

[105] D. Cataldi, Z. Bin Z. Abidin, G. Cataldi, V. Straser, A. A. Siyad, M. S. Radzi, Z. Hassan, A. N. Zulkiplee, M. Abdullah, N. S. A. Hamid. (2023). Experimentation of the RDF network for research on pre-seismic electromagnetic signals. New Concepts In Global Tectonics Journal Vol 11, N 3, September 2023. Pp 233-249.

[106] V. Straser, D. Cataldi, G. Cataldi. (2024). Comparison of Electromagnetic Signals Before an Earthquake Using the Radio Direction Finding Method. The Case of Po Plain Valley (Italy). MedGU 2022. Recent Research on Geotechnical Engineering, Remote Sensing, Geophysics and Earthquake Seismology pp 279–283. February 21, 2024. DOI: 10.1007/978-3-031-48715-6_60.

[107] D. Cataldi, G. Cataldi, V. Straser. (2024). Electromagnetic signals that preceded the M4.8 magnitude earthquake that occurred between New Jersey and New York on April 5, 2024. New Concepts in Global Tectonics Journal. Volume 12, Number 2, June 2024. Pp. 154-162.

[108] D. Cataldi, G. Cataldi, V. Straser. (2024). Electromagnetic signals that preceded the destructive earthquakes that occurred in Taiwan between April 2 and 3, 2024. New Concepts in Global Tectonics Journal. Volume 12, Number 2, June 2024. Pp. 132-141.

NCGT Journal
New Concepts in Global Tectonics

New Concepts in Global Tectonics Journal
Volume 13, Number 10, December 2025

ISSN number; ISSN 2202-0039

Seismotectonics of Karachi Periclinal Foredeep, Pakistan

Haleem Zaman Magsi, Nazir Zaman Magsi Baloch
Seismoenergy As Future Energy Resource (Project) 703
Dominion Business Centre 1, Bahria Town Karachi, Pakistan

Corresponding Author:
Haleem Zaman Magsi.
Seismoenergy As Future Energy Resource (Project) 703
Dominion Business Centre 1,
Bahria Town Karachi, Pakistan
Email:
zamanhaleemmagsi@gmail.com

Abstract: The seismicity of southern Pakistan is shaped by high activity in the western Makran–Ormara and eastern Kutch–Hyderabad domains, yet the intervening Karachi Periclinal Foredeep remains comparatively quiescent. This study examines the seismogeodynamic behaviour of the foredeep, drawing on seismic catalogues (1989–2025), recent swarm earthquake sequence (June–October 2025), and regional fault system analyses. While earlier interpretations described the foredeep's seismicity as diffuse or energy-deficient, evidence from focal depth distributions indicates seismic events spanning both upper and lower seismogenic layers, with clustering in confined focal volumes. Major bounding faults—including the Kirthar, Lakhra–Mubarak, and Kachi–Gharo faults—are interpreted as structural barriers that attenuate lateral seismic energy transmission from adjacent tectonic domains. This boundary-controlled behaviour is consistent with the stagnant–burstable–emission zone framework, wherein limited energy accumulation within small focal volumes restricts seismic magnitudes. Although the probability of large earthquakes remains low, the potential for moderate events poses localized hazards for Karachi's densely populated and infrastructure-vulnerable setting. These findings refine the regional seismic hazard assessment and contribute to broader models of individual tectonic elements.

Keywords: Karachi Periclinal Foredeep; seismicity; fault-bounded domains; intraplate tectonics; seismic hazard assessment

Introduction:

Karachi Metropolitan city, Pakistan had experienced low-moderate earthquakes in June-July 2025 (Fig.1). The absence of significant strong earthquakes in surrounding of Karachi Metropolitan City in June-Jule 2025 suggests that the recorded tremors are unlikely to be aftershocks . The geographic region encompassing Karachi and its surroundings lacks an active volcanic system, making volcanic eruptions highly improbable. Nonetheless, this area stays susceptible to substantial seismic activity, highlighting the complex tectonic processes (MonaLisa, and M. Qasim Jan 2015; Kukowski N., 2002; Namdarsehat , P et al., 2024 , Shah et al., 2023) underlying its seismotectonic vulnerability.

Notable historical and modern major earthquakes, such as those in Debal (magnitude 7.5–8), Shahbander (magnitude 7.5), and Awaran (magnitude 7.7), which occurred approximately 60–100 km east and 314 km northwest of Karachi, respectively (Bilham et al., 2007, Bilham 1999 2004; Javid Iqbal et al., 2017; Magsi 1983; Quittmeyer & Jacob, 1979) further emphasize this vulnerability (Fig.1).

The foci transition of seismic bursts of June-July 2025 from upper seismogenic layer (Magsi 2013) to mantle underscore the necessity for detailed investigations into the nature and genesis of ongoing seismogeodynamics, including the potential for future seismic events despite their intensity does not increase seismic zoning map category (Magsi 2014, Gulraiz et al., 2012; Naseer et al., 2015).

The low -moderate seismic bursts that impacted Karachi and its environs during the June–July 2025 period (Fig. 1), in conjunction with the historical and modern seismicity of southern Pakistan (Bilham 1999, 2004 2009, Bilham et al., 2007; Javed Iqbal et al., 2017; Magsi 1983; Quittmeyer & Jacob, 1979), as well as projections of potential earthquakes with intensities reaching up to 9.0 (Gulraiz et al., 2012; Naseer et al., 2015), collectively underscores the critical need for a comprehensive seismogeodynamic assessment of the Karachi Periclinal Foredeep region.

Swarm seismic burst can be considered precursory signals, reflecting ongoing seismotectonic processes, such as the transitions of seismic foci from upper and lower seismogenic layers (Magsi, 2013) towards the mantle (Fig.

ISSN number; ISSN 2202-0039

2), consistent with seismoenergy-reservoir structures within the seismogeodynamic environment zone.

Quittmeyer and Jacob (1979) and Quittmeyer et al. (1979) classified the seismicity of the southern Kirthar Ranges covering Karachi periclinal foredeep as diffuse, citing weak correlations with mapped surface faults. Conversely, studies (Sarwar and Alizai 2013, Hamid et al. 2012, and Mirza et al. 2024) associate regional seismicity with active faults in the Karachi Foredeep and adjoining areas, including a wrench fault traversing Karachi city (Sarwar & Alizai, 2013) and the Pab, Kirthar, Hab, Jhimpir, Surjan, Ornach–Nal, and Rann of Kutch faults (Mirza et al., 2024).

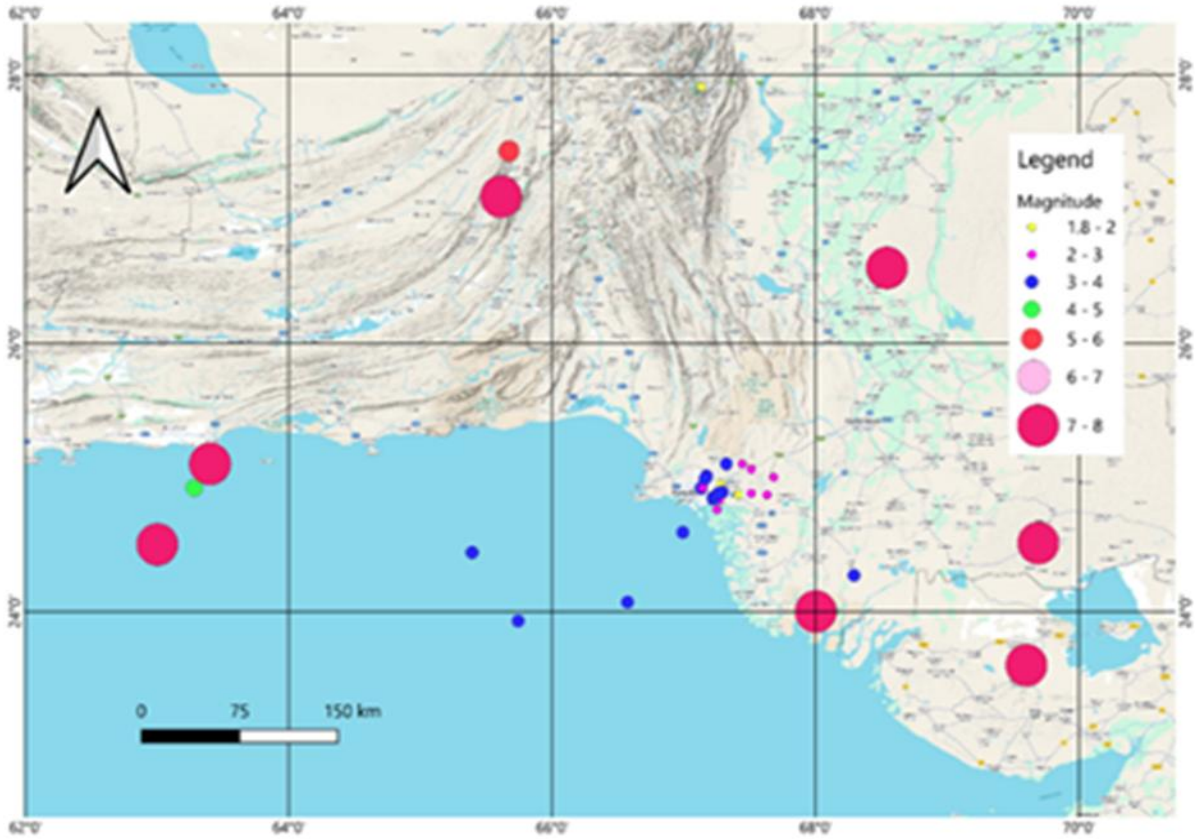

Fig. 1. Epicentres of swarm earthquakes June-Juley 2025 epicentres (PMD 2025) and historical and modern great seismic bursts (Bilham et al., 2007, Javed Iqbal et al., 2017, Magsi 1983, Quittmeyer and Jacob 1979, USGS catalogue 2025).

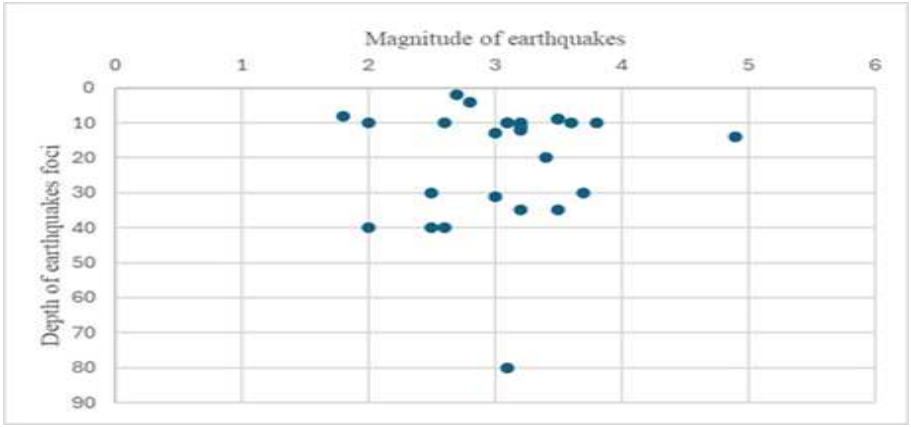

Fig.2. Magnitude and foci depth of swarm earthquakes June-July 2025.

NCGT Journal
New Concepts in Global Tectonics
New Concepts in Global Tectonics Journal
Volume 13, Number 10, December 2025
ISSN number; ISSN 2202-0039

However, Gorshkov (1984) challenges the conventional view that faults accumulate energy leading to earthquakes. Similarly, Magsi (1983, 1985, 2014) argues that faults do not source and reservoir seismoenergy but instead act as conduits for its emission (Magsi, 2017). Building on this perspective, Magsi Baloch and Magsi Baloch (2024) propose a model of lithospheric segmentation composed of stagnant, burstable, and emission zones, with the burstable zones representing the loci of seismic activity (Fig.3). Considering these evolving interpretations, the present study seeks to classify the Karachi Foredeep according to the lithospheric zoning framework proposed by Magsi Baloch and Magsi Baloch (2024). This classification aims to enhance understanding of the regional seismic hazard and to inform future strategies for seismic risk assessment and mitigation.

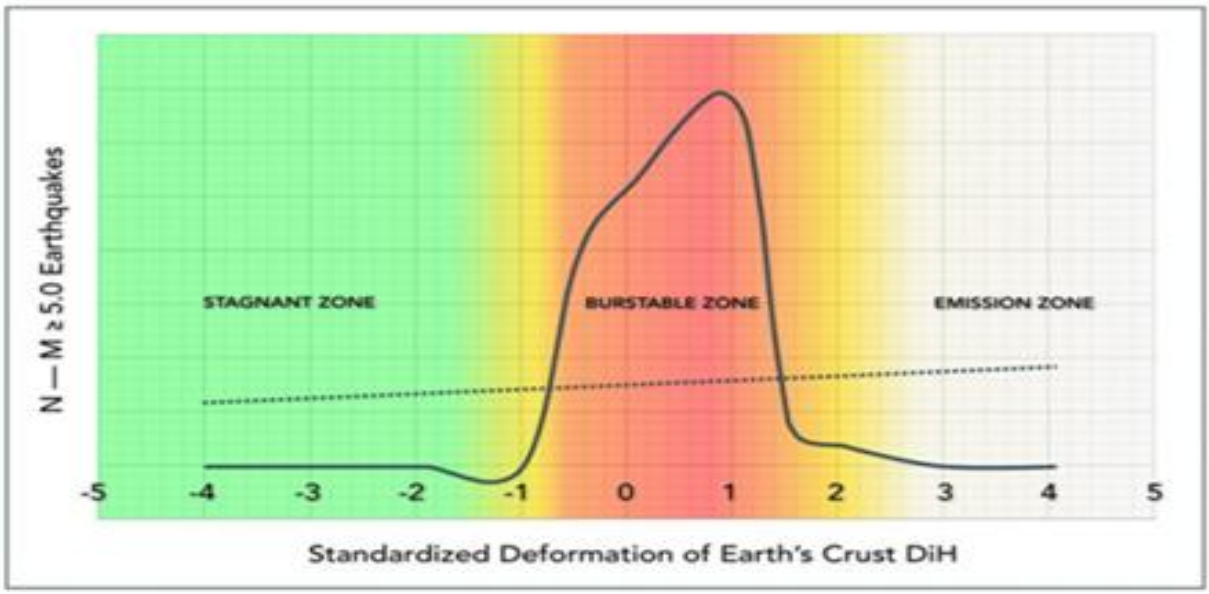

Fig.3. Spatial zones of geodynamic stress as stagnant, burstable, and emission zones (after Magsi Baloch and Magsi Baloch 2024).

Seismicity:

The seismicity of southern Pakistan (Asad ur Rahman et al., 2021; Bilham 1999, 2004, 2009, Bilham et al., 2007; Javid Iqbal et al., 2017; Magsi, 1983; Quittmeyer & Jacob, 1979; Tirmizi et al., 2023; USGS Catalogue, 2025), encompassing both modern and historical earthquakes with magnitudes ≤ 8.1, (Fig.4) delineates two principal seismotectonic flanks adjacent to the Karachi Periclinal Foredeep. Six major seismic bursts, with magnitudes ranging from 7.0 to 8.1, have been documented in the western flank (Bilham 2004, 1999, Bilham et al., 2007) also term as Makran zone (Quittmeyer et al., 1979). In contrast, eastern flank consists of the Sindh and Kutch zones (Khan et al., 2002) have collectively experienced five strong earthquakes. Despite western and eastern flanks are undergoing significant seismic activity, the Karachi Periclinal Foredeep is experiencing low to moderate seismic bursts (Fig. 4). Analysis of contemporary seismicity reveals two distinct spatial patterns in the distribution of earthquake epicentres along the western Makran and eastern Sindh seismic provinces, relative to the Karachi Periclinal Foredeep (Fig. 4). In the Makran Seismotectonic Zone, the alignment of epicentres exhibits a directional shift in axis from NE to N as it approaches the foredeep. Conversely, the seismicity in the Sindh Seismotectonic Zone trends NW relative to the foredeep. Notably, the NE- and NW-trending axes of these two zones intersect at the Khuzdar uplift (Voskresenskiy et al., 1971), also referred to as the Khuzdar Knot (Sarwar & De Jone, 1979). Nabi et al. (2024) reported no definitive seismic source within the Karachi Periclinal Foredeep, attributing its relatively low seismicity to insufficient conditions for substantial seismoenergy accumulation. Instead, it is plausible that active faults facilitate the dissipation of seismoenergy rather than its storage (Magsi, 2014, 2017).

NCGT Journal
New Concepts in Global Tectonics
New Concepts in Global Tectonics Journal
Volume 13, Number 10, December 2025
ISSN number; ISSN 2202-0039

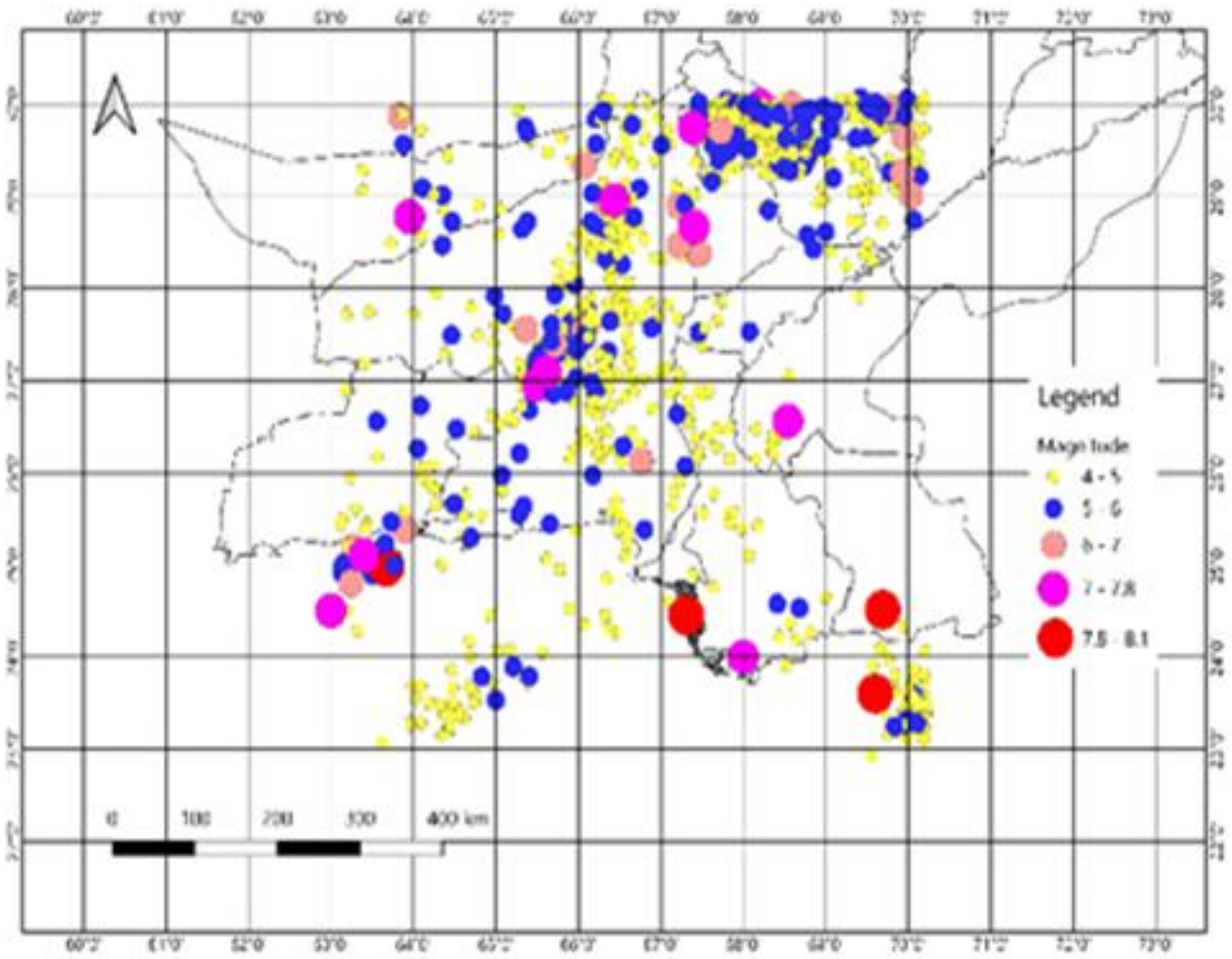

Fig.4. Historical and Modern Seismicity of Southern Pakistan (after (Bilham et al., 2007; Javid Iqbal et al., 2017; Magsi, 1983; Quittmeyer & Jacob, 1979; USGS Catalogue, 2025).

The Pakistan Meteorological Department (PMD) recorded low-magnitude seismic events impacting the southern sector of the Karachi Periclinal Foredeep during June–July 2025 (Fig.1). Of these, 15 earthquakes with magnitudes ≤ 3.8 were concentrated in the Malir and Eastern districts of the Karachi metropolitan division (Fig.5). On one notable day, six seismic bursts occurred in rapid succession (PMD Catalogue, 2025), demonstrating the clustered nature of recent local seismicity. These events originated from both upper and lower seismogenic zones within the crust (Magsi, 2013), with one event sourced from the mantle. Two additional earthquakes occurred at unusually shallow depths of 2 km and 4 km, respectively (Fig. 2). The June–July 2025 seismic swarm therefore highlights the need for a comprehensive evaluation of the seismotectonic environment of the Karachi Periclinal Foredeep. Such an assessment requires the formulation and application of a three-dimensional geodynamic model that incorporates stagnant, burstable, and emission zones to more accurately characterize its seismogeodynamic behaviour.

New Concepts in Global Tectonics Journal
Volume 13, Number 10, December 2025
ISSN number; ISSN 2202-0039

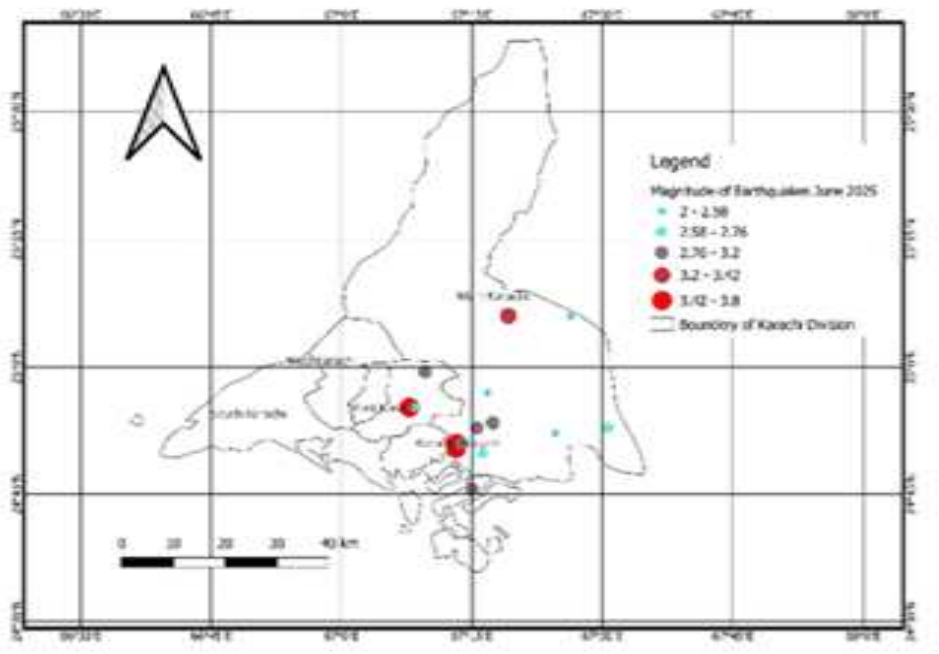

Fig.5. Earthquake epicentres of June-July 2025 in Karachi City.

Tectonic Setting:

The Karachi Periclinal Foredeep (KPF) is superimposed on a series of structural elements established during the Oligocene (Voskresenskiy et al., 1971). Its axis is gently inclined westward. The KPF is bordered to the west by the Kirthar Meganticlinorium and to the north by the Badra–Sanbak Saddle. Along its eastern margin, it adjoins both the Badra–Sanbak Saddle and the Sindh Monocline (Voskresenskiy et al., 1971; Magsi, 1983). South–southwestward, the trough terminates into the Arabian Sea (Fig. 6).

Sarwar and De Jong (1979) identified an autonomous tectonic entity, Khuzdar–Karachi Block situated on the western margin of the Indian plate. Khuzdar-Karachi tectonic block domain encompasses the Khuzdar transverse uplift, Kirthar foredeep, and Karachi periclinal trough, Badra-Sanbak folded saddle, and Kotri-Hyderabad uplift developed along the margin of the Indian Platform slope (Voskresensky et al., 1971). However, Fazal et al. (2016) prefers to recognize only the Sulaiman and Kirthar Folded Belts along with its respective foredeeps. omitting the Khuzdar and Karachi blocks. They specifically exclude the Karachi Foredeep and the Hub (Porali) Foredeep (Siddiqui and Jadoon 2013) from the Sulaiman-Kirthar foredeep belt.

Sarwar and de Jong (1979) suggested that the Khuzdar-Karachi Block undergoes a counterclockwise rotational motion along with Indian Plate, which influences the intricate dynamic processes within the Indo-Pakistani Plate. Siddiqui and Jadoon (2013) corroborated rotational kinematic pattern and suggest it deemed crucial in the genesis and evolutionary history of the Porali Trough during the Oligocene epoch. While, according to Voskresensky et al. (1971) and Magsi (1983), the Hub (Porali) trough and Karachi periclinal foredeep are coeval features that amalgamated during the Oligocene period.

Schelling (1999) discerns a bifurcation of Kirthar folded belt into central and southern segments, with the Manchar strike-slip fault demarcating the interface between the east-vergent imbricate fan characteristic of the Karachi arc and the west-vergent structural regime of the Central Kirthar Range. Schelling (1999) introduced a detachment model to explain the eastward displacement of the southern Kirthar folded belt, positing that the detachment surface is located within the shale-dominated Cretaceous Sember - Goro Shale (Sarwar & De Jong, 1979) source of development of structure elements. While Sarwar and Alizai (2013) propose mechanism linking the eastward migration of the southern Karachi Arc with a wrench fault system that transects the urban area of Karachi. in the Karachi periclinal trough.

ISSN number; ISSN 2202-0039

The Karachi arc (Sarwar and De Jong 1979) is moving eastward along the Sembar–Goru Shale (Cretaceous) décollement surface (Sarwar & De Jong, 1979; Sarwar and Alizai 2013, Schelling, 1999). Its northern and southern boundaries are defined by the Manchar Lake strike-slip fault (Schelling, 1999) and the Proto Karachi–Keenjhar boundary strike-slip fault (Haleputo et al., 2025), respectively.

Continued subsidence of the Hyderabad Graben facilitates this progressive eastward "crawling" of the Karachi Arc (Sarwar, 2004). Although once regarded as a distinct tectonic entity, the Karachi Arc is now interpreted as part of the South Kirthar Fold Belt (Haleputo, 2025, Schelling, 1999; Khalid et al., 2023; Zaigham & Mallick, 2000). The Manchar Lake strike-slip fault separates the Central and Southern Kirthar belts (Schilling, 1999). Together, the Manchar Lake and Karachi–Keenjhar strike-slip faults exert primary control on both the eastward displacement of the Karachi Arc and the subsidence of the Hyderabad Graben (Sarwar, 2004; Haleputo et al., 2025).

The Fault Tectonic Map of South Asia (Kuznetsov, 1980) delineates major Early to Middle Proterozoic basement faults, including the Kirthar Fault, an unnamed fault active during the — P. N=Q period, and an inferred fault associated with the Owen‑Murray Fault System. Author termed the unnamed active fault as the Kachi–Gharo Fault, while the inferred (hidden) fault corresponds to the Lakhra–Mubarak Fault. The Kirthar Fault comprises two segments: a northern thrust segment and a southern strike-slip segment, which merges with the inferred Lakhra–Mubarak Fault (Fig.7). The Lakhra–Mubarak Fault trends transversely across the southern Kirthar Fold Belt (Schelling, 1999) and extends southward to join the Owen–Murray Fault System in the Arabian Sea.

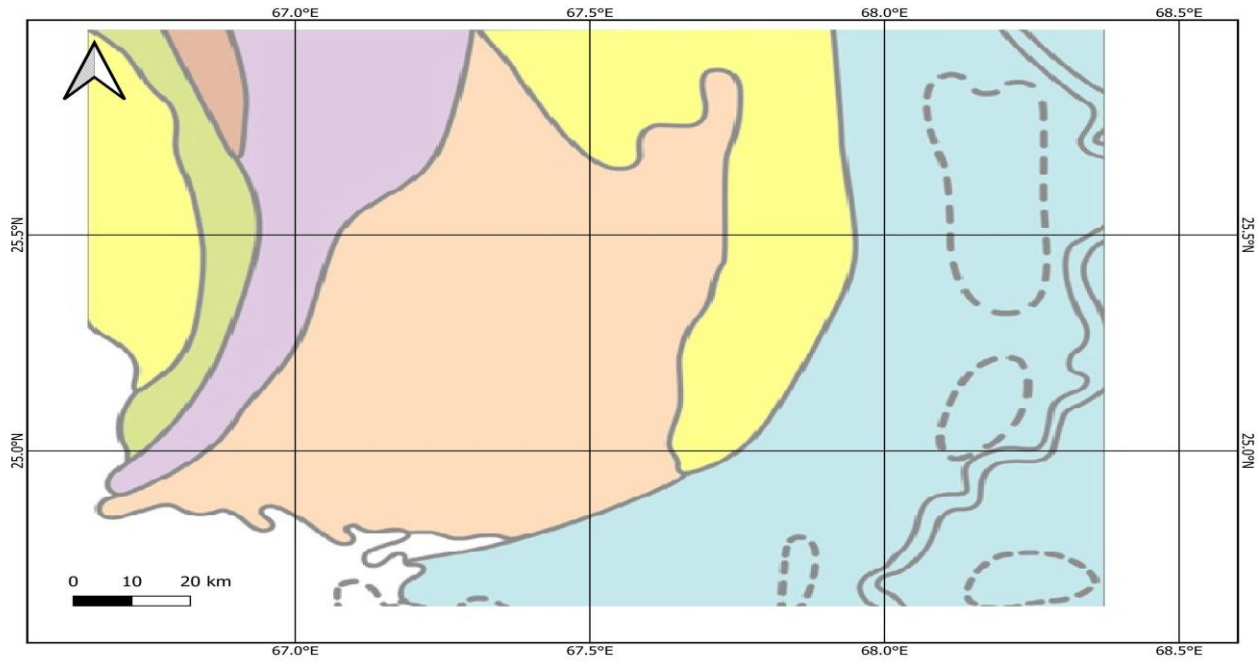

Fig.6. Karachi Periclinal Foredeep and adjacent tectonic elements (After Voskresenskiy et al., 1971 with some changes).

A comparison of the tectonic map of Voskresenskiy et al. (1971) with Kuznetsov's (1980) fault map indicates that the Lakhra–Mubarak Fault, running transversely through the northern part of the southern Kirthar Fold Belt, forms the western boundary of the Karachi Periclinal Trough. In contrast, the Kachi–Gharo Fault, active in the Paleogene and Neogene, defines its eastern boundary (Fig. 7).

The eastern flank of the Karachi Trough is dominated by submeridional anticlinal structures, typically manifested as asymmetric brachanticlines. The northern segment is relatively uplifted, exhibiting hyposymmetric topography with gentle arches developed within Upper Paleogene sediments. The southern segment is more deeply submerged and contains Miocene strata overlain locally by coarse-grained Palaeocene deposits. In this region, bedding is largely subhorizontal, and fold structures are weakly expressed.

ISSN number; ISSN 2202-0039

Along the western margin, the trough forms a relatively simple monocline, whereas the eastern margin is structurally broader and more complex, comprising several chains of east-verging asymmetric brachanticlines. Fold strikes are predominantly submeridional but curve southwestward toward the southern end of the trough.

In the northern segment of the trough, folds are well developed and clearly delineated. Anticlines display gently arched cores with low-angle western limbs (2–20°) and steep eastern limbs (40–90°), often modified by flexures. Three principal anticline zones—Rahuja, Sari Singh, and Benir—expose the Oligocene Nari Formation in their cores, with localized uplifts ranging from 100 to 650 m. The southern trough is dominated by the Miocene Gaj Formation, overlain by Pliocene clastic of the Manchar Formation. Numerous small-amplitude, linear folds occur here, typically lacking distinct periclinal closures, and subhorizontal bedding predominates. Notable structures in this segment include the Drigh Road Anticline (Karachi) and the Pir Mango Structural Nose. Authors suggest block folding (Belousov 1980) as mechanism of the brach folds

Discussion:

The seismicity landscape of southern Pakistan is characterized by high seismic activity in the western and eastern regions (Bilham et al., 2007). In contrast, the Karachi Periclinal Foredeep, positioned between these high seismicity zones, exhibits significantly lower to moderate seismic activity (Quittmeyer & Jacob, 1979; Bilham et al., 2007; Javid Iqbal et al., 2017, USGS Catalogue 2025). Elevated seismicity in the western domain has been attributed to the complex interactions at the triple junction of the Indian, Eurasian, and Ormara microplates (Kukowski et al., 2002), as well as to the subduction of the Arabian Plate beneath the Eurasian Plate (Abbas & Zia, 2021; Bilham et al., 2007; Gulraiz et al., 2013, Namdarsehat et.al., 2024). In the east, seismicity is often associated with hidden faults (Bilham et al., 2007), while Sarwar (2004) suggested that the junction of the Hyderabad graben, Kutch graben, and Karachi arcs also plays a significant role in shaping seismic activity in the eastern flank domine.

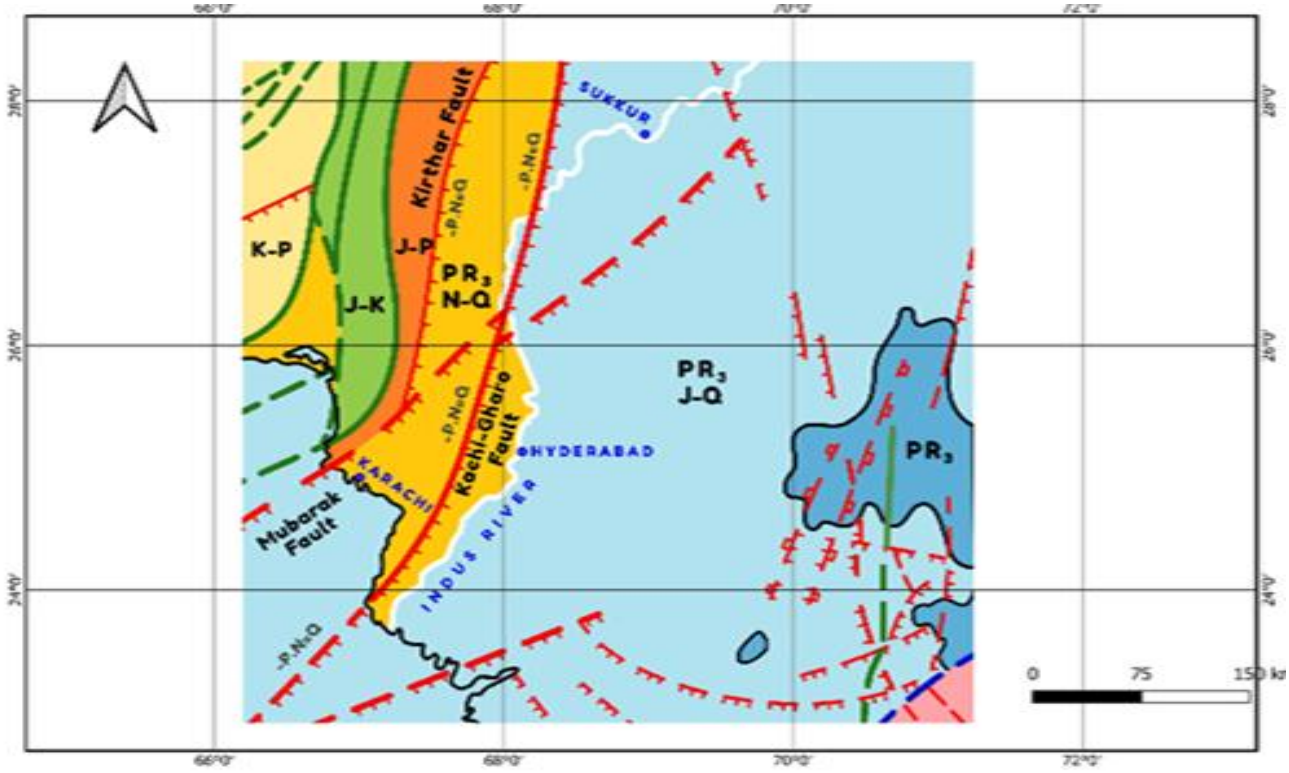

Fig.7. Regional faults of Karachi Periclinal Foredeep and adjacent regions (after Kuznetsov's 1980 with some changes).

The low seismicity Karachi Periclinal Foredeep has been interpreted in varying ways (Fig.8). Quittmeyer et al. (1979) described its seismicity as diffuse, whereas Nabi et al. (2019) suggested the absence of primary seismic energy sources within the trough. Subsequent studies, however, identified several active faults in and around Karachi—including the Wrench, Pub,

Kirthar, Hab, Jhimpir, Surjan, Ornach-Nal, and Rann of Kutch faults—which are thought to influence the foredeep's seismicity (Gulraiz et al., 2013; Hamid et al., 2012; Mirza et al., 2024; Naseer et al., 2015; Sarwar & Alizai, 2013). Magsi (1985, 2014, 2017) argued that these structures primarily act as conduits for seismic energy dissipation rather than as independent sources of seismic bursts (Magsi 2014,2015, 2017).

The seismogeodynamic behaviour of the Karachi Periclinal Foredeep is further complicated by energy transmigration from adjacent tectonic domains. Abbas & Zia (2021), Bilham et al. (2007), Gulraiz et al. (2013) and Sarwar (2004) suggested that seismic energy may migrate laterally into the basin from the east and west and influences on seismicity of Karachi Periclinal Foredeep. However, Xiaowa et al. (2021) reasoned that regional faults act as boundaries separating seismogenic blocks. In this context, the Kirthar Fault, as well as the inferred Lakhra–Mubarak and Kachi–Gharo faults, delineate the western, Karachi Periclinal foredeep, and eastern domains respectively (Fig.7). These boundary faults likely impede the lateral propagation of seismic energy into the foredeep, a hypothesis supported by the absence of seismic energy extension from the Indus–Kohistan Seismic Zone to north of the Main Mantle Thrust (Monaliza et al., 2009).

Seismic events recorded in southern Karachi Periclinal Foredeep during June–July 2025 (M 1.8–4.9) highlight the dynamic but subdued character of the region (PMD Catalogue 2025). Fifteen events were concentrated in the Malir and eastern districts of Karachi (Fig.6), including six earthquakes occurring within a single day. 89 % of earthquakes foci spanned both in upper and lower seismogenic layers (Magsi, 2013), with one event originating from the mantle and 7% in upper riding cover layer (2–4 km depth). The vertical distribution of foci within the June–July 2025 tremor sequence a complex genesis of these events, extending from the upper riding cover layer of crust to the mantle involving both shallow and deep crustal processes (Fig.8).

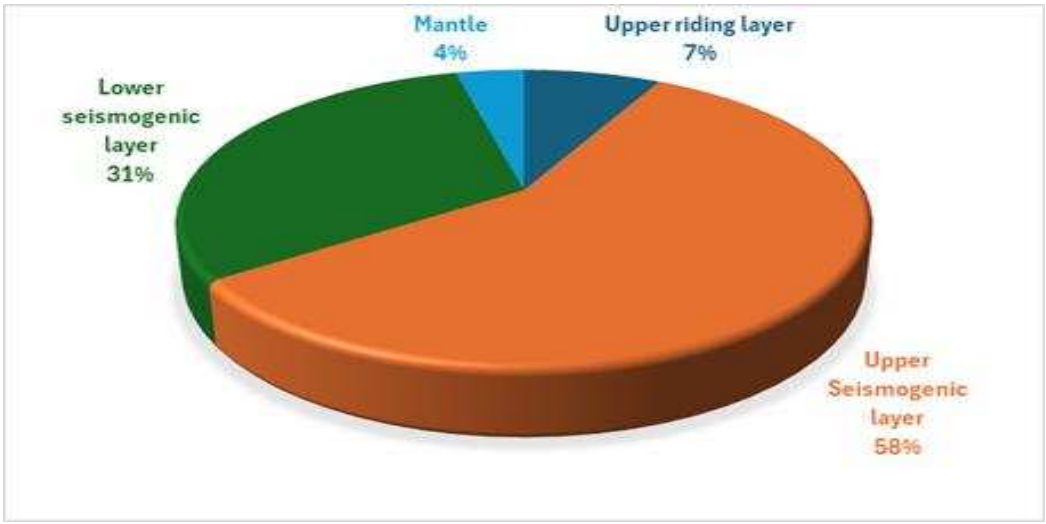

Fig.8. Vertical Distribution of Earthquake Foci of June-July 2025 in Karachi City.

The depth variability and clustering raise questions about the mechanisms governing seismicity in the foredeep. Swarm earthquakes are often linked to slow-slip events along plate boundaries (Farge and Brodsky 2025, Obara 2020, Supino et al., 2020) and to Moho-related seismic bursts (Kalenda & Neumann, 2013). However, these processes are not strongly evident in the Karachi Periclinal Foredeep. Takemura et al. (2022) proposed that fluid migration near plate interfaces initiates slow-slip events, but such mechanisms are geographically restricted to subduction margins., such, a mechanism of the Makran subduction zone, where the Arabian Plate is subducting beneath the Eurasian Plate as the Makran zone, and are not directly applicable to the Karachi Periclinal Foredeep. This spatial disparity underscores the need for alternative frameworks to explain foredeep seismicity.

Given the absence of a direct causal relationship between slow-slip seismic events and the Karachi Periclinal Foredeep, alternative hypotheses are necessary to explain the seismicity patterns observed in this region. The present analysis supports a seismogeodynamic model in which regional fault systems act primarily as boundaries, attenuating seismic energy flux from the adjacent tectonic domains rather than transmitting it into the foredeep. This attenuation exerts only a minimal modulatory influence on the basin's seismotectonic processes, providing a plausible explanation for the region's consistently low seismicity.

Its low seismicity is best explained by the buffering role of

ISSN number; ISSN 2202-0039

the bounding faults and the presence of small volume foci that create explosive zones in the seismogenic layers of earth' crust. This interpretation provides a more detailed understanding of the tectonic behaviour of the foredeep and provides a conceptual framework that complements, but goes beyond, traditional fault-controlled seismicity models

The distribution of seismic foci from June–July 2025 (Fig.2) within the upper and lower seismogenic layers of Pakistan (Magsi, 2013), coupled with the seismicity (Fig.4) observed between 1909 and 2025 (Bilham et al., 2007; Javid Iqbal et al., 2017; Magsi, 1983; Quittmeyer and Jacob, 1979; USGS Catalogue, 2025), supports the application of the seismotectonic model of stagnant zone, burstable zone, and emission zone (Magsi Baloch & Magsi Baloch, 2024) for Karachi Periclinal Foredeep. This framework emphasizes accumulation of seismoenergy in the three-dimensional volume (focus) confined "burstable zones" within the upper and lower seismogenic layers, from which energy is eventually released. Small focal volumes (Gorshkov 1984) in the burstable zone in the upper and lower seismogenic layers (Magsi 2013) formed in result of earth's crust crushing (Magsi 1985) and as small volume folds (Haleputo, 2025a, b) collectively suggests that the Karachi Periclinal Foredeep represents a seismogenic domain characterized by small focal zones and limited energy release

Conclusion:

The seismicity of the Karachi Periclinal Foredeep is defined by its relative quiescence when compared with the adjacent western and eastern tectonic domains of southern Pakistan (Bilham et al., 2007). While the foredeep is characterized by generally low to moderate levels of seismic activity, the punctuated earthquake sequence of June–October 2025 highlights that seismic events within this basin tend to occur in both the upper and lower seismogenic layers (Magsi, 2013). These events, however, remain limited in magnitude and extent, primarily due to the restricted volume of the foci that comprise the burstable zone (Magsi Baloch & Magsi Baloch, 2024).

Regional fault systems—including the Kirthar, Lakhra–Mubarak, and Kachi–Gharo structures—appear to act as structural boundaries that impede the lateral transfer of seismic energy into the Karachi Periclinal Foredeep. This interpretation is consistent with the stagnant–burstable–emission zone framework (Magsi Baloch & Magsi Baloch (2024).

In contrast to models that attribute earthquake swarms to slow-slip behaviour and fluid migration along subduction interfaces (Takemura et al., 2022; Supino et al., 2020), the Karachi Periclinal Foredeep demonstrates a distinct seismogeodynamic regime. Its relatively low seismicity is more effectively explained by the limited energy accumulation possible within small, three-dimensional focal volumes confined to the burstable zones of the crust.

Taken together, these observations suggest that the Karachi Periclinal Foredeep functions as a transitional seismogenic domain, where fault-bounded energy barriers, focal volume dynamics, and crustal deformation collectively govern seismic expression. Understanding this interplay not only sharpens the regional seismic hazard framework for southern Pakistan but also contributes to the broader study of intraplate seismicity in foredeep basins worldwide. For Karachi city—situated directly atop this foredeep—these findings imply that while the probability of large-magnitude earthquakes remains low, localized moderate events within the burstable zones could still present significant hazard potential given the city's dense population and vulnerable infrastructure.

Acknowledgement: The author(s) gratefully acknowledged the Pakistan Meteorological Department (PMD) US Geological Survey (USGS) for providing linkage of catalogues that formed the basis of this research. Sincere thanks are also extended to the academic and research community whose contributions to the study of regional tectonics and seismicity provided the foundation for this work. The author(s) further appreciate the constructive insights and guidance offered by colleagues and reviewers, which enhanced the quality and clarity of this study.

Funding Information: This research received no specific grant from any funding agency in the public, commercial, or not-for-profit sectors.

Author's Contributions: Haleem Zaman Magsi conceptualized and designed the study, performed data collection and analysis, interpreted the results and drafted the manuscript. Nazir Zaman Magsi Baloch prepared figures. Both authors reviewed, edited, and approved the final version of the manuscript**.**

Ethics: This study did not involve human participants, animals, or sensitive personal data. All data used were

ISSN number; ISSN 2202-0039

obtained from publicly available seismic catalogues and published research. The authors declare that the research was conducted in accordance with ethical standards and relevant guidelines for scientific integrity.

Reference:

Abbas Haider and Zia ur Rehman 2021. Evaluation of seismicity of Karachi city in the context of modern building code. Arabian Journal of Geosciences 14: 65.p.1-12. https://doi.org/10.1007/s12517-021-06462-3.

Asad ur Rahman, Fawad Ahmed Najam, Saeed Zaman Atif Rasheed Rana 2021. An updated probabilistic seismic hazard assessment (PSHA) for Pakistan. Bulletin of Earthquake Engineering. https://doi.org/10.1007/s10518-021-01054-8.

Bilham, R., Lodi, S., Hough, S., Bukhary S., Khan A., and Rafeeqi S. 2007. Seismic Hazard in Karachi, Pakistan: Uncertain Past, Uncertain Future. Seismological Research Letters Volume 78, No.6. Pp.601- 613

Bilham R. 2009. The seismic future of cities. Bull Earthquake E. DOI 10.1007/s10518-009-9147-0.

Bilham, R., 1999, Slip parameters for the Rann of Kachchh, India, 16 June 1819, earthquake quantified from contemporary accounts, in Stewart, I. S. & Vita-Finzi, C. (Eds) Coastal Tectonics. Geological Society London, v. 146, p. 295-318.

Bilham, R., 2004, Earthquakes in India and the Himalaya: tectonics, geodesy and history, Annals of Geophysics, v. 47, p. 839-858.

Farge G., and Brodsky E.E. 2025. The big impact of small quakes on tectonic tremor synchronization Sci. Adv. 11, eadu7173pp.1-10.

Farhana Sarwar, Saleem Iqbal, Muhammad Qaisar, Abdul Rehman, Faiza Akhtar,2016. Earthquake Statistics and Earthquake Research Studies in Pakistan. Open Journal of Earthquake Research, 5, 97-104. s. http://www.scirp.org/journal/ojer http://dx.doi.org/10.4236/ojer.2016.52007.

Gorshkov, G.P., 1981. Fault or deformation of the medium? In the book geologic - geophysical research methods in seismic-prone zones. Abstracts of All-Union session hazardous areas (2-6 September 1981) Frunze 12-13. (In Russian).

Gorshkov, G. P. (1984): Regional seismotectonics of the territory of the south of the USSR. Moscow: Nauka, 272 p. (in Russian).

Gulraiz Hamid, Khalil A. Mallick, Syed Zeeshan Jaferi, Imran A. Siddiqui, Ibraheem Azmat 2013. Structural and Tectonic Control of Karachi (Pakistan) and the Possibilities of Seismic Hazards. International Journal of Natural and Engineering Sciences 7 (2): 01-07, www.nobel.gen.tr

Halepoto A.A., Agheem M.H, Hakro A., Shabeer Ahmed and Ahmedani S.B.2025 Geometry and Kinematics of the Gentle to Open Fault-propagation Fold having Four-way Dip Enclosure: Outcrop and Lineament Analysis of the Rois Anticline, Southern Kirthar Fold Belt, Pakistan Journal of Himalayan Earth Sciences Volume 58, No. 1, pp. 88-106.

Halepoto A.A., Agheem M.H, Hakro A., Shabeer Ahmed and Ahmedani S.B.2025. Lateral strike-slip deformation and possible transition of extensional faults to strike-slip faults in the foreland fold belt: a regional to outcrop tectonic synthesis of the Southern Kirthar Fold Belt, northwestern Indian Plate, Pakistan. Journal of Asian Earth Sciences 291. 106678. https://doi.org/10.1016/j.jseaes.2025.106678.

Javed Iqbal, Jadoon I., Raja I., 2017. The Balochistan Earthquake 2013: Emergence of A New Island in The Arabian Sea. SDRP Journal Of Earth Sciences & Environmental Studies. volume:2 Issue:1 pp.1-13. www.siftdesk.org.

Khan, A. M., Abbasi, A. and Khattak, G., 2002. Geological Control on Natural Hazards: Earthquakes and mass movement hazards in Pakistan. Geol. Bull. Univ. Peshawar, v. 35, p. 1-8.

Kukowski N., Schillhorn T., Flueh E. and Huhn K. 2002. Newly identified strike-slip plate boundary in the northeastern Arabian Sea. Geology; v. 28; no. 4; p. 355–358.

Magsi, H.Z., 1983. Seismotectonics of Pakistan. Ph. D. Thesis, p.155 (in Russian).

Magsi, H.Z., 1985. Evaluation of seismic danger zones in Pakistan based on the interpretation of Landsat data. Bulletin of the International Institute of Seismology and

Earthquake Engineering, Building Research Institute, Ministry of Construction, Japan. v. 22, p. 133-137.

Magsi, H.Z., 2013. Seismogenic layers in Pakistan. New Concepts in Global Tectonics Journal, v. 1, no. 4, p. 29-33. www.ncgt.org

Magsi, N. 2014. Relation of seismicity with surface faults in Pakistan: an overview. New Concepts in Global Tectonics Journal, v. 2, no. 1, p.42 -55. www.ncgt.org.

Magsi, H.Z. 2017 Seismotectonics of the Nanga Parbat - Haramosh Massif, Gilgit Baltistan, Pakistan. New Concepts in Global Tectonics Journal, v. 5, no. 4, p.590 -590 www.ncgt.org.

Magsi, N., & Magsi Baloch, S. 2025. Seismotectonics of the Karakoram Folded Belts (in preparation).

Magsi Baloch, H.Z., & Magsi Baloch, N., 2024. In the search of earthquakes: An overview. New Concepts in Global Tectonics Journal, v. 12, no. 3, p.228-239 www.ncgt.org.

Mirza, M.Q. Yasir Bashirb, and Syed Haroon Alic 2024 Application of Probabilistic Seismic Hazard Assessment for Earthquake Hazard: Case Study of Karachi City, Pakistan. Journal of Earth Sciences and Technology. Vol. 5, No. 1, 20–33

MonaLisa, and M. Qasim Jan 2015. Awaran, Pakistan, Earthquake of Mw 7.7 in Makran Accretionary Zone, 24 September 2013: Preliminary Seismotectonic Investigations. Proceedings of the Pakistan Academy of Sciences 52 (2): 159-168.

Nabi A, Xiaodong Liu, Zhijun Gong, Abbas Aliand Umair Khalil.2019. Seismic potential and neotectonic studies at Karachi, Gadap and Hub areas, southern Kirthar Fold Belt, Pakistan. Pacific International Journal, Vol. 2(4), 142-149; ISSN (Print) 2663-8991, ISSN (Online) 2616-48251DOI:10.55014/pij.v2i4.86.
https://rclss.com/index.php/pij

Nakata, T., Otsuki, K. and Khan, S.H., 1990. Active faults stress field, and plate motion along the Indo-Eurasian plate boundary. In: M. Kono and B.C. Burchfiel (Editors), Tectonics of Eastern Asia and Western Pacific Continental Margin. Tectonophysics, 181:83-95.

Namdarsehat, P.; Milczarek, W.; Motavalli-Anbaran, S.-H.; Khaledzadeh, M. 2024. Makran Subduction Zone: A Review and Synthesis. Geosciences, 14, 219. https://doi.org/10.3390/geosciences14080219

Naseer Ahmed, Shahid Ghazi, and Perveiz Khalid 2015. On the variation of b-value for Karachi region, Pakistan through Gumbel's extreme distribution method. Acta Geod Geophys. DOI 10.1007/s40328-015-0122-8

Obara K., 2020. Characteristic activities of slow earthquakes in Japan. Proc. Jpn. Acad., Ser. B 96 No. 7 pp. 297-315.

Pakistan Meteorological Department Bulletin June- July 2025 https://seismic.pmd.gov.pk/bulletins.php.

Quittmeyer, R.L. and Jacob, K.H., 1979. Historical and Modern Seismicity of Afghanistan, NW India, South Iran and South Asia. Bull. of Seism. Soc. America, v. 69, no. 3 p. 773-825.

Quittmeyer, R.L., Farah, A. and Jacob, K.H., 1979. The Seismicity of Pakistan and its relation to surface faults. In: Farah, A. and DeJong, K.A. (eds.), Geodynamics of Pakistan. Geol. Surv. Pak., Quetta, p. 271-284.

Sarwar, G. and K.A. DeJong, 1979, Arcs, Oroclines, Syntaxes: The curvatures of mountain belts in Pakistan, in: A. Farah and K.A. DeJong (eds.); Geodynamics of Pakistan. Geol. Surv. Pakistan, Quetta, p.341-349.

Sarwar, G. 2004. Earthquakes and the Neo-Tectonic Framework of the Kutch-Hyderabad-Karachi Triple Junction Area, Indo-Pakistan. Pakistan Journal of Hydrocarbon Research.Vol.14, p.35-40,

Sarwar, G., & Alizai, A. 2013. Riding the mobile Karachi arc, Pakistan: Understanding tectonic threats. Journal of Himalayan Earth Sciences v. 46 no.2, 9-24.

Schelling, D.D., 1999. Frontal structural geometries and detachment tectonics of the northeastern Karachi arc, southern Kirthar Range, Pakistan. In: Macfarlane, A., Sorkhabi, R.B., Quade, J. (Eds.), Himalaya and Tibet: Mountain Roots to Mountain Tops. Geological Society of America, Boulder, Colorado, pp. 287–302. https://doi.org/10.1130/0-8137-2328-0.28

Shah F., Miraj M., Ali A., Ahsan N., Mehmood T., Sajida M., Salaam A, and Fazal A. (2023). Tectonics of

ISSN number; ISSN 2202-0039

Jacobabad–Khairpur High and Its Impact on Petroleum Fields of the Region, Southern Indus Basin, Pakistan: A Case Study. Geotectonics, 2023, Vol. 57, No. 3, pp. 346–358.

Supino, S., Poiata N., Festa G., Vilotte J.P., Satriano C., & Obara K., 2020. Self-similarity of low-frequency earthquakes. Scientific Reports. 10:6523 | https://doi.org/10.1038/s41598-020-63584-6

Takemura S, Hamada Y., Okuda H., Okada Y, Okubo K., Akuhara T, Noda A., and Tonegawa T., 2023. A Review of Shallow Slow Earthquakes Along the Nankai Trough. Earth, Planets and Space (2023) 75:164. https://doi.org/10.1186/s40623-023-01920-6

Tirmizi, O.; Khan, S.D.; Mirzaee, S.; Fattahi, H. 2023. Hazard. Potential in Southern Pakistan: A Study on the Subsidence and Neotectonics of Karachi and Surrounding Areas. Remote Sens.15, 1290. https://doi.org/10.3390/rs15051290.

USGS. (2025). Earthquake Catalogue for Pakistan. U.S. Geological Survey.

Voskresensky, I., Kravchenko, K., Movshovich, E. and Sokolov, B., 1971. Outline of Geology of Pakistan. M. Nedra, p. 166. (in Russian).

Xiaowa, QIN Siqing, XUE Lei, ZHANG Ke, CHEN Hongran, ZHAI Mengyang 2021. Partition method of seismogenic tectonic block and its corresponding seismic zone. Geological Review. Vol. 67 No. 2 pp.325- 338 Doi: 10. 16509 / j. georeview. 2021. 02. 004.

NCGT Journal
New Concepts in Global Tectonics

New Concepts in Global Tectonics Journal
Volume 13, Number 10, December 2025

ISSN number; ISSN 2202-0039

HISTORY OF OCEANIC WATER

Vadim V. Gordienko
S.I. Subbotin Institute of Geophysics, NASU, Kiev, Ukraine
gordienkovadim39@gmail.com

Abstract: Views on the origin and evolution of water on planet Earth vary significantly. They mainly pertain to the amounts of water and the mechanisms of its incorporation within crustal and mantle rocks. Conclusions from various sections of geography, geology, geochemistry, cosmochemistry, and cosmogony have been employed for their foundation. An analysis of numerous data makes it possible to conclude with sufficient confidence that the emergence of water is associated with the final stage of planet formation, which began following the buildup of 60 to 90 percent of its volume. It was during that period of time that, among other chondrites, hydrous carbonatite chondrites were supplied to the accretion zone. After analyzing various sources that deal with their contribution to the formation of water, this process can be correlated with geological and geophysical data on the processes that occurred during the Earth's early history. This involved assumptions made by this author on the global asthenosphere, which is a relic of the primordial magmatic ocean. It is precisely this information that has enabled us to estimate the volume of substance from which the emergence of the magmatic ocean made it possible to extract water. By matching the above independent results, we can claim with a high degree of probability that water to fill the ocean was available (in one form or another) throughout the entire explored geological history of planet Earth.

Keywords: magmatic ocean; the nature of water on planet Earth.

Introduction

The origin and evolution of oceans is one of the major issues in geological studies. We can move closer to its solution, in particular, by exploring the water within them. Perceptions regarding the origin of oceanic water, its age, changes in its volume and salinity in the course of geological history that one can find in various publications differ significantly [Budyko et al., 1987, Hay et al., 2006; Mikhailov et al., 2007; Orlenok, 2010; Shu et al., 1990, etc.]. The arguments used by authors to substantiate their viewpoints are no less different. In many cases, they could not even be correlated because they had been obtained with the help of information from different sections of geography, geology, geochemistry, cosmochemistry, cosmogony, and so on. Nevertheless, it appears that in recent years one has become increasingly aware of the general recognition that water on Earth is largely primordial in origin and that it emerged at early stages of geological history following the splitting of the substance into nucleus and shells.

The lengthy and intricate course of the material condensation, the accretion of internal planets within the Solar System that brought about such an event, contains numerous elements that have not so far been explained explicitly [Meteorites…., 2006; White, 2020]. Some of them fall in the category of science this author is not familiar with, and so it remains to be guided by opinions of experts — mainly listed in [Grimm et al., 1989, Lunine, 2006, Peslier et al., 2017, etc.], even though I do not always share their views.

Nevertheless, since the separation of the core is also a well-proven geological fact, it is possible to conclude that, at this specific point of the process, the very fact that results obtained independently by dissimilar techniques do coincide, enhances its credibility.

Of course, recognition of the authenticity of the event in question is insufficient for answering many questions regarding the evolution of the contemporary ocean and, probably, of its precursors, as well. It appears worthwhile to analyze those problems with special reference to geological and geophysical information since only its incorporation makes it possible, at various historical stages, to make use of the data, perhaps incomplete, often just fragmentary, yet pertaining to the same evolutionary process in question. The geological theory proposed by this author [Gordienko, 2022] enables us to incorporate in the analysis results of the antecedent evolution of the Solar System substance and carry out their independent quantitative comparison with contemporary oceans. This has become possible owing to the revelation of the "magmatic ocean" and conservation of its bottomset throughout the entire history of planet Earth, after the shells are disclosed.

The Magmatic Ocean and the Global Asthenosphere

The aforementioned portion was identified as the global asthenosphere [Gordienko, 2017; Gordienko et al., 2025, etc.] - a zone of partial melting within the mantle (**Fig.1**).

NCGT Journal
New Concepts in Global Tectonics

New Concepts in Global Tectonics Journal
Volume 13, Number 10, December 2025

ISSN number; ISSN 2202-0039

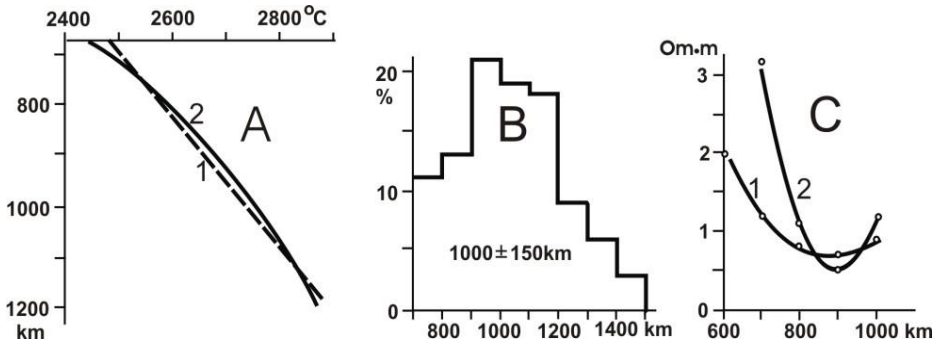

Fig.1. Criteria for identifying the global asthenosphere:
A — the thermal model of the Precambrian platform's mantle: 1 - temperature of mantle rocks' solidus, 2 - temperature distribution; B — histogram of the distribution of velocity heterogeneity in the mantle of various regions of continents and oceans at depths ranging from 700 to 2000 km; C— variation with depth of the specific electrical resistance of mantle rocks according to laboratory data (1) and results of geomagnetic-variation probing(2).

The thermal evolution model for the mantle is based on the concept of the initial temperature (T) distribution that prevailed about 4.2 billion years ago. If we disregard aspects of the process that are not essential for our purpose, it was due to the antecedent accretion (that led to the planet's heating by 1,500-2,500° C, on the average, depending on the process scheme used), to the Earth's differentiation into the core and outer shells (which was responsible for the average rise in temperature by 1,200° C) during 10-100 millions of years [Early…, 1980; Ringwood, 1981, Peslier et al., 2017 and others), and to the formation of a "magma ocean" with a depth of about 1,000 km. "The magma ocean is becoming enriched with volatile and incoherent elements by contrast with solid magma, which is becoming very dry and devoid of volatile elements" (The Early History of the World, 1980, p. 28), with crustal material being removed from it. The process is accompanied by intensive heat and mass transfer (in all likelihood, through continuous convection) and by a cooling of the tectonosphere to the level of rock solidus temperature. Once this temperature is reached, the viscosity of the mantle material increases significantly, and continuous convection at the rate required for enabling heat and mass transfer during actual active processes becomes unlikely. Subsequent temperature changes are linked to conductive cooling through the surface, emission of radiogenic heat (with an intensity varying with time and, in the absence of heat losses, capable of heating the upper mantle of a future platform by 2,000-2,500° C), and to heat efflux through advection during active processes. Additional sources of heat (its generation or absorption) can emerge during the displacement of the top of the polymorphic transformation zone in the upper mantle's lower portion.

When calculating thermal changes models reflecting the effects of heat and mass transfer, we superposed results of displacement of the material in each active episode of the region's history on the initial model (distribution of solidus temperature down to 1,000-1,100 km depths 4.2 billion years ago) and results of its evolution under the effect of heat generation and heat release through the surface.

The choice of endogenous regimes was tied to the type of preceding thermal model. If the temperatures exceeded solidus within a broad range of depths greater than 200 km, the situation was assumed to be suitable for the emergence of convection within the asthenosphere and of a geosynclinal process. Also taken into account was the presence of a gradient exceeding adiabatic in the asthenosphere or in a portion thereof. It was precisely such a segment of the asthenosphere that was considered suitable for a convective interfusion of the material and for shaping an asthenolith that floated upwards. If the asthenosphere was thinner, conditions were considered suitable for rifting or for a single activation episode (during which the material moved like at the initial stage of rifting). In that case, as a rule, the material was removed from the asthenosphere or its portion about 100 km thick, less frequently 50 km thick. In the absence of the asthenosphere or its insignificant thickness (less than 50 km), the estimation (implying just the evolution of the background and smoothing of previous temperature anomalies) continued until the required conditions were obtained. To simplify calculations, the diameter of a single quantum of tectonic action (QTA – a minimum volume of material capable of changing position) was in all cases considered to amount to 50 km. Every geosynclinal or rifting event was matched by the transfer of three QTAs. When necessary, restriction of emerging heat sources in length and width was taken into account.

Of course, the modelling that was carried out does not reflect the only plausible version of the sequence of active processes in the platform's tectonosphere. When the heat model did not make it possible to opt for a type of endogenous regimes conclusively, considered several varieties of the process with different thermal properties of the medium and different types of the process, so that active process could start or the time-span of the "tectonic quiescence" could be extended to enable a more complete "maturation" of conditions for subsequent heat and mass transfer. In all cases, we observed largely the same pattern. There is nothing

New Concepts in Global Tectonics Journal
Volume 13, Number 10, December 2025

ISSN number; ISSN 2202-0039

that could be added to or removed from the estimated heat and mass transfer episodes.

Computations performed for the depths beneath the zone under study have revealed a peculiar situation. Within a depth range of about 700-1,100 km, a layer with insignificant partial melting left by the "magma ocean" has remained intact throughout the entire geological history. This global asthenosphere is commensurable in volume with the outer core and is larger than the inner core. Presently available velocity models of the mantle do not detect it.

From the depths of 200-250 km, the density of the liquid is higher than that of the crystalline material with the same composition, and for that reason, no floating asthenoliths take shape in the global asthenosphere. Low viscosity causes seismicity to cease in the upper part of the asthenosphere at an approximate depth of 700 km.

The perception derived with the help of the method described above regarding the volume of the magmatic ocean (0.47 trillion km³, the volume of the entire planet Earth equaling 1.08 trillion km³) from which water could form, is in harmony with the recent conclusion to the effect that the stage of our planet's formation culminated with the volume of about 70±20% of its present volume. Later (from 10 to 100-150 million years from the beginning of accretion, when the planet accumulated a mass reaching 99% of the present mass), the surface collected meteorite materials uniform in age and isotopic composition (D/H); the role of comets was negligibly small. The parameters of that material are similar to those of the rocks on Earth. More specifically, even if large fragments from other parts of the Solar System are within the Earth (the material of the last stage of accretion does not contain enough iron necessary for building the core), they are situated in the deep lower mantle and in the core. It is there, according to the adopted accretion model, that the substance may be found that was supplied to planet Earth during the period of asteroids (planetesimals) hitting the Earth. "The number of water-rich bodies in the 'feeding zone' of the Earth is increasing (with time — author). The Earth began relatively dry, i.e., poor in water, and received its first significant influx of volatiles after reaching 60-90% of its present size. The subsequent accretion was dominated by bodies rich in volatiles. For example, water-rich fragments of the mantle or undifferentiated materials originating from the primordial asteroid belt (such as carbonaceous chondrites)… or between and beyond the giant planets" [Peslier et al., 2017, p.766]. The authenticity of associating the material of Earthly origin precisely with chondrites was put in doubt after analysis of the results of isotopic comparison (D/H) with other elements. However, the aforementioned procedure often turns out to be less substantiated than that for deuterium and hydrogen. This has been shown, in particular, by E.M. Galimov for carbon [Galimov, 1973]. There exists "…. the process of heterogeneous fractionation of carbon isotopes, which could be used for studying a vast range of geological processes. At the same time, however, it is precisely the presence of subtle and multiform isotopic effects in the process of graphite formation that must caution us against resorting to excessively straightforward conclusions regarding graphite genesis based on measurements of its isotopic composition." [Galimov, 1973, pp. 352-353].

The Amount of Water on Earth

The total amount of the free water on Earth (on its surface and its vicinity) is 1.46 billion km³, which is by 4% larger than the amount of ocean water [Mikhailov et al., 2007].

Determination of water concentration in crystalline rocks of the crust and mantle within the former magmatic ocean was carried out using the data quoted in numerous publications [Anderson, 1989; Babushkina et al., 2009; Bolfan-Casanova, 2005; Drybus et al., 2022; Katayama et al., 2006; King et al., 2008, Natural…, 2003; Norton, 2002; Otani et al., 2009; Peslier et al., 2017; Ryabchikov, 1985; Solovova, 2004; White, 2020, and others]. Generally speaking, the methods of study and the available material differed considerably. The results were divided into two groups, largely in terms of estimates outside direct measurements of water amounts in real rock samples. It has to be pointed out that "…. most of 'water' on the Earth is actually trace amounts of hydrogen within rock-forming silicate minerals that make up the planet's crust and mantle" [Peslier et al., 2017, p. 746]. For the problem being tackled, this is quite a reasonable way to get an estimate: What is being determined is the concentration of water that may occur within different "baggings" at any moment of geological history. The concentration of water is much greater in crystalline rocks than of the moisture in the pores. Some reference information is listed in **Fig. 2.**

NCGT Journal
New Concepts in Global Tectonics

New Concepts in Global Tectonics Journal
Volume 13, Number 10, December 2025

ISSN number; ISSN 2202-0039

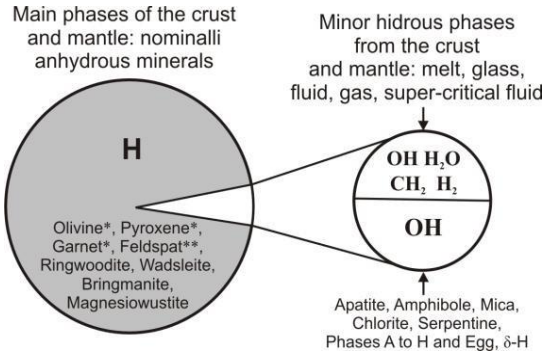

Fig. 2. "Diagram illustrating "water" species present during various phases in the Earth's mantle and crust [Preslier et al., 2017, p. 746].

The size of the pie slices represents the approximate volume percentage of the phases. The main reservoir of water in the mantle is nominally anhydrous minerals where hydrogen (H) enters their lattice in defects, and bonds to structural oxygen (gray field) [Bell and Rossman, 1992]." *Olivine, pyroxene and garnet can incorporate water as H2 under reduced conditions [Yang et al., 2016]. **K-feldspar can sometimes incorporate water as H2O and NH4 [Johnson and Rossman, 2004]".

The average content of water in the continental crust (amphibolite + granulites) is estimated at approximately 1,3 mass % (0,1-5%), whereas in the oceanic crust (basalt + gabbro) its content is about 1,5 mass % [Bodnar et al., 2013]. The total amount of that type of water is 0.26 billion km³. The depths from which the study samples, were derived are limited by the location of magma chambers capable of producing the melt of rather low density. They are limited by the level of pressure over which the liquid becomes denser than hard rocks of the same composition. As a rule, such pressure for real rocks is reached at a depth of approximately 250 km. Xenolites from the layer of 0-250 km are very common in regions that experienced magmatism of diverse composition and age [Peslier et al., 2017, etc.]. The data for both identified groups within that depth range do not differ significantly. In the case of one such group, there is no information on the eclogite concentration in the mantle, but this may be just accidental.

One may come across some microscopic samples, which are difficult to identify, from the depth interval of 250-400 km ("xenoliths within xenoliths"). Water content in them differs little from that in samples taken from more shallow depths. This author believes it is unlikely for the substance from the zone transitional between the upper and the lower mantle or from the lower mantle to reach the surface [Gordienko, 2017, etc.].

A detailed analysis of this problem was performed by A.V. Ivanov. His study slightly mitigates the limitations. It is impossible petrologically to prove that the substance from the lower mantle and/or from the boundary between the lower mantle and the core could reach the surface. It is just a speculative theory. "Petrological studies of the substance that rose to the surface from the deepest levels have shown that the relevant depth is limited to upper levels of the lower mantle (approximately 650-700 km), i.e., to the depth of the deepest earthquakes. Ferropericlase inclusions found in some diamonds do not rule out the involvement of deeper mantle levels, yet they do not provide explicit validation of such a theory either. Nor do geochemical data explicitly confirm the involvement of the lower mantle substance in the processes of magma generation beneath volcanically active areas. At the same time, they testify to a complete material isolation of the core from processes in the upper mantle" [Ivanov, 2010, p. 87].

One of the groups of data presents results on water concentration beneath the bottom of the magmatic ocean in the lower mantle and even in the core. We are naturally talking only about the results of modelling, moreover, for the part of the planet that formed while remaining "dry". The magnitudes do not differ from those that applied to the bottom part of the magmatic ocean.

There exists an assumption claiming that water was trapped in the aforementioned part of the Earth in the course of very intense mass exchange through the mechanism detailed in the plate tectonics concept (PTC). Many geologists (including this author) point to a disagreement between this concept and the real facts [Bluman, 2008, Frolov et al., 2011, Gordienko, 2017, Radich, 1984, Storetvedt, 1997, etc.], whereas supporters of the concept have been reiterating for many decades their speculative points in favour of the concept, without even performing obvious experimental verifications of at least its basic elements. Therefore, we cannot rely on the PTC conclusions as reliable points.

Some publications [Bolfan-Casanova, 2005; Peslier et al., 2017, etc.] mention abnormally large water contents in the transition zone between the upper and lower mantle. They claim that up to 18 oceans exist in that depth interval [Peslier et al., 2017]. More specifically, they insist that rock structures formed under PT conditions within the transition zone might contain the corresponding amount of water. No such phenomenon is assumed to exist above or below that zone. That is, rocks differ not just in terms of conditions, but also by their composition. It is claimed that the transition zone contains "a cemetery of slabs" — fragments of oceanic crust that sank there. For this author, such an idea is totally unacceptable in principle. Moreover, it is not even in conformity with the main stipulations of plate tectonics. "The productivity" of the spreading zone (for which proponents of the PTC do not determine in terms of magmatic intensity on mid-oceanic ridges, but simply claim that it is equal

NCGT Journal
New Concepts in Global Tectonics

New Concepts in Global Tectonics Journal
Volume 13, Number 10, December 2025

ISSN number; ISSN 2202-0039

in volume to the area of the crust from the mid-oceanic ridges to the subduction zone) is by orders of magnitude lower than is required for supporting the postulated subsidence of the plates. Focal zones occurring at depths no less than 400 km have only been identified at just 10% of continent-ocean contacts.

Water is quite abundant in the presumably sinking oceanic crust (see above). However, in the case of required subsidence, no slab is capable of delivering that water to the transition zone. It is precisely by its melting that plate tectonics proponents account for island arcs' magmatism. The melting process occurs at relatively shallow depths (50-150 km) and is very intense ("the Pacific ring of fire"). Under such conditions [Peslier et al., 2017], the rocks lose virtually all their water.

Publications on water abundance in rocks of the transition zone to the lower mantle quote numerous results of temperature and pressure determinations that do not reflect the real situation. For example, it is claimed in [Gu et al., 2022, etc.] that ringwoodite occurs at a depth of 660 km under the pressure of about 23 GPa, and the temperature of 1,650°C. The temperature is actually 600-700°C higher. The possibility of such errors was corroborated by an analysis, reported in [Yu et al., 2011]. In fact, with temperature increase, water content reduces to normal for mantle rocks [Bolfan-Casanova, 2005].

The veracity of hydration in the transition zone was checked out seismologically, and the result was negative. "The velocity data do not provide any proof that wadsleyite or ringwoodite could be globally hydrated as a result of subduction or initial conditions on the Earth [Houser, 2016, p. 94]. Over the entire territory of Northern Eurasia between the Pacific and Atlantic oceans, the results of studying the structure of the upper mantle with the help of nuclear explosions have revealed a velocity jump of longitudinal seismic waves of 0.6-0.7 km/sec at the top of the transition zone [Pavlenkova et al., 2014]. This conforms to the transformation of olivine into ringwoodite without "water addition".

[Piani et al., 2020] assume that the mantle contains amounts of water much greater than in the ocean. This assumption was based on revealing 1% of water in rare enstatite chondrites. The composition of those chondrites resembles the composition of the mantle. It might be assumed that the mantle formed precisely from them. The composition of enstatite is as follows: MgO - 40%; SiO_2 - 60%. The real mantle contains 45% SiO_2 and 39% MgO. The rest are oxides of Fe, Al, and Ca. How come the authors decided that enstatite's composition is similar to the mantle's? Other arguments also contradict the above hypothesis, but what we have provided is sufficient.

The estimated amount of water in mantle rocks of the former magmatic ocean, as presumed in the publications listed above, suggests a median quantity of 0.8±0.2 billion km³, together with crustal rocks — 1.06 billion km³, and together with liquid surface and subsurface water - approximately 2.5 billion km³.

The computation of the amount of water introduced into the shell of the Earth by meteorites prior to the formation of the magmatic ocean was performed using the data reported in the following publications: [Anderson, 1989; Bondar et al., 2013; Braukmüller et al., 2018; Grimm et al., 1989; Lunine, 2006; Marakushev et al., 2010, 2006; …, Natural…., 2023, Norton, 2002, Peslier et al., 2017, White, 2020, etc.]. It was assumed that only carbonaceous chondrites that occupy about 4.6% of the entire substance supplied over that period of time contributed a substantial input to the entire mass. Those formations differ markedly in composition and properties. Five groups have been identified within the mentioned class of meteorites. Small amounts of nongrouped specimens were also identified. Their characteristics were not described due to their scarcity and insignificant water content (**Fig. 2**). Unfortunately, information on specific contents of water in carbonaceous chondrites is scarce. Nevertheless, we may hope that the average values obtained for each group are reliable enough.

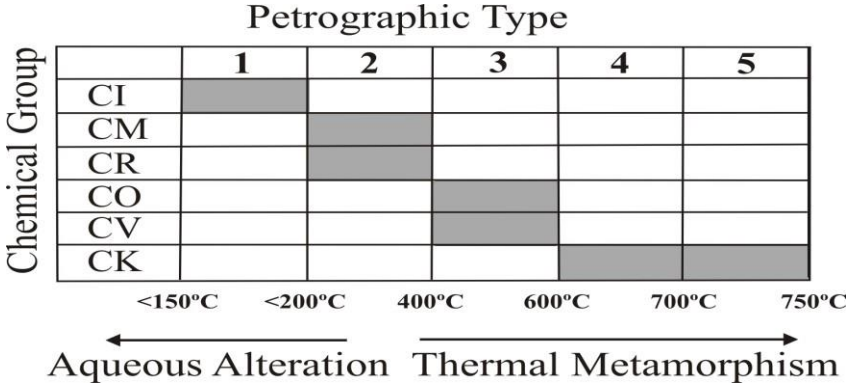

Fig. 3. Carbonaceous chondrites are classified based on a combination of their primary (chemical) composition and levels of secondary (aqueous and thermal processing (Sephton, 2002, Natural…, 2023).

NCGT Journal
New Concepts in Global Tectonics

New Concepts in Global Tectonics Journal
Volume 13, Number 10, December 2025

ISSN number; ISSN 2202-0039

Based on publications [Marakushev et al., 2010; Meteorites…, 2006; Natural…, 2023, Norton, 2002, Peslier et al., 2017, White, 2020, etc.], it is possible to get an idea on the formation of chondrites, including carbonaceous ones. It can be presumed that they come into being during the disintegration of asteroids. Their maximum quantity originates from upper layers, whereas deeper layers are involved more seldom. The substance of the inner core (iron meteorites) got onto the Earth in tiny quantities during the latest period. They do not exceed about 3%, and the rest are silicate formations. In other words, the main part of the Earth's iron core (16% in volume) was supplied earlier, during the period of planetesimals' fallout.

It is generally recognized that the quantity of chondrites CI with the highest water content (about 20%) must be much greater than in other groups. However, their preservation after hitting the Earth's surface is minimal. They turn out to be very fragile formations with the lowest degree of thermal metamorphism. Upon hitting the surface, they, as a rule, turn into dust which easily undergoes erosion. The quantity of authentic chondrite samples does not exceed several dozen.

The following approach was applied for relative (in comparison with carbonaceous chondrites from other groups) restoration of such samples. The catalog of meteorites [Natural…, 2023] lists over 500 carbonaceous chondrite samples from known groups, petrological types, and temperature of metamorphism. Presumably, they represent, in required proportion, sets of samples to which we can ascribe the average temperature of metamorphism and compare the derived distribution with a normal one (**Fig. 4**).

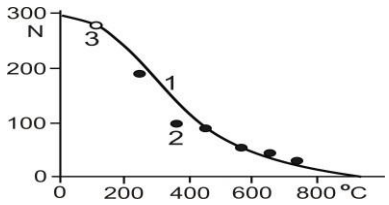

Fig. 4. The quantity of carbonaceous chondrites with dissimilar temperatures of metamorphism [Natural…, 2023]. 1— the graph of normal distribution, 2 — points characterizing the quantity of samples in each group and the mean temperature of their metamorphism, 3 — position of the CI point for the temperature of metamorphism ranging from 50 to 100°C.

It is obvious that the distribution of carbonaceous chondrites' varieties is close to normal; the average deviation of the points from the graph does not exceed 15% of the graph deviation from the horizontal axis. The quantity of the CI meteorites that had to be in the set is 280. The total number of carbonaceous chondrites (including CI) in the Meteorite Catalogue of the Natural History Museum (London) among all meteorites is 4.6%, i.e., it coincides with the world average.

Table. Water contents in Carbonaceous Chondrites groups [Braukmüller et al., 2018, Grimm et al., 1989, Meteorotes…, 2006; Norton, 2002, Peslier et al., 2017, White, 2020, etc.].

Chemical Group (Petrographic type)	Water content (vol.%)	Relative quantity [%]	Part of the average water content (vol.%)
CI (1)	20	34	6.8
CM (2)	13	24	3.1
CR (2)	11	11	1.2
CO (3)	4	13	0.5
CV(3)	3	7	0.2
CK(4,5)	1.5	11	0.2

The mean concentration of water in all carbonaceous chondrites is 12%, so that it will amount to 0.55% in the future magmatic ocean. The total amount of water supplied by meteorites at the final stage of formation of the Earth will be 2.6 billion km³. Clearly, the technique described here cannot guarantee an accurate result. This goal could rather be achieved by its correlation with the quantity established through a totally different manner. In the given case, the agreement is full. Naturally, we should not attribute any decisive significance to that coincidence. The above description of the procedure that was used to obtain results, even though it involves rather sound judgments, is in fact approximate. Once more detailed data appears, our results can be supplemented or revised. For the time being, we will accept in further constructions the probability that oceanic water has existed on the Earth in contemporary mass right from the moment of crystallisation of the magmatic ocean rocks 4.2 billion years ago. A larger figure could certainly be used, but for the Hadean period, very few objects or events with sufficiently accurate dating are known that could be compared to calculated data.

New Concepts in Global Tectonics Journal
Volume 13, Number 10, December 2025

ISSN number; ISSN 2202-0039

Conclusions

The study has shown that the coordination of numerous data from various spheres of knowledge makes it possible to determine the origin of water on planet Earth is achievable. We managed, with their help, to specify in more certain terms - certain processes, such as the formation of the magmatic ocean and the mobilization of water delivered to the upper part of the shell at the final stage of accretion, including the introduction of meteorites.

The results obtained make it possible to inspect other aspects in the formation and functioning of the oceans on planet Earth.

Acknowledgements. The author would like to express special thanks to Mrs. Rita Schneider for translating this paper from Russian.

Reference

Anderson D. (1989). Theory of the Earth. Boston: *Blackwell Scientific Publications*, 384 p.

Babushkina M.S. Nikitina L.P., Goncharov A.G., & Ponomareva N.I., (2009). Water in the structure of minerals in mantle peridotites as controlled bythermal and redox conditions of the upper mantle. *Geology of Ore Deposits*. Vol. 51, pp. 712–722.

Bell D., Rossman G. (1992). Water in Earth's mantle: the role of nominally anhydrous minerals. *Science*. Vol. 255, pp. 1391-1397. DOI: 10.1126/science.255.5050.1391

Bluman B.A. (2008). Weathering of basalts and unconformities in the oceanic crust: possible geodynamic implications. *Regional geology and metallogeny.* No. 35, pp. 72-86 (in Russian). http://www.evgengusev.narod.ru/tecto/bluman-2008.html

Bodnar R., Azbej T., Becker S., Cannatelli C., Fall A., Severs M. (2013). Whole Earth geohydrologic cycle, from the clouds to the core: The distribution of water in the dynamic Earth system. *The Geological Society of America. Special Paper 500*, pp. 431–461.

Bolfan-Casanova N. (2005). Water in the Earth's mantle. *Mineralogical Magazine*. Vol. 69 (3): pp. 229-257. https://doi.org/10.1180/0026461056930248

Braukmüller N., Wombacher F., Hezel D., Escoube R., Münker C. (2018). The chemical composition of carbonaceous chondrites: Implications for volatile element depletion, complementarity and alteration. *Geochimica et Cosmochimica Acta*. Vol. 239, pp. 17-48. https://doi.org/10.1016/j.gca.2018.07.023

Budyko M.I., Ronov A.B.,Yanshin A.L. (1987). History of the Earth's atmosphere. Berlin; New York : *Springer-Verlag*, 139 p.

Drajbus G., Yagoutts E., Wenke K. (1997). Water in the Earth's mantle. *Geologiya i Geofizika* Vol. 38, pp. 269-275 (in Russian).

The Early history of the Earth. Ed. B. Windley. (1976.) Moscow: *Mir*, 619 p. (in Russian).

Frolov V.T., Frolova T.I. (2011). Origin of the Pacific. Moscow: *MAKS Press*. 52 p. (in Russian).

Galimov E.M. (1973). Carbon isotopes in petroleum geology. Moscow: *Nedra*. 384 p. (in Russian).

Gordienko V.V. (2017). Thermal processes, geodynamics, deposits. 283 p. https://ivangord2000.wixsite.com/tectonos

Gordienko V.V. (2022). About geological theory. *Geophysical Journal*. No 2. pp. 68-92.

Gordienko V.V., Logvinov I.M. (2025). On the Earth's global asthenosphere. *Geophysical Journal*. No 2, pp.187-192 (in Ukrainian).

Grimm R., McSween H. (1989). Water and the Thermal Evolution of Carbonaceous Chondrite Parent Bodies. *Icarus.* Vol. 82, pp. 244-280. https://doi.org/10.1016/0019-1035(89)90038-9

Gu T., Pamato M.G., Novella D. et al. (2022). Hydrous peridotitic fragments of Earth's mantle 660 km discontinuity sampled by a diamond. *Nature Geoscience*. Vol. 15, pp. 950–954. https://doi.org/10.1038/s41561-022-01024-y

Hay W., Migdisov A., Balukhovsky A., Wold C., Flogel S., Soding E. (2006). Evaporites and the salinity of the ocean during the Phanerozoic: implications for climate, ocean circulation and life. *Palaeogeography, Palaeoclimatology, Paleoecology*, Vol. 240, pp. 3-46.

Houser C. (2016). Global seismic data reveal little water in the mantle transitian zone. *Earth and Planetary Science Letters*. Vol. 448, pp.94-101.

Ivanov A.V. (2010). Deep-seated geodynamics: process boundaries on the basis of geochemical and petrological data. *Geodynamics & Tectonophysics*. No. 1. pp. 87-102 (in Russian). https://doi.org/10.5800/GT-2010-1-1-0008

Johnsoin E., Rossman G. (2004). A survey of hydrous species and concentrations in igneous feldspars. *American Mineralogist*. Vol. 89, pp. 586-600.

Katayama I., Nakashima S., Yurimoto H. (2006). Water content in natural eclogite and implication for water transport into the deep upper mantle. *Lithos*. V. 86, Issues 3–4, pp. 245-259.

ISSN number; ISSN 2202-0039

King A., Daly L., Rowe J. et al. (2022). The Winchcombe meteorite, a unique and pristine witness from the outer solar system. *Science Advances.* Vol 8, No. 46. https://doi.org/10.1126/sciadv.abq3925

Kovalenko V.I., Naumov V.B., Girnis A.V., Dorofeeva V.A., Yarmolyuk V.V. (2006). Estimation of the average contents of H2O, Cl, F, S in the depleted mantle based on the compositions of melt inclusions and quench glasses of mid-ocean ridges. *Geochemistry International*, 3, p. 243-266 (in Russian).

Li, Z., Lee T., Peslier A., Lenardic A., Mackwell S. (2008). Water contents in mantle xenoliths from the Colorado Plateau and vicinity: Implications for the mantle rheology and hydration-induced thinning of continental lithosphere, *Journal of Geophysical Research Atmospheres*, 113, B09210, doi:10.1029/2007JB005540

Lunine J. (2006). Origin of Water Ice in the Solar System. Meteorites and the early Solar system II. *University of Arizona Press*. pp. 309–319.

Marakushev A.A. Glazovskaya L.I., Marakushev S.A. (2010). Correlation of the formation of iron-silicate and carbonaceous matter in carbonaceous chondrites. *Dokl. RAS*, Vol. 434, No. 5, pp. 664–669 (in Russian).

Meteorites and the early Solar system II. Ed. D. Lauretta and H. McSween. (2006). 943 p. *University of Arizona Press*.

Mikhailov V.N., Dobrovolsky A.D., Dobrolyubov S.A. (2007). Hyidrology. 2nd ed. Moscow: *Higher education textbook*. 464 p. (in Russian).

Natural History Museum. London. (2023). Meteorite Catalogue. https://doi.org/10.5519/10.5519/tqfuwle7

Norton, O. (2002).The Cambridge Encyclopedia of Meteorites. Cambridge: *Cambridge University Press*. 354 p.

Orlenok V.V. (2010). Global volcanism and oceanization of the Earth and planets. Kaliningrad: *I. Kant RSU*. 196 p. (in Russian)

Otani E., Zhao D. (2009). The role of water in the deep upper mantle and transition zone: dehydration of stagnant slabs and its effects on the big mantle wedge. *Russian Geology and geophysics*. Vol. 50. No. 12, pp. 1073-1078. https://doi.org/10.1016/j.rgg.2009.11.006

Pavlenkova N.I., Pavlenkova G.A. (2014). The Earth's crust and upper mantle structure of the Northern Eurasia from the seismic profiling with nuclear explosions. Moscow. GEOKART: *GEOS*. 191 p. (in Russian).

Peslier A., Schönbacher M., Busenmann H., Karato S. (2017). Water in the Earth's interior: distribution and origin. *Space Science Reviews*. Vol. 212. Issue 1-2. pp. 743-810. DOI 10.1007/s11214-017-0387-z

Piani L., Marrocchi Y., Rigaudier T. et al. (2020). Earth's water may have been inherited from material similar to enstatite chondrite meteorites. *Science*. Vol 369, Issue 6507, pp. 1110-1113. DOI: 10.1126/science.aba1948

Ringwood A.E. (1981). Composition and petrology of the Earth's mantle. Moscow: *Nedra*. 584 p. (in Russian).

Rudich E.M. (1984). Expanding Oceans: Facts and Hypotheses. Moscow: *Nedra*. 251 p. (in Russian).

Ryabchikov I.D. (1985). Aqueous solutions in the upper mantle and problems of the Earth's degassing. In the book: Groundwater and the evolution of the lithosphere. Vol. 1. Moscow: *Nauka*, pp. 176-187 (in Russian).

Sephton N.A. (2002). Organic compounds in carbonaceous meteorites. *Natural Product Reports*. Vol. 19, pp. 292-311. DOI:10.1039/B103775G

Shu L., Conway M., Zhang X., Hu S., Chen L., Han J., Zhu M., Li Y. (1999). Lower Cambrian vertebrates from South China. *Nature*. Vol. 402, Issue 6757, pp. 42—46. DOI:10.1038/46965

Sobotovich E.V., Bartnitsky E.N., Tson O.V., Kononenko L.V. (1982). Handbook of Isotope Geochemistry. Moscow: *Energoizdat*. 240 p. (in Russian).

Solovova I.P. (2004). Mantle magmas and fluids from the study of inclusions in minerals. Dis. Dr. geol.-min. Sciences. Moscow: *IGEM RAN*, 335 p. (in Russian).

Storetvedt K. (1997). Our evolution planet. Earth history in new perspective. Bergen: *Alma mater forlag*. 456 p.

White W.M. (2020). Geochemistry. 2nd Edition. *Wiley-Blackwell*. 960 p.

Yang X., Keppler H., Li Y. (2016). Molecular hydrogen in mantle minerals. *Geochemical Perspectives Letters* v2, n2, pp. 160-168. doi: 10.7185/geochemlet.1616

Yu, Y. G., Wentzcovitch, R. M., Vinograd, V. L. & Angel, R. J. (2011). Thermodynamic properties of $MgSiO_3$ majorite and phase transitions near 660 km depth in $MgSiO_3$ and Mg_2SiO_4: A first principles study. *Journal of Geophysical Research*. Vol. 116, Issue B2, pp. 31–19. https://doi.org/10.1029/2010JB007912

New Concepts in Global Tectonics Journal
Volume 13, Number 10, December 2025

ISSN number; ISSN 2202-0039

ABOUT THE NCGT JOURNAL

The NCGT Newsletter, the predecessor of the NCGT Journal, was begun as a result of discussions at the symposium "Alternative Theories to Plate Tectonics" held at the 30th International Geological Congress in Beijing in August 1996. The name is taken from an earlier symposium held in association with the 28th International Geological Congress in Washington, D. C. in 1989. The first issue of the NCGT Newsletter was December 1996. The NCGT Newsletter changed its name in 2013 to the NCGT Journal. Aims of the NCGT Journal include:

1. Providing an international forum for the open exchange of new ideas and approaches in the fields of geology, geophysics, solar and planetary physics, cosmology, climatology, oceanography, electric universe, and other fields that affect or are closely related to physical processes occurring on Earth from its core to the top of its atmosphere.
2. Forming an organizational focus for creative ideas not fitting readily within the scope of dominant tectonic models.
3. Forming the basis for the reproduction and publication of such work, especially where there has been censorship or discrimination.